Oriented Matroid Analysis of Thermochemical Reaction Systems

Samuel W. Peterson

June 30, 2000

Acknowledgements

This Master's thesis is based upon my work as a research assistant for the Department of Geology at the University of Minnesota from September, 1999, to May, 2000. There are many people to whom I am grateful for making this possible. I would first like to thank my good friend and mentor, Professor Jesus de Loera, who introduced me to the beautiful world of combinatorial geometry. Thanks to my friends and family for all of their support and encouragement throughout my years as a graduate student. For seeing me through graduation, I thank my academic advisor, Professor Fadil Santosa, and the Minnesota Center for Industrial Mathematics. Thank you Michel Schrameck and Professor Paul Garrett for helping me with CGI stuff. Thanks to Jörg Rambau for providing such a brilliant piece of software as TOPCOM. Special thanks to Jürgen Richter-Gebert and Ulrich Kortenkamp at ETH Zurich. Most of all, I would like to thank my advisors Professors Jim Stout, Victor Reiner, and Paul Edelman. I learned so much from the three of you throughout this year and had a lot of fun in the process. It has been a huge honor for me to work under such brilliant individuals.

Abstract

We address the problem of phase diagram construction for thermochemical reaction systems. The spatial representation of chemical phases in composition space imposes a discrete set of geometric relationships between them. These relationships restrict the phase diagram topology to a relatively small set of possibilities. Oriented matroid theory allows us to completely describe the geometry and enumerate the candidate topologies for systems of n components and $n+1$, $n+2$, and $n+3$ phases. The computations involved can be done very quickly on a computer. We have designed a Java applet called `CHEMOGALE` which performs the geometric analysis for a user input chemical system. Output is provided in a graphical format consistent with the conventions of geochemists, including the generation of the closed net, Euler Sphere, and straight line nets of potential solutions. We give user instructions for this program in Chapter 3. Similar instructions may be found on the program's web site at `http://www.math.umn.edu/~reiner/CHEMOGALE.html`. Finally, we include an appendix with the complete classification of all combinatorially distinct chemographies for non-degenerate systems of four components and seven phases.

Chapter 1

1.1 Introduction

Given any set of substances in a closed system at fixed temperature and pressure, various interactions between them may be possible. These interactions are limited to a finite set of chemical reactions in which some set of physically homogeneous substances, called *phases*, react to form a totally different set of substances and vice versa. The pressure and temperature of the system decide which set of phases is produced and which is consumed. With enough time, the consumption process runs the reactions out of vital phases. At this point, the phases and their amounts become fixed and the system has reached a state of *equilibrium*. A closed system will maintain equilibrium until the pressure and temperature change enough to reverse some of the reactions. After this change, a new equilibrium will be obtained. We are interested in exactly how the equilibrium state depends on the pressure and temperature. For example, a geologist examining a rock may find a set of several coexisting minerals (phases). This set is the result of a particular pressure and temperature acting on elements existing in the region for an extended period of time. The minerals which exist in the rock and those absent from the rock (but whose compositional elements are present) together limit the pressure and temperature at the time the rock was formed to a bounded set of possibilities. Our problem, in general, is to examine how this set is determined.

1.2 Reactions and Mass Balance

When dealing with any chemical system, it is vital to know the phases involved and how those phases interact with each other. This information is contained in a list of relations called *mass balance equations*. The set of mass balance equations for a reaction system consists of sets of phases, each divided disjointly into a left-hand and right-hand side, for which the total mass of each element within the left-hand side is equal the total mass of the same element within the right-hand side. Since it is necessary that every chemical reaction conserve the mass of the particles involved, the list of mass balance equations completely

defines all reactions which are possible for a system. The general form for a mass balance equation is:

$$a_1 p_{l_1} + a_2 p_{l_2} + \cdots + a_n p_{l_n} \rightleftharpoons b_1 p_{r_1} + b_2 p_{r_2} + \cdots + b_m p_{r_m},$$

where p_{l_i} and p_{r_i} are the phases of the system and $a_1, a_2, \ldots, a_n, b_1, b_2, \ldots, b_m$ are numerical coefficients representing the numbers of moles or other quantity of each phase. The distinction between left and right-hand sides is completely arbitrary.

Consider a very simple system involving the three physical states of H_2O: ice, water, and steam. The phase interactions in this system include ice melting and water freezing, water evaporating and steam condensing, and ice sublimating and steam depositing. The mass balance equations are very simple because H_2O is the only molecule involved. We will abbreviate ice, water, and steam by $H_2O_{(s)}$, $H_2O_{(l)}$, and $H_2O_{(g)}$, respectively. The possible mass balance equations are:

(1) $H_2O_{(s)} \rightleftharpoons H_2O_{(l)}$

(2) $H_2O_{(s)} \rightleftharpoons H_2O_{(g)}$

(3) $H_2O_{(l)} \rightleftharpoons H_2O_{(g)}$

(4) $H_2O_{(s)} + H_2O_{(l)} \rightleftharpoons 2H_2O_{(g)}$

(5) $H_2O_{(s)} + H_2O_{(g)} \rightleftharpoons 2H_2O_{(l)}$

(6) $H_2O_{(l)} + H_2O_{(g)} \rightleftharpoons 2H_2O_{(s)}$

Notice, however, that equation (4) is the sum of equations (2) and (3). Similarly, equation (5) is a combination of equations (1) and (2), and equation (6) is a combination of equations (1) and (3). Thus it is unnecessary to list (4), (5), and (6), since their information is already contained in (1), (2), and (3). Because of this redundancy scientists only include, in the set of mass balance equations, those relations which cannot be obtained by some combination of other relations in the list.

As another example, consider a reaction system involving water (H_2O), and the minerals quartz (SiO_2), andalusite (Al_2SiO_5), diaspore ($AlO(OH)$), pyrophyllite ($Al_2(OH)_2(Si_4O_{10})$), and kaolinite ($Al_2Si_2O_5(OH)_4$). This system has 13 mass balance equations:

(1) $2AlO(OH) + 2SiO_2 + H_2O \rightleftharpoons Al_2Si_2O_5(OH)_4$

(2) $2AlO(OH) + 4SiO_2 \rightleftharpoons Al_2(OH)_2(Si_4O_{10})$

(3) $2AlO(OH) + Al_2(OH)_2(Si_4O_{10}) + 2H_2O \rightleftharpoons 2Al_2Si_2O_5(OH)_4$

(4) $Al_2Si_2O_5(OH)_4 + 2SiO_2 \rightleftharpoons Al_2(OH)_2(Si_4O_{10}) + H_2O$

(5) $Al_2SiO_5 + SiO_2 + 2H_2O \rightleftharpoons Al_2Si_2O_5(OH)_4$

(6) $Al_2SiO_5 + Al_2Si_2O_5(OH)_4 + 5SiO_2 \rightleftharpoons 2Al_2(OH)_2(Si_4O_{10})$

(7) $2Al_2SiO_5 + Al_2(OH)_2(Si_4O_{10}) + 5H_2O \rightleftharpoons 3Al_2Si_2O_5(OH)_4$

(8) $Al_2SiO_5 + 3SiO_2 + H_2O \rightleftharpoons Al_2(OH)_2(Si_4O_{10})$

(9) $2AlO(OH) + SiO_2 \rightleftharpoons Al_2SiO_5 + H_2O$

(10) $6AlO(OH) + Al_2(OH)_2(Si_4O_{10}) \rightleftharpoons 4Al_2SiO_5 + 4H_2O$

(11) $4AlO(OH) + 3SiO_2 \rightleftharpoons Al_2SiO_5 + Al_2Si_2O_5(OH)_4$

(12) $2Al_2SiO_5 + 3H_2O \rightleftharpoons 2AlO(OH) + Al_2Si_2O_5(OH)_4$

(13) $10AlO(OH) + 3Al_2(OH)_2(Si_4O_{10}) \rightleftharpoons 4Al_2SiO_5 + 4Al_2Si_2O_5(OH)_4$

It is important to keep in mind that the mass balance equations do not impose a direction on the reactions in general. In other words, it is possible for the reaction to run from left to right or from right to left or both, depending on the pressure and temperature. At a fixed pressure and temperature, the final equilibrium state is the direct result of the combined directions of all the reactions involved.

1.3 The Phase Diagram

Chemists map the stable equilibria associated with any pressure and temperature in a chemical system into a *phase diagram*. With pressure values along the positive vertical axis and temperature values along the positive horizontal axis, the phase diagram partitions the first quadrant of the two dimensional coordinate system into the various possible phase equilibria. The partitioning is defined by curves which correspond to mass balance equations for phases in the system. The region on one side of a curve consists of pressure-temperature pairs for which the reaction runs left to right, while on the other side of the curve, the reaction runs right to left. Chemists refer to the regions as *divariant fields* because within them, both temperature and pressure are free to vary independently while maintaining the same set of equilibrium phases. Pressure and temperature coordinates along the reaction curve boundaries represent conditions for which all phases involved in the reaction are in chemical equilibrium. These curves are referred to as *univariant curves*, because there is only one degree of freedom among pressure-temperature coordinates which lie along them. The exact point at which multiple univariant curves intersect represents a pressure and temperature at which all phases involved in the intersecting curves are in equilibrium. This is called an *invariant point* because the phase equilibrium represented cannot be maintained for any other pressure-temperature pair.

A simple illustration is the phase diagram for the ice, water, steam system. Figure 1.1 shows the three regions labeled by their respective phases, $H_2O_{(s)}$, $H_2O_{(l)}$, and $H_2O_{(g)}$. As we would expect, the region for ice contains points of low temperature and high pressure. Water exists at slightly higher temperatures

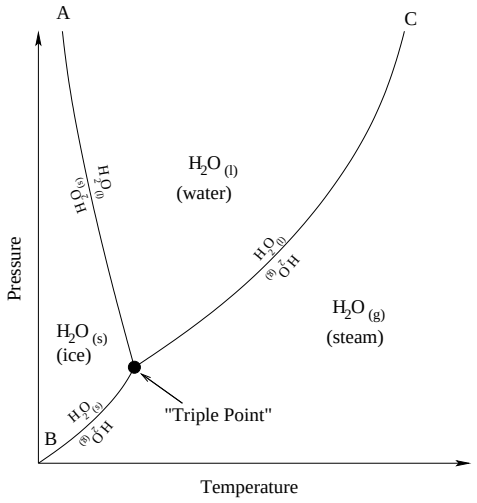

Figure 1.1: The phase diagram for the three physical states of H_2O.

when the pressure is sufficiently high. Finally, H_2O is in steam form at high temperatures with sufficiently low pressures. The univariant curves are labeled with the stable phases on their respective sides. The point at the intersection of all three curves is the exact pressure and temperature at which ice, water, and steam can all exist in equilibrium, and is called the triple point.

The phase diagram fully defines the relationships between the chemicals and states involved in a reaction and the pressure and temperature imposed on them. The combination of phases present at any equilibrium state corresponds to some region on the phase diagram. Only pressure-temperature coordinates contained in this region are feasible for the given outcome. Of course, for the H_2O example given above, the regions are very large and cover a wide range of pressure and temperature configurations. More complicated systems, however, involving many interacting phases yield very complex phase diagrams in which the regions defined are much more confining.

1.4 Gibbs Energy

Chemists are often faced with the task of constructing the phase diagram for a given chemical system. The key to this problem is to understand the roles that pressure and temperature play in each reaction of the system. Scientists quantify this role in terms of *Gibbs free energy* or simply, *Gibbs energy*. Every phase in a reaction system has an intrinsic Gibb's energy function associated with it. The value of this function depends solely on temperature and pressure, provided there are no chemical composition changes. The Gibb's energy of a substance is inversely related to its stability at the input pressure and temperature. Also,

the value of the Gibb's energy per mole is additive across different phases. In other words, the Gibb's energy associated with a particular collection of phases at a given pressure and temperature is equal to the sum of the Gibb's energy of each multiplied by its molarity. In this way, we can group the Gibb's energies in each of the left and right sides of the mass balance equations into $G_l(P,T)$ and $G_r(P,T)$, respectively. Reactions always favor the direction which minimizes the Gibbs energy. So if $G_l(P_0,T_0) > G_r(P_0,T_0)$, the reaction will tend towards the right side when run at pressure P_0 and temperature T_0, and vice versa when $G_l(P_0,T_0) < G_r(P_0,T_0)$.

As an example, let us consider the simple and familiar system involving the three states of H_2O. Recall the three mass balance equations for the system:

(1) $H_2O_{(s)} \rightleftharpoons H_2O_{(l)}$

(2) $H_2O_{(s)} \rightleftharpoons H_2O_{(g)}$

(3) $H_2O_{(l)} \rightleftharpoons H_2O_{(g)}$

Referring back to figure 1.1, we can make general observations about the Gibbs Free energy:

- For P,T pairs lying in region $H_2O_{(s)}$, reactions (1) and (2) have $G_l(P,T) < G_r(P,T)$.
- For P,T pairs lying in region $H_2O_{(l)}$, reaction (1) has $G_l(P,T) > G_r(P,T)$ and reaction (3) has $G_l(P,T) < G_r(P,T)$.
- For P,T pairs lying in region $H_2O_{(g)}$, reactions (2) and (3) have $G_l(P,T) > G_r(P,T)$.
- For P,T pairs lying on curve A, reaction (1) has $G_l(P,T) = G_r(P,T)$, and reactions (2) and (3) have $G_l(P,T) < G_r(P,T)$.
- For P,T pairs lying on curve B, reaction (2) has $G_l(P,T) = G_r(P,T)$, reaction (1) has $G_l(P,T) < G_r(P,T)$ and reaction (3) has $G_l(P,T) > G_r(P,T)$.
- For P,T pairs lying on curve C, reaction (3) has $G_l(P,T) = G_r(P,T)$, and reactions (1) and (2) have $G_l(P,T) > G_r(P,T)$.
- For P,T at the triple point, all three reactions have $G_l(P,T) = G_r(P,T)$.

Unfortunately, the Gibbs energy function is not well known for every phase. For the most part, the function cannot be derived and instead must be found experimentally. This requires carefully controlled laboratory experiments at varied pressure and temperature configurations. Typically, conclusive results can only be obtained after several repeated iterations for each data point. Human error and measurement uncertainty can produce data which is not sufficiently accurate. The fatal result is that the topology of the phase diagram is misrepresented. Even with guaranteed perfect data, there may be unresolvable ambiguity

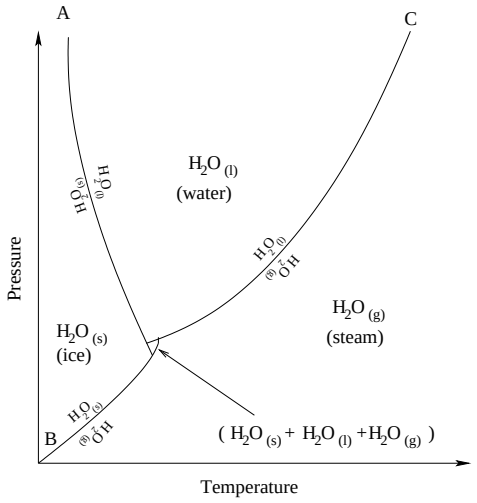

Figure 1.2: An alternative phase diagram for the ice, water, steam system which is topologically incorrect.

in the phase diagram. For instance, consider an alternative phase diagram for the ice, water, and steam system shown in figure 1.2. This version is almost correct, except the simultaneous equilibrium of ice, water and steam exists in a divariant field instead of a single invariant point. No amount of laboratory runs can resolve the ambiguity between a single point and a very tiny region. For these reasons, chemists require a way in which to determine the exact topology of the phase diagram for the system in question. Once this is done, thermodynamic and experimental data will serve to properly orient and size the diagram in the pressure-temperature plane. For many systems, the correct topology, or at least a small set of feasible topologies, can be mathematically determined just from the list of phases involved. In the next chapter, we explain the relationship between our chemical problem and the recently introduced mathemtical theory of oriented matroids.

Chapter 2

2.1 Composition Space: An Introduction

Throughout this chapter, we incorporate some powerful mathematics into our chemical problem. In order for this discussion to be effective, the fundamental link between the mathematics and the chemistry must be established. This link lies in what chemists refer to as *composition space*. When studying relationships among some set of objects, it is natural to spatially organize them in such a way that very similar items are close together while very distinct items are far apart. Chemical compounds are no exception. For instance, given a particular phase, we can base its nearness to other phases on the similarity of their chemical composition. We demonstrate this concept with a simple example.

Example 2.1.1 Consider the chemical reaction system involving pure carbon (C), pure oxygen (O_2), carbon dioxide (CO_2), and carbon monoxide (CO). Since all of the molecules are composed of either carbon or oxygen or both, we can represent all of them on a two dimensional coordinate system with carbon along the x-axis and oxygen along the y-axis. It is straightforward, then, that the coordinates for carbon would be $(1, 0)$, for oxygen $(0, 2)$, for carbon dioxide $(1, 2)$, and for carbon monoxide $(1, 1)$. Since we are not given the amounts of each substance, it is appropriate to treat their coordinates as directions corresponding to the ratios of carbon and oxygen in each. The result is the set of four vectors shown in figure 2.1.

It is easy to see the generalization of this model, in which the number of common elements determines the number of coordinate axes. Representing reaction systems this way is very intuitive and encodes a great deal of information. Exactly what that information is and how to extract it, is the focus of this chapter. We wish to discuss reaction systems in a purely general sense, so our chemical model space will be $\mathbb{R}^n$ - the real coordinate space with n being an arbitrary number of axes. The mathematics we present warrants a bit of introduction to expose some important concepts of $\mathbb{R}^n$ and establish a working vocabulary. In the next section, we take the time to introduce and review some general notions about the real vector space $\mathbb{R}^n$. It will be assumed that the reader is somewhat

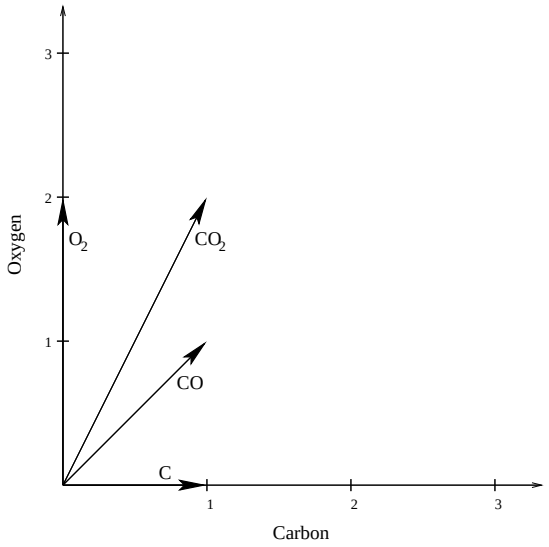

Figure 2.1: The composition space for a system of carbon (C), oxygen (O_2), carbon dioxide (CO_2), and carbon monoxide (CO).

comfortable with the basic properties and notations associated with this space (if not, we recommend [1] for a review).

2.2 Fundamentals of $\mathbb{R}^n$

All of the objects, operations, and so forth, that we present in this paper exist in the real vector space $\mathbb{R}^n$ for some finite n. All numerical values will be elements of the set of real numbers $\mathbb{R}$, which we call scalars and represent with italic letters (e.g. a, b, x_0, x_1, v_0, v_1, etc.). Vectors in the space are ordered n-tuples of real numbers, and we write them as boldface letters (e.g. $\mathbf{x}, \mathbf{v}, \mathbf{z}$, etc.). The letter $\mathbf{e}$ is reserved to denote the *standard basis vectors* of $\mathbb{R}^n$, namely $\mathbf{e}_1 = (1, 0, 0, \ldots, 0)$, $\mathbf{e}_2 = (0, 1, 0, 0, \ldots, 0)$, ..., $\mathbf{e}_n = (0, 0, \ldots, 1)$. For a particular vector, we always use the same letter for the individual components as for the vector itself. So the expanded form of a vector $\mathbf{x} \in \mathbb{R}^n$ is generalized by $\mathbf{x} = (x_1, x_2, \ldots, x_n)$.

To avoid any confusion, we must make a distinction between a *linear* discussion of $\mathbb{R}^n$ and an *affine* one. Within the linear treatment of $\mathbb{R}^n$, vectors are like arrows with "heads" at the location specified by the coordinates and "tails" at the origin. Anytime we describe something as linear, we mean that it includes the origin. On the other hand, in the affine case, vectors represent points floating in space. Things described as affine do not necessarily contain the origin, and may instead be translated arbitrarily far away from it in any direction. For simplicity, we will refer to n-tuples as vectors in the linear case and points in the affine case. In general, we will use the letter $\mathbf{v}$ to be a vector

and $\mathbf{x}$ to be a point.

Script letters are used to denote some (possibly infinite) set of objects. Specifically, $\mathcal{V}$ will represent a set of vectors $(\mathbf{v}_1, \ldots, \mathbf{v}_m)$ and $\mathcal{X}$ will represent a set of points $(\mathbf{x}_1, \ldots, \mathbf{x}_m)$. We reserve regular capital letters (A, H, F etc.) to stand for special sets called *affine subspaces*. An affine subspace in $\mathbb{R}^n$ is a vector space of dimension less than or equal to n which has been embedded (positioned somehow) in $\mathbb{R}^n$. Familiar affine subspaces of $\mathbb{R}^3$ are points (dimension = 0), lines (dimension = 1), and planes (dimension = 2). A *linear subspace* is an affine subspace which includes the origin. Note that by our definition $\mathbb{R}^n$ is a linear subspace of itself. We give special attention to the affine subspaces of dimension $n-1$, called *hyperplanes*, and reserve for them the letter H. It is always true that a hyperplane $H \subset \mathbb{R}^n$ divides $\mathbb{R}^n$ into two halves called *half-spaces*. The two halfspaces are distinguished by arbitrarily assigning one to be positive and the other to be negative. We then refer to these closed halfspaces as H^+ and H^-, respectively. The hyperplane itself contains the only points shared between the two halfspaces, so $H^+ \cap H^- = H$. Figure 2.2 contains examples of hyperplanes and the halfspaces they define for $\mathbb{R}^1$, $\mathbb{R}^2$, and $\mathbb{R}^3$. An affine hyperplane can always be described by an affine functional of the form

$$f_H(\mathbf{x}) = a_0 x_0 + a_1 x_1 + ... + a_n x_n + a_{n+1}.$$

The value yielded by the functional describes the position of the input point $\mathbf{x}$ relative to H. If $f_H(\mathbf{x}) = 0$, then x lies directly on H; if $f_H(\mathbf{x}) > 0$, then x is properly within H^+; and if $f_H(\mathbf{x}) < 0$, then x is properly within H^-. A hyperplane which contains the origin must therefore have a functional which evaluates to zero when the origin is input. Such a hyperplane is called a *central* hyperplane, and is described by a linear functional of the form:

$$l_H(\mathbf{x}) = a_0 x_0 + a_1 x_1 + ... + a_n x_n$$

If H is a central hyperplane, then $l_H(\mathbf{v}) = 0$ whenever $\mathbf{v} \in H$; $l_H(\mathbf{v}) > 0$ whenever the head of $\mathbf{v}$ points into H^+; and $l_H(\mathbf{v}) < 0$ whenever the head of $\mathbf{v}$ points into H^-.

All of the mathematics presented in this paper is from the realm of *discrete geometry* or simply finite geometry. Therefore, most of the discussions revolve around a finite set of vectors or points. We use matrices to conveniently represent and manipulate the sets that we deal with. The vectors in a set $\mathcal{V} = (\mathbf{v}_1, \mathbf{v}_2, \ldots, \mathbf{v}_m) \subset \mathbb{R}^n$ are written as the columns of a matrix as follows:

$$\mathcal{V} = \begin{pmatrix} v_{11} & v_{21} & \cdots & v_{m1} \\ v_{12} & v_{22} & \cdots & v_{m2} \\ \vdots & \vdots & \ddots & \vdots \\ v_{1n} & v_{2n} & \cdots & v_{mn} \end{pmatrix}.$$

Likewise, the set of points $\mathcal{X} = (\mathbf{x}_1, \mathbf{x}_2, \ldots, \mathbf{x}_m) \subset \mathbb{R}^n$ has the expanded matrix

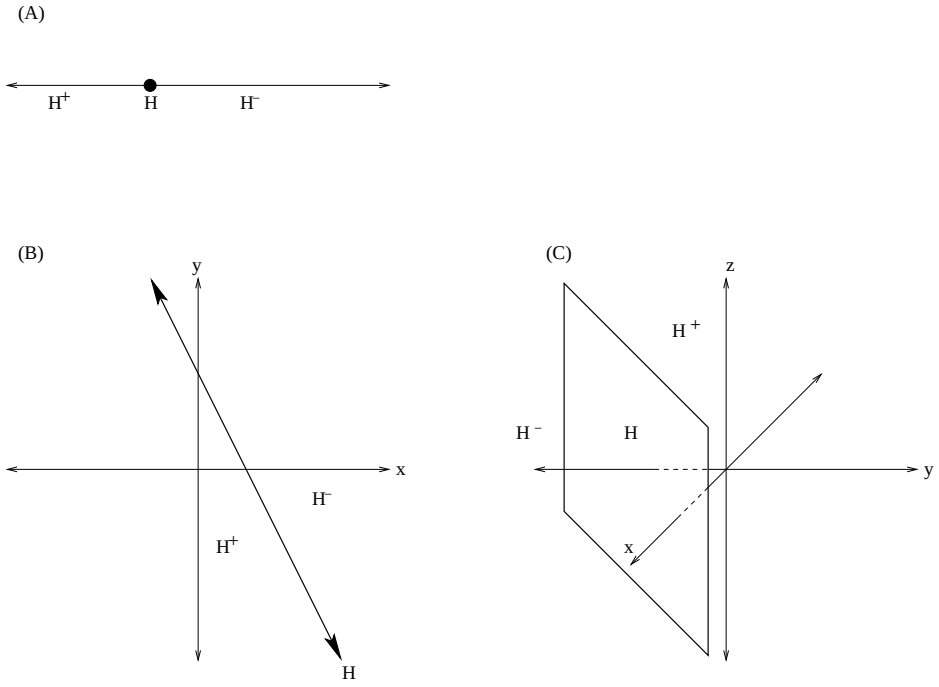

Figure 2.2: (A) A hyperplane H in $\mathbb{R}^1$. (B) A hyperplane H in $\mathbb{R}^2$. (C) A hyperplane H in $\mathbb{R}^3$.

form:

$$\mathcal{X} = \begin{pmatrix} x_{11} & x_{21} & \cdots & x_{m1} \\ x_{12} & x_{22} & \cdots & x_{m2} \\ \vdots & \vdots & \ddots & \vdots \\ x_{1n} & x_{2n} & \cdots & x_{mn} \end{pmatrix}.$$

By representing sets of vectors and points in this way, we can establish mathematical descriptions and operations for them.

An important notion for sets of vectors or points is *dependence*. A *linear dependence* for a set of vectors $\mathcal{V} \in \mathbb{R}^n$ is a non-zero vector $\mathbf{z} \in \mathbb{R}^m$ such that $\mathcal{V}\mathbf{z} = \mathbf{0}$. If such a $\mathbf{z}$ exists, we say that $\mathcal{V}$ is *linearly dependent*. When no such $\mathbf{z}$ exists, then $\mathcal{V}$ is linearly *independent*. A linearly independent set of n vectors in $\mathbb{R}^n$ constitutes a *basis* for $\mathbb{R}^n$. The set $\mathcal{B} = (\mathbf{b}_1, \mathbf{b}_2, \ldots, \mathbf{b}_n)$ is a basis set for $\mathbb{R}^n$ if and only if any vector $\mathbf{v} \in \mathbb{R}^n$ can be written uniquely as

$$\mathbf{v} = c_1\mathbf{b}_1 + c_2\mathbf{b}_2 + \cdots + c_n\mathbf{b}_n.$$

We say that a set of vectors $\mathcal{V} \in \mathbb{R}^n$ *spans* $\mathbb{R}^n$ if and only if it contains some subset which is a basis for $\mathbb{R}^n$.

An *affine dependence* for a set of points $\mathcal{X} \in \mathbb{R}^n$ is a non-zero vector $\mathbf{z} \in \mathbb{R}^m$ such that $\mathcal{X}\mathbf{z} = \mathbf{0}$ and $z_1 + z_2 + \cdots + z_n = 0$. The set $\mathcal{X}$ is *affinely dependent* if such a $\mathbf{z}$ exists and affinely *independent* otherwise. A set of points $\mathcal{X} \in \mathbb{R}^n$ is said to affinely span $\mathbb{R}^n$ if and only if it contains some subset $\mathcal{X}' \subseteq \mathcal{X}$ such that $\mathcal{X}'$ is affinely independent and $|\mathcal{X}'| = n + 1$. We also say that such a set is *full-dimensional*.

A vector configuration $\mathcal{V} \in \mathbb{R}^n$ is *acyclic* if it spans $\mathbb{R}^n$ and there exists a central hyperplane H such that $l_H(\mathbf{v}_i) > 0$ for all $\mathbf{v}_i \in \mathcal{V}$. Whenever $\mathcal{V}$ is an acyclic vector configuration, we can find an affine hyperplane $H_\mathcal{V}$ which lies between the origin and the heads of all of the vectors in $\mathcal{V}$. The vectors in $\mathcal{V}$ poke through the hyperplane, giving a set of points on $H_\mathcal{V}$ which we call the *affine slice* of $\mathcal{V}$. Figure 2.3 shows an example of this for a set of vectors in $\mathbb{R}^3$. Also, if $\mathcal{V}$ is acyclic then we may construct its *convex cone*:

$$cone(\mathcal{V}) = \{\mathbf{u} \in \mathbb{R}^n : u = c_1\mathbf{v}_1 + c_2\mathbf{v}_2 + \cdots + c_m\mathbf{v}_m, c_i \geq 0\}.$$

In other words, the convex cone of $\mathcal{V}$ is the set of all non-negative combinations of vectors in $\mathcal{V}$. Figure 2.4 shows examples of convex cones defined by acyclic vector configurations in $\mathbb{R}^2$ and $\mathbb{R}^3$. Since every spanning set in $\mathbb{R}^n$ has at least n vectors, $\mathcal{V}$ must have at least n vectors to be acyclic. In fact, any linearly independent set of n vectors is an acyclic vector configuration in $\mathbb{R}^n$. The cones formed from such sets are the simplest cones we can define in $\mathbb{R}^n$ and are called *simplicial* cones.

Related to the convex cone of a vector configuration in $\mathbb{R}^n$ is the *convex hull* of a point configuration in $\mathbb{R}^{n-1}$. Given $\mathcal{X}$, a set of m points which affinely span $\mathbb{R}^{n-1}$, we can construct the set $\mathcal{H}_+(\mathcal{X})$, which contains all hyperplanes H for which $\mathcal{X} \subset H^+$. The convex hull of $\mathcal{X}$ is the set

$$conv(\mathcal{X}) = \bigcap_{H \in \mathcal{H}_+(\mathcal{X})} H^+.$$

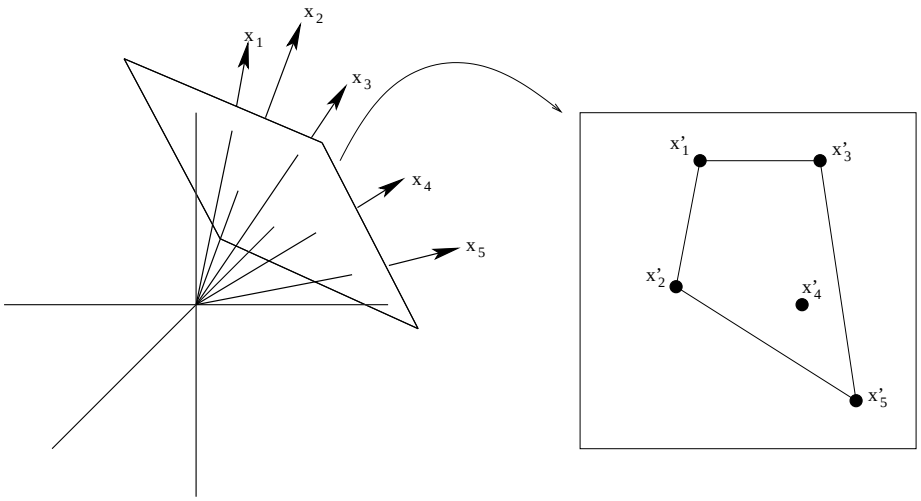

Figure 2.3: An acyclic vector configuration in $\mathbb{R}^3$ sliced by an affine hyperplane to yield a set of points in $\mathbb{R}^2$.

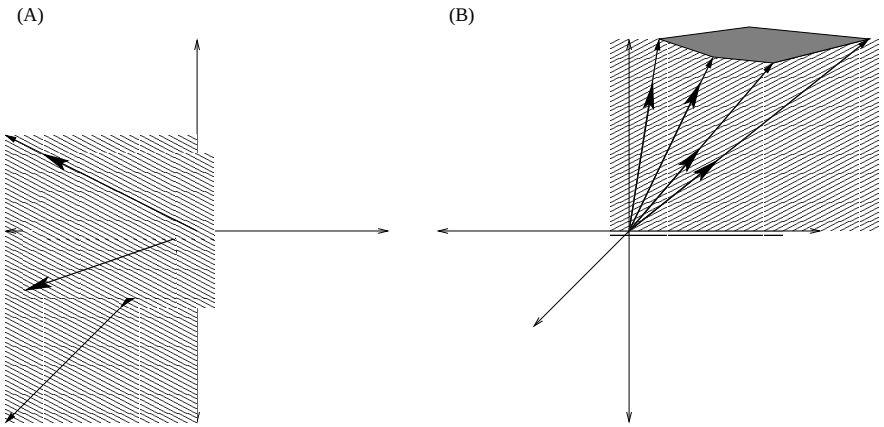

Figure 2.4: (A) The convex cone formed by an acyclic vector arrangement in $\mathbb{R}^2$. (B) The convex cone formed by an acyclic vector arrangement in $\mathbb{R}^3$.

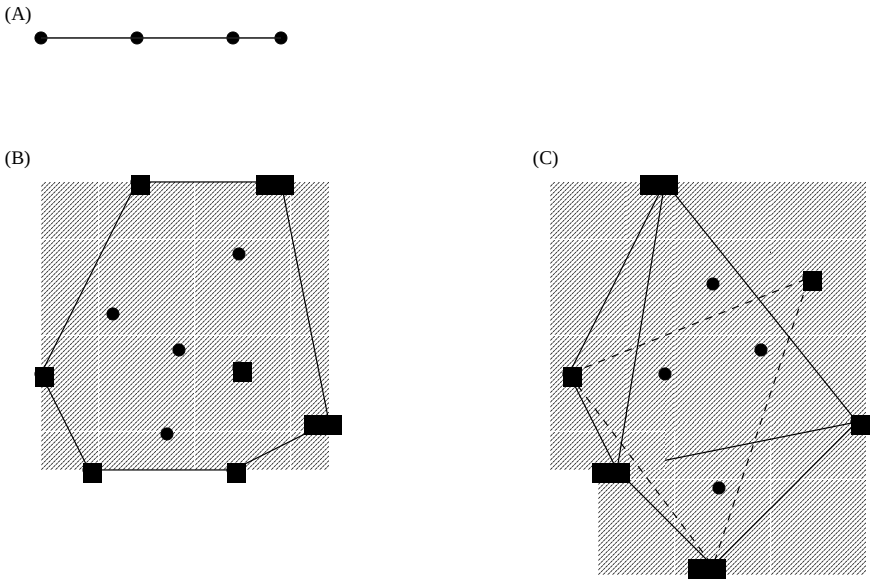

Figure 2.5: The convex hull of point configurations in (A) $\mathbb{R}^1$, (B) $\mathbb{R}^2$, and (C) $\mathbb{R}^3$.

In other words, the convex hull of $\mathcal{X}$ is the set of points which lie in the positive half-space of every hyperplane in $\mathcal{H}_+(\mathcal{X})$. Convex hulls have the significant property that if $\{\mathbf{y}_1, \mathbf{y}_2, \ldots, \mathbf{y}_r\} \subset conv(\mathcal{X})$, then it is true that $\lambda_1\mathbf{y}_1 + \lambda_2\mathbf{y}_2 + \cdots + \lambda_r\mathbf{y}_r \subset conv(\mathcal{X})$ whenever $\lambda_1 + \lambda_2 + \cdots + \lambda_r = 1$ and $\lambda_i \geq 0$ for all $1 \leq i \leq r$. Put another way, given any subset of points in the convex hull, any point that lies between them must also be in the convex hull. We give illustrations of convex hulls for point sets in one, two, and three dimensions in figure 2.5. We say that a point configuration $\mathcal{X}$ is convex if and only if $conv(\mathcal{X}') \neq conv(\mathcal{X})$ for every proper subset $\mathcal{X}' \subset \mathcal{X}$. In order for a configuration to affinely span $\mathbb{R}^{n-1}$, it must have at least n elements. Thus the simplest convex configurations that can be realized in $\mathbb{R}^{n-1}$ contain n affinely independent points. Such a configuration is called a *simplex* (pl. *simplices*). For example, simplices define line segments in $\mathbb{R}^1$, triangles in $\mathbb{R}^2$, and tetrahedra in $\mathbb{R}^3$.

There is an interesting relationship between convex cones in $\mathbb{R}^n$ and convex hulls in $\mathbb{R}^{n-1}$. The convex hull of any set of points in $\mathbb{R}^{n-1}$ can always be realized as the affine slice of the convex cone of some set of vectors in $\mathbb{R}^n$. Conversely, the affine slice of the convex cone of a set of points in $\mathbb{R}^n$ is always the convex hull of a set of points in $\mathbb{R}^{n-1}$. As one would expect, the affine slice of any simplicial cone in $\mathbb{R}^n$ defines a simplex in $\mathbb{R}^{n-1}$ and any simplex in $\mathbb{R}^{n-1}$ corresponds to the affine slice of a simplicial cone in $\mathbb{R}^n$.

One more useful notion for describing sets of vectors or points is *degeneracy*. A set of vectors $\mathcal{V} \in \mathbb{R}^n$ is degenerate if there exists some linearly dependent

subset $\mathcal{V}' \subseteq \mathcal{V}$ such that $|\mathcal{V}'| = n$. Similarly, a set of points $\mathcal{X} \in \mathbb{R}^{n-1}$ is degenerate if there exists some affinely dependent subset $\mathcal{X}' \subseteq \mathcal{X}$ with $|\mathcal{X}'| = n$. Sets which are not degenerate are said to be in *general* position or called *generic* sets. For example, a set of points in $\mathbb{R}^2$ is generic if no three points are collinear and in $\mathbb{R}^3$ if no four points are coplanar. A set of vectors in $\mathbb{R}^2$ is generic if no two vectors are collinear and in $\mathbb{R}^3$ if no three vectors are coplanar. Degeneracies such as these often cause computational algorithms to diverge or geometric generalizations to fail. For most of our derivations, they do not pose a significant problem.

2.3 More on Composition Space: Components and Phases

In order to perform an effective analysis of reaction systems in general, we must adopt some conventions for description and classification. For this, we introduce the *components* of a chemical reaction system. To a chemist, components are the basic building blocks of a system. In other words, every phase in the system should be able to be described by specific amounts of each component.

Although the idea of a component is somewhat intuitive, it can be firmly defined in terms of our above discussion of the real vector space. We can represent the global composition space as $\mathbb{R}^{98}$ with one dimension for each naturally occurring element. A phase is any physically homogeneous substance made up of non-negative amounts of the elements, and so every phase vector is contained in the positive orthant of $\mathbb{R}^{98}$. Given this fact, is easy to show that any configuration of phase vectors $\mathcal{V}$ in this space is acyclic. Just choose H such that $l_H(\mathbf{v}) = v_1 + v_2 + \ldots + v_{98}$. The components of the system, $\mathcal{C}$, can be any acyclic, linearly independent set of at most n vectors for which $\mathcal{V} \subseteq cone(\mathcal{C})$. In particular, any phase vector $\mathbf{v}_p$ of the system can be written as $\mathbf{v}_p = \lambda_{p_1}\mathbf{c}_1 + \lambda_{p_2}\mathbf{c}_2 + \cdots + \lambda_{p_n}\mathbf{c}_n$ with $\mathbf{c}_i \in \mathcal{C}$ and $\lambda_{p_i} \geq 0$. We can replace each phase vector $\mathbf{v}_p \in \mathbb{R}^{98}$ with $\mathbf{v}'_p = (\lambda_{p_1}, \lambda_{p_2}, \ldots, \lambda_{p_n})$, yielding the acyclic vector configuration $\mathcal{V}'$ in the new composition space $\mathbb{R}^n$. Thus the n components of the system correspond to each of the n coordinate axes in $\mathbb{R}^n$.

In the example given earlier involving the phases carbon, oxygen, carbon dioxide, and carbon monoxide, we defined the components to be C and O. The ice, water, and steam system has just the single component H_2O. Depending on the number of components (i.e. the dimension of the composition space), chemists label a system *unary* ($n = 1$), *binary* ($n = 2$), *ternary* ($n = 3$), *quaternary* ($n = 4$), etc. The number of phases involved is often specified in terms of how many more phases there are than components. For example, if a system has three more phases than components, then that system is said to have n components and $n+3$ phases. The system in example 2.1.1 would be described as a binary system with $n + 2$ phases. As will be seen later, there is great mathematical significance in this convention.

Since the phase vectors for any system always define an acyclic vector con-

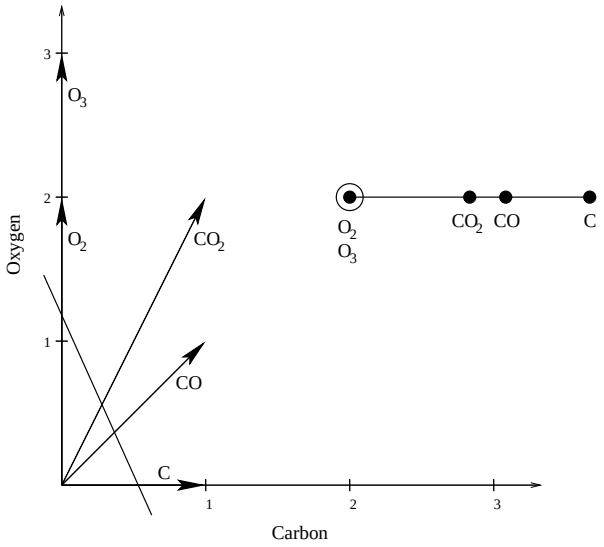

Figure 2.6: A degenerate set of phase vectors and their associated chemography.

figuration in $\mathbb{R}^n$, it is possible to slice them by an affine hyperplane to yield a point configuration in $\mathbb{R}^{n-1}$. The resulting configuration is called the *chemography* of the system and imposes a discrete geometry among the phases. We note that the chemography of a system may have multiple points in the same location. For example, consider adding ozone (O_3) to the phases in example 2.1.1. The new vector configuration has O_2 and O_3 parallel to each other. Figure 2.6 shows that slicing by an affine hyperplane yields a chemography with the two phases overlapping (as indicated by the circle around the point). In the ice-water-steam system, the situation is even worse. All three phases in the system have the exact same chemical composition (H_2O), thus they are represented by the same vector in the composition space. Degeneracies such as these create no inconsistencies in our geometric analysis. As we will see, the geometry of the chemography contains a perfect description of a system's chemical interactions. To understand this, we must familiarize ourselves with some of the concepts of discrete geometry. Therefore, we resume our mathematical discussion in the next few sections. Bear in mind, however, that phrases like "given a set of m points in $\mathbb{R}^{n-1}$..." and "given a set of m vectors in $\mathbb{R}^n$..." are equivalent to "consider a chemical reaction system with m phases and n components...".

2.4 Triangulations

One of the most important mathematical notions for our problem is a *triangulation* of a point configuration. We will briefly define and discuss the mathematical

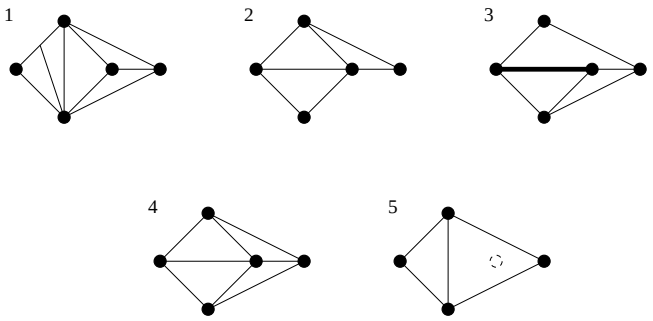

Figure 2.7: Five sets of simplices for a point configuration. The first three are not triangulations.

concept of triangulation before explaining how it relates to our problem. For a more thorough treatise of the vast topic of triangulations, we recommend chapter seven of Gelfand, Kapranov, and Zelvisky [7].

A *triangulation* of a set of points $\mathcal{X}$ in $\mathbb{R}^{n-1}$ is any decomposition of $conv(\mathcal{X})$ into a finite set of simplices $\mathcal{T}$ such that:

(1) If σ is a simplex in $\mathcal{T}$, then σ is a subset of $\mathcal{X}$.

(2)

$$\bigcup_{\sigma \in \mathcal{T}} conv(\sigma) = conv(\mathcal{X})$$

(3) The intersection of the convex hulls of any two simplices in $\mathcal{T}$ is the convex hull of a simplex in $\mathbb{R}^d$, $d < n-1$, which is a sub-simplex of both.

Figure 2.7 shows five simplicial decompositions of a set of points in $\mathbb{R}^2$. In the first case, some of the simplices are not the convex hulls of points strictly from the set, thus violating (1). The second does not fit the definition of a triangulation because (2) does not hold. The third decomposition is not a triangulation, since the highlighted edge violates (3). The fourth, and fifth pictures represent valid triangulations. In the fifth decomposition, one of the interior points is not used to define any simplex. Notice that this does not violate any of our criteria for a valid triangulation.

We say that a triangulation is *regular* if it can be realized as part of the boundary of a convex hull when its vertices are "lifted" to one higher dimension. Lifting points from $\mathbb{R}^{n-1}$ to $\mathbb{R}^n$ simply involves tacking an extra value onto the ends of their coordinate vectors. No matter what values we tack on, any triangulation of the original points is topologically feasible for the lifted points. That is, the convex hulls of simplices (no longer full-dimensional after lifting) will not intersect each other improperly. The regularity of a triangulation $\mathcal{T}$ of a point configuration $\mathcal{X}$ is usually demonstrated by lifting the points in $\mathcal{X}$ in

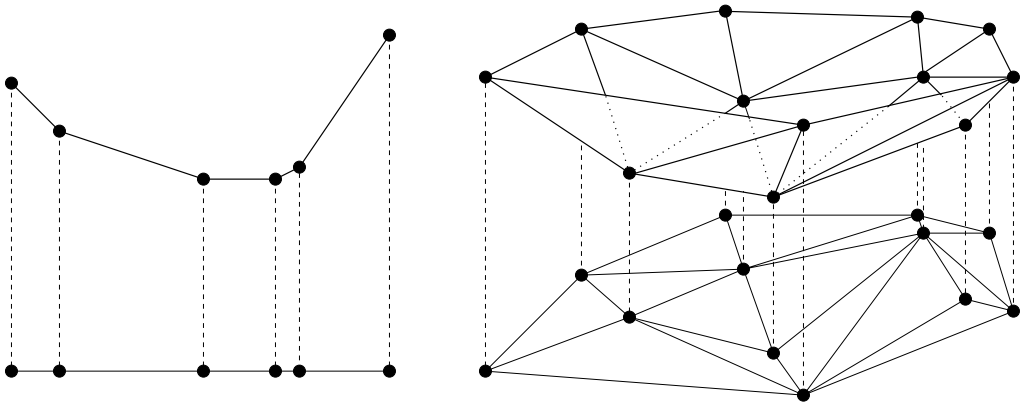

Figure 2.8: Examples of regular triangulations in two and three dimensions with corresponding lower hulls.

such a way that the simplices of $\mathcal{T}$ define the underside of the convex hull of the lifted points in $\mathbb{R}^n$. This "underside" of the lifted points, formed by regular triangulations, is known as the *lower hull*. Figure 2.8 shows two examples of a triangulation of a point configuration becoming a lower hull when the points are lifted. Both of the triangulations shown are thus regular.

It is perhaps surprising that there exist triangulations which are non-regular. Such triangulations never form a lower hull when the points are lifted to one higher dimension. The occurrence of non-regular triangulations increases as the dimension and/or the number of points increases. Non-regular triangulations, however, can occur for sets in as low as two dimensions with as few as six points. Figure 2.9 shows such a set and its non-regular triangulation. Regularity among triangulations is an active topic of research in mathematics. Much of the theory is fascinatingly complex and there are still many open problems.

In order to understand what triangulations have to do with our chemical problem, consider a reaction system with n components and $n+q$ phases, labeled $p_1, p_2, \ldots, p_{n+q}$. The chemography of this system is a set of $n+q$ points $\mathcal{X}$ in $\mathbb{R}^{n-1}$, where the point $\mathbf{x}_i$ corresponds to the phase p_i. Fix the temperature and pressure of the system at (P_0, T_0). We can then lift the points of the chemography to $\mathbb{R}^n$ by tacking on the values of the Gibbs Energy, $G_{P_0,T_0}(p_i)$, as the nth coordinate. The lower hull of the lifted points corresponds to some regular triangulation $\mathcal{T}$ of the points in $\mathcal{X}$. From $\mathcal{T}$, we get all of the information about the final equilibrium state of the reaction. If $\sigma = \{\mathbf{x}_{\sigma_1}, \mathbf{x}_{\sigma_2}, \cdots, \mathbf{x}_{\sigma_n}\}$ is a simplex in $\mathcal{T}$, then it is possible for any of the phases $\{p_{\sigma_1}, p_{\sigma_2}, \ldots, p_{\sigma_n}\}$ to coexist at equilibrium for the given pressure and temperature. Conversely, if the points $\{\mathbf{x}_i, \mathbf{x}_j\}$ are not together on at least one simplex of $\mathcal{T}$, then it is impossible for the phases $\{p_i, p_j\}$ to coexist at equilibrium for the given pressure and temperature. Furthermore, if the point $\mathbf{x}_i$ is not part of any simplex,

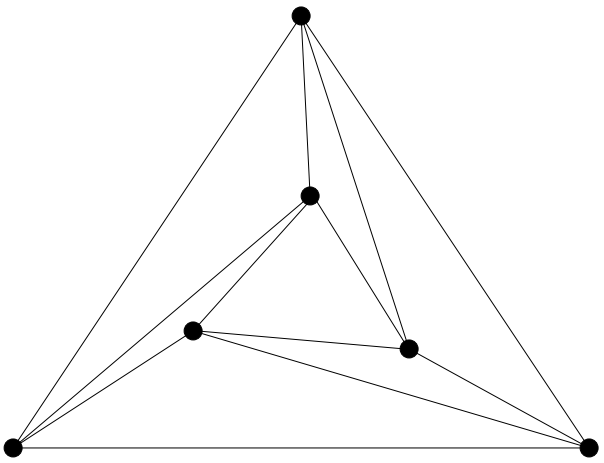

Figure 2.9: An example of two dimensional triangulation which is non-regular.

then the phase p_i will never appear at equilibrium for the given pressure and temperature. To illustrate what we mean, let us consider a simple example.

Example 2.4.1 Suppose we have a system with two components, labeled c_1 and c_2, and five phases, labeled p_1, p_2, p_3, p_4, and p_5. The phases have the following coordinates in composition space: $p_1 = (1, 0)$, $p_2 = (0, 2)$, $p_3 = (2, 2)$, $p_4 = (1, 3)$, and $p_5 = (2, 3)$. Figure 2.10 shows the phases in composition space ($\mathbb{R}^2$) and the corresponding chemography in $\mathbb{R}^1$. Assume that at pressure P_0 and temperature T_0, the Gibbs energies are:

1. $G_{P_0,T_0}(p_1) = 82.5$
2. $G_{P_0,T_0}(p_2) = 56.1$
3. $G_{P_0,T_0}(p_3) = 101.4$
4. $G_{P_0,T_0}(p_4) = 41.8$
5. $G_{P_0,T_0}(p_5) = 66.2$

The lifted points and their lower hull are shown in figure 2.11. From the figure, we can see that the lower hull corresponds to the regular triangulation $\mathcal{T}_0 = \{\{\mathbf{x}_2, \mathbf{x}_4\}, \{\mathbf{x_4}, \mathbf{x}_1\}\}$, and thus the only possible equilibrium configuration is p_2 coexisting with p_4, and/or p_4 coexisting with p_5.

Suppose at another pressure and temperature (P_1,T_1) the Gibbs Energies are:

1. $G_{P_1,T_1}(p_1) = 90.0$
2. $G_{P_1,T_1}(p_2) = 61.2$

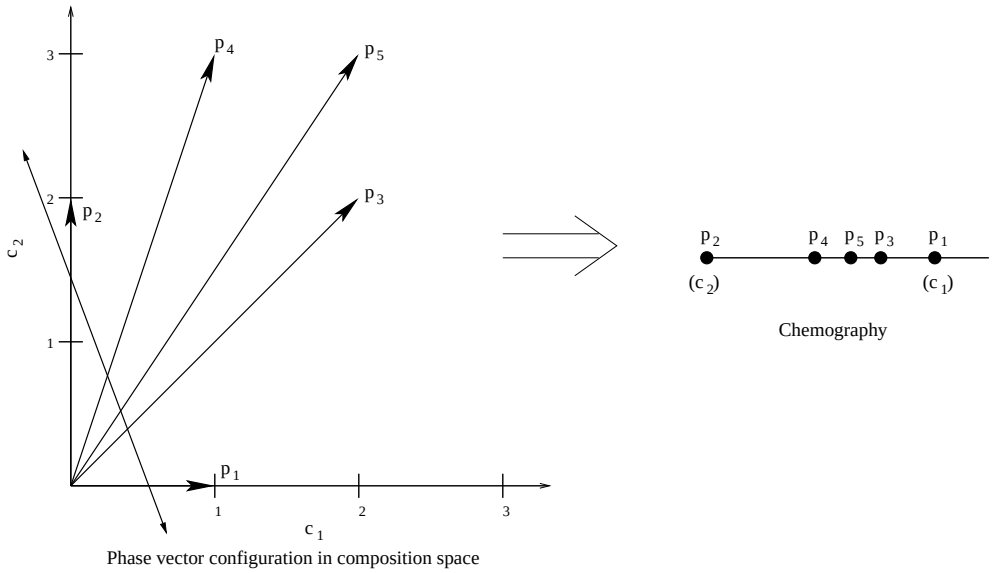

Figure 2.10: Composition space vectors in $\mathbb{R}^2$ representing the phases in example 2.4.1 and the corresponding chemography in $\mathbb{R}^1$.

3. $G_{P_1,T_1}(p_3) = 80.3$
4. $G_{P_1,T_1}(p_4) = 50.1$
5. $G_{P_1,T_1}(p_5) = 55.4$

The lower hull for this pressure and temperature is shown in figure 2.12. Notice that the Gibbs Energy for p_5 has dropped below the line from p_4 to p_1. Now the lower hull corresponds to the triangulation $\mathcal{T}_1 = \{\{\mathbf{x}_2, \mathbf{x}_4\}, \{\mathbf{x}_4, \mathbf{x}_5\}, \{\mathbf{x_5}, \mathbf{x_1}\}\}$. At this pressure and temperature, it is therefore only possible for p_2 and p_4 to coexist, p_4 and p_5 to coexist, and p_5 and p_1 to coexist.

It is important to emphasize that nature only allows the coexistence of phases on the **lower hull** of the lifted chemography and that the triangulation which yields the equilibrium information must therefore be **regular**. If the associated triangulation for the chemography of a reaction system were non-regular, the immediate implication would be that the system has not reached equilibrium. In these cases, nature has not yet completed its minimization of the total Gibbs energy of the system.

All of the triangulations for a point configuration (both regular and non-regular) are completely determined by the respective locations of the points. Therefore, the chemography alone determines all of the possible phase equilibria for a chemical system. In the next few sections, we develop some powerful theory which will allow us to enumerate what these possibilities are.

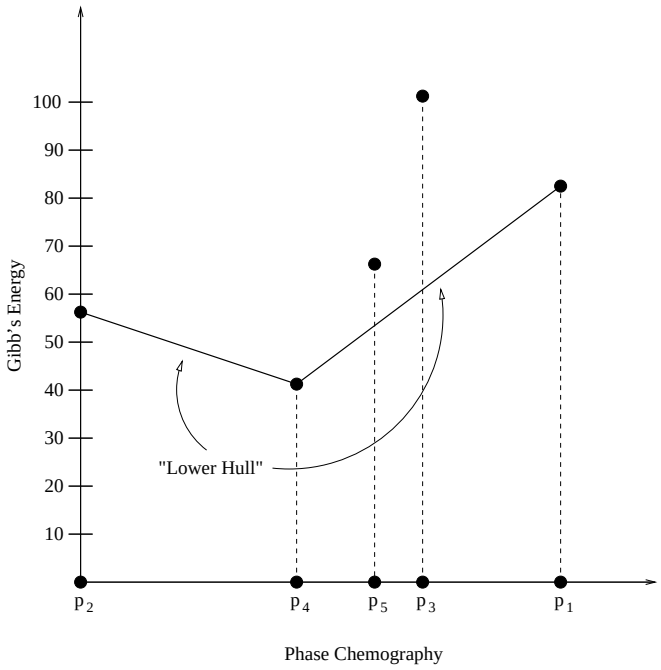

Figure 2.11: The phase chemography lifted by Gibbs Energy values at pressure P_0 and temperature T_0 in example 2.4.1.

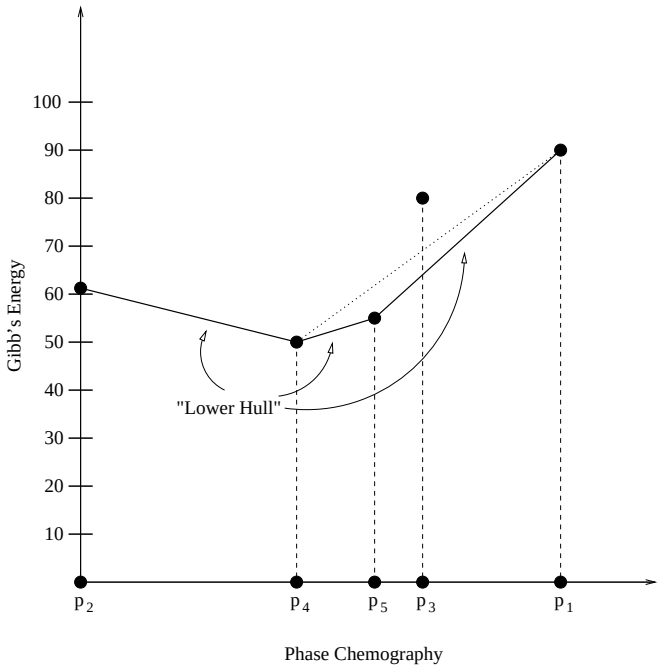

Figure 2.12: The phase chemography lifted by Gibbs Energy values at pressure P_1 and temperature T_1 in example 2.4.1.

2.5 Oriented Matroids

Enumerating all possible triangulations for a set of points $\mathcal{X}$ in $\mathbb{R}^{n-1}$ can be seen as a counting problem. The question we are asking is: What are the possible sets of n-tuples of elements in $\mathcal{X}$ which satisfy the three criteria of a triangulation? This problem has been intensively studied in the last fifty years in the field of combinatorial geometry.

At the lowest level, we are interested in codifying the spatial relationships among points in $\mathbb{R}^{n-1}$. What is needed is a convenient way to describe these relationships. Such a description was initiated by the independent authors, Jon Folkman and Jim Lawrence [6], and Robert G. Bland and Michel Las Vergnas [3] in the 1970s in what is called *oriented matroid* theory. The theory of oriented matroids has grown to be quite extensive in the past few decades. A thorough treatment of the theory is given in Björner, Las Vergnas, Sturmfels, White, and Ziegler [2]. We shall only cover the basics of the theory which will help us to more deeply understand triangulations. Specifically, we will define and explain two dual combinatorial descriptions of a point configuration in terms of *circuits* and *cocircuits*. As we will see later, these descriptions have great chemical significance when applied to systems in composition space.

For $\mathcal{X}$ a set of m points in $\mathbb{R}^n$ with $m \geq n$, recall that the affine dependences consist of all vectors $\mathbf{z} \in \mathbb{R}^m$ $(\mathbf{z} \neq \mathbf{0})$ such that $\mathcal{X}\mathbf{z} = \mathbf{0}$ and $z_1 + \cdots + z_m = 0$. Certainly, if $\mathbf{z}$ is an affine dependence of $\mathcal{X}$, then so is $c\mathbf{z}$ for any $c \neq 0$. For this reason, we *normalize* the dependences so that:

$$\sum_{i \in \mathcal{P}(\mathbf{z})} z_i = -\sum_{i \in \mathcal{N}(\mathbf{z})} z_i = 1,$$

where $\mathcal{P}(\mathbf{z}) = \{i : z_i > 0\}$ and $\mathcal{N}(\mathbf{z}) = \{i : z_i < 0\}$. From our previous discussion of convex hulls, we see that

$$\mathbf{y}_{\mathcal{P}} = \sum_{i \in \mathcal{P}(\mathbf{z})} z_i \mathbf{x_i}$$

is in the convex hull of $\{x_i : i \in \mathcal{P}(\mathbf{z})\}$ and

$$\mathbf{y}_{\mathcal{N}} = \sum_{i \in \mathcal{N}(\mathbf{z})} -z_i \mathbf{x_i}$$

is in the convex hull of $\{x_i : i \in \mathcal{N}(\mathbf{z})\}$. But by the restriction $\mathcal{X}\mathbf{z} = \mathbf{0}$, we must have $\mathbf{y}_{\mathcal{P}} = \mathbf{y}_{\mathcal{N}} = \mathbf{y}$. Geometrically, an affine dependence of $\mathcal{X}$ simply corresponds to two nonempty disjoint subsets $\mathcal{X}_{\mathcal{P}}, \mathcal{X}_{\mathcal{N}} \subset \mathcal{X}$ for which $\text{conv}(\mathcal{X}_{\mathcal{P}}) \cap \text{conv}(\mathcal{X}_{\mathcal{N}}) \neq \emptyset$. A *minimal affine dependence* is defined to be an affine dependence for which every proper subset $\mathcal{S} \subset \mathcal{X}_{\mathcal{P}} \cup \mathcal{X}_{\mathcal{N}}$ is affinely independent. We will write $\mathcal{A}_{\mathcal{X}}$ for the set of minimal affine dependences of a point configuration $\mathcal{X}$. Every affine dependence is a finite sum of minimal affine dependences. Therefore, the set of affine dependencies of $\mathcal{X}$ forms a vector subspace $A_{\mathcal{X}} \subseteq \mathbb{R}^m$ which is spanned by $\mathcal{A}_{\mathcal{X}}$. To help clarify all this, we give an example.

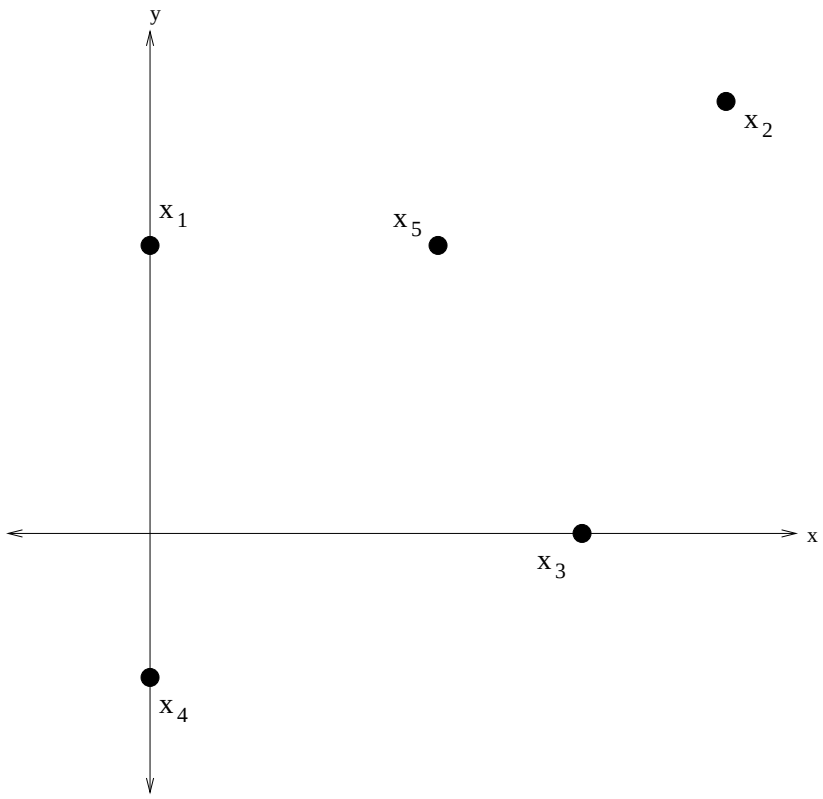

Figure 2.13: The point configuration $\mathcal{X} \subset \mathbb{R}^2$ in example 2.5.1

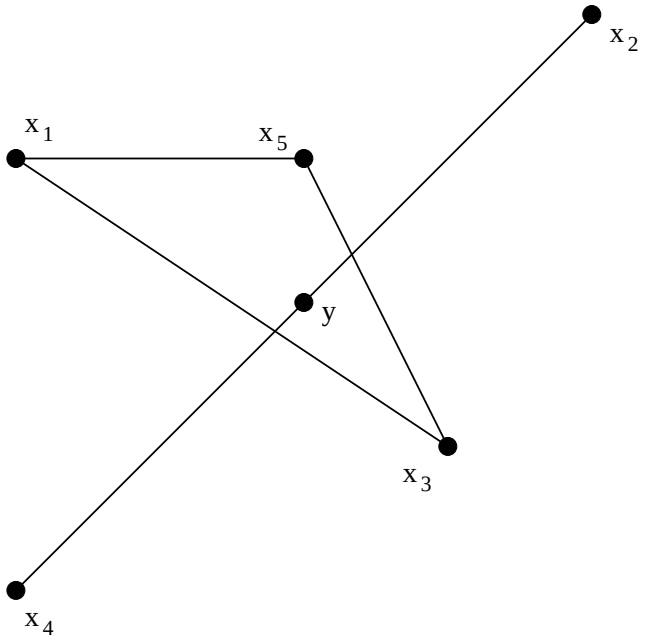

Figure 2.14: The geometric interpretation of the (non-minimal) affine dependence **z** in example 2.5.1.

Example 2.5.1 Let

$$\mathcal{X} = \begin{pmatrix} 0 & 4 & 3 & 0 & 2 \\ 2 & 3 & 0 & -1 & 2 \end{pmatrix}$$

be the point configuration in $\mathbb{R}^2$ shown in figure 2.13. There is an affine dependence given by

$$\mathbf{z} = \begin{pmatrix} \frac{1}{4} \\ -\frac{1}{2} \\ \frac{1}{2} \\ -\frac{1}{2} \\ \frac{1}{4} \end{pmatrix}$$

This particular $\mathbf{z}$ has $\mathcal{X}_\mathcal{P} = \{\mathbf{x}_1, \mathbf{x}_3, \mathbf{x}_5\}$ and $\mathcal{X}_\mathcal{N} = \{\mathbf{x}_2, \mathbf{x}_4\}$. The reader may check that this choice of $\mathbf{z}$ is valid by verifying that $X\mathbf{z} = \mathbf{0}$, $z_1 + z_2 + z_3 + z_4 + z_5 + z_6 = 0$, $z_1 + z_3 + z_5 = 1$, and $-z_2 - z_4 = 1$. We compute $\mathbf{y}$ as defined above to get

$$\mathbf{y} = \mathbf{y}_\mathcal{P} = \mathbf{y}_\mathcal{N} = \begin{pmatrix} 2 \\ 1 \end{pmatrix}$$

The geometric interpretation of $\mathbf{z}$ is shown in figure 2.14. We can see that $\mathbf{z}$ is not a minimal affine dependence since there is a proper subset of $\mathcal{X}_\mathcal{P} \cup \mathcal{X}_\mathcal{N}$ which is not affinely independent. One such subset is $\{\mathbf{x}_1, \mathbf{x}_2, \mathbf{x}_3, \mathbf{x}_4\}$ for which the affine dependence is

$$\mathbf{z}' = \begin{pmatrix} \frac{2}{5} \\ -\frac{9}{20} \\ \frac{3}{5} \\ -\frac{11}{20} \\ 0 \end{pmatrix}$$

This dependence has

$$\mathbf{y} = \mathbf{y}_\mathcal{P} = \mathbf{y}_\mathcal{N} = \begin{pmatrix} \frac{9}{5} \\ \frac{4}{5} \end{pmatrix}$$

We can see that $\mathbf{z}'$ has $\mathcal{X}_\mathcal{P} = \{\mathbf{x}_1, \mathbf{x}_3\}$ and $\mathcal{X}_\mathcal{N} = \{\mathbf{x}_2, \mathbf{x}_4\}$ and that $\mathbf{z}'$ is a minimal affine dependence. Figure 2.15 shows the geometric interpretation of $\mathbf{z}'$.

It is true that $\mathcal{X}$ is completely determined by $\mathcal{A}_\mathcal{X}$ up to an affine coordinate change (see Ziegler [22]). The positions of the points relative to each other, however, can be described in a slightly simpler format called the *circuits* of $\mathcal{X}$. We generate the circuit $\mathbf{c}_i$ of $\mathcal{X}$ by replacing $\mathbf{z}_i \in \mathcal{A}_\mathcal{X}$ by $sign(\mathbf{z}_i) = (sign(z_1), sign(z_2), \ldots, sign(z_m))$, where

$$sign(x) = \begin{cases} 0, & \text{if } x = 0 \\ +, & \text{if } x > 0 \\ -, & \text{if } x < 0 \end{cases}$$

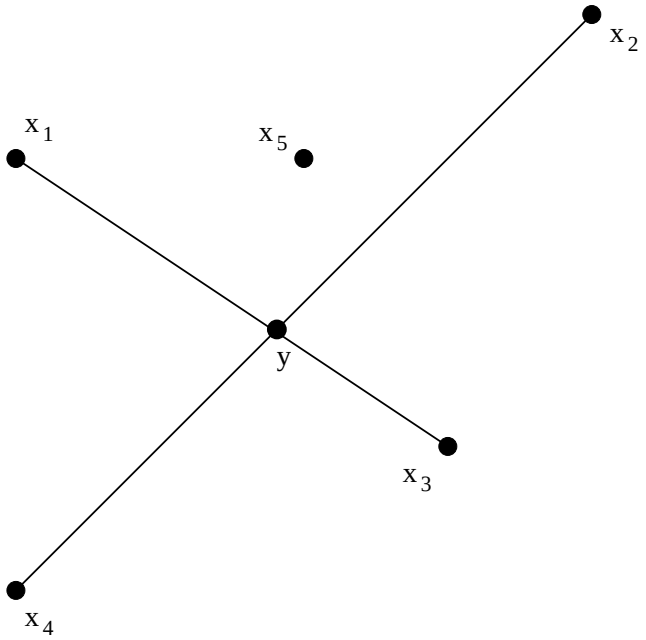

Figure 2.15: The geometric interpretation of the (minimal) affine dependence $\mathbf{z}'$ in example 2.5.1.

We define $-\mathbf{c}_i$ to be $sign(-\mathbf{z}_i)$. The set of circuits of $\mathcal{X}$ is defined as $\mathcal{C}(X) = \{sign(\mathbf{z}) : \mathbf{z} \in \mathcal{A}_\mathcal{X}\}$. For $\mathcal{X}$ in example 2.5.1, there was a minimal affine dependence

$$\mathbf{z}' = \begin{pmatrix} \frac{2}{5} \\ -\frac{9}{20} \\ \frac{3}{5} \\ -\frac{11}{20} \\ 0 \end{pmatrix}$$

which has the corresponding circuit

$$SIGN(\mathbf{z}') = \begin{pmatrix} + \\ - \\ + \\ - \\ 0 \end{pmatrix}.$$

Looking back at our chemical model, we see that the set of mass balance equations is just the set of minimal affine dependencies for the system's chemography. For each $\mathbf{z} \in \mathcal{A}_\mathcal{X}$, the equation

$$\sum_{i \in \mathcal{P}(\mathbf{z})} z_i \mathbf{x_i} = \sum_{i \in \mathcal{N}(\mathbf{z})} -z_i \mathbf{x_i}$$

corresponds to the mass balance equation

$$\sum_{i \in \mathcal{P}(\mathbf{z})} z_i p_i \rightleftharpoons \sum_{i \in \mathcal{N}(\mathbf{z})} z_i p_i.$$

This is intuitive in the sense that mass is balanced whenever the sum of components for the reactant phases is equal to the sum of components for the product phases. The circuits $\mathcal{C}(\mathcal{X})$ simply provide the distinction between left-hand and right-hand sides (via distinction between + and −) for all of the mass balance equations.

There is another combinatorial description for a set of points $\mathcal{X} \in \mathbb{R}^{n-1}$, which is dual to the set of circuits, called the *cocircuits* of $\mathcal{X}$. While the circuits stemmed from affine dependences among the points in $\mathcal{X}$, the cocircuits are generated from affine hyperplanes in $\mathbb{R}^{n-1}$. Recall from section 2.2 that an affine hyperplane H is defined by an affine functional f_H, which maps points $\mathbf{y} \in \mathbb{R}^{n-1}$ to $\mathbf{ay} + b = f_H(\mathbf{y}) \in \mathbb{R}$. If we apply f_H to the set $\mathcal{X}$, we get the row vector $(f_H(\mathbf{x}_1), f_H(\mathbf{x}_2), \ldots, f_H(\mathbf{x}_m)) = (\mathbf{ax}_1 + b, \mathbf{ax}_2 + b, \ldots, \mathbf{ax}_m + b)$. Remember that the sign (+, −, or 0) of $f_H(\mathbf{x})$ relates whether $\mathbf{x}$ lies in H^+, H^-, or H, respectively. We will denote $\mathcal{H}_\mathcal{X}$ to be the set of hyperplanes in $\mathbb{R}^{n-1}$ which are spanned by points in $\mathcal{X}$. That is, $\mathcal{H}_\mathcal{X}$ is the set of all hyperplanes H for which $f_H(\mathbf{x}) = 0$ for at least $n-1$ distinct points in $\mathcal{X}$. We apply this notion to the set of points given in example 2.5.1.

Example 2.5.2 Given the point configuration $\mathcal{X}$ from example 2.5.1, the set $\mathcal{H}_\mathcal{X}$ consists of ten hyperplanes in $\mathbb{R}^2$. Figure 2.16 shows all of the hyperplanes

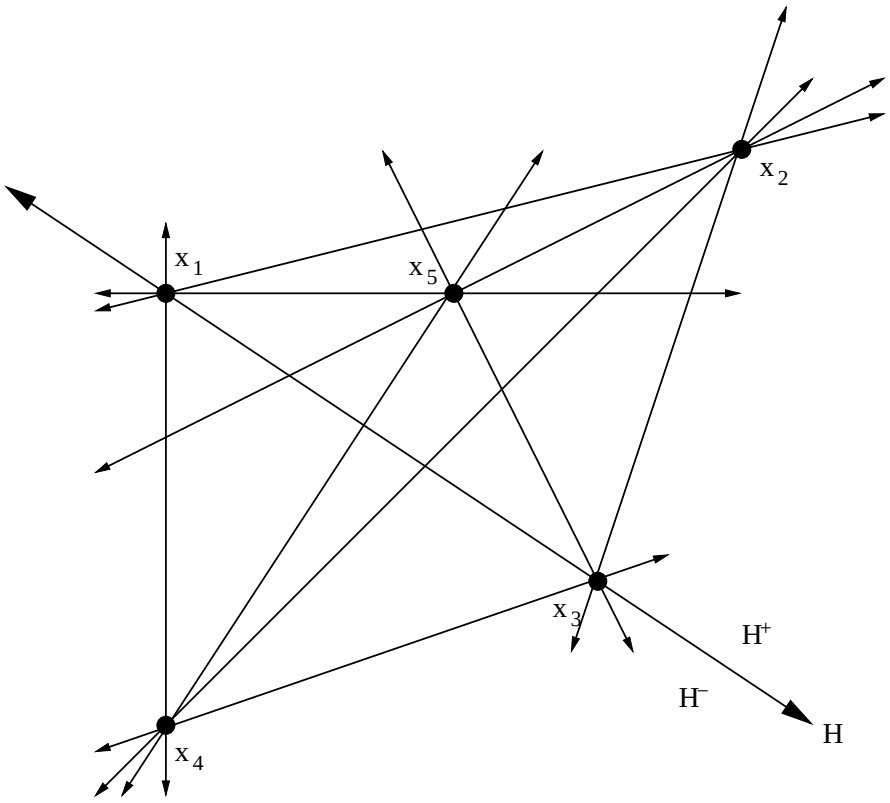

Figure 2.16: All hyperplanes which are spanned by the point configuration $\mathcal{X} \subset \mathbb{R}^2$ from example 2.5.2.

in $\mathcal{H}_\mathcal{X}$ with arbitrarily assigned orientations. Hyperplane $H \in \mathcal{H}_\mathcal{X}$, shown in 2.16, is spanned by $\{\mathbf{x}_1, \mathbf{x}_3\}$ and has the affine functional $f_H(\mathbf{x}) = 2x + 3y - 6$. Applying f_H to $\mathcal{X}$, we get the row vector $(0, 11, 0, -9, 4)$. This implies that $\mathbf{x}_1$ and $\mathbf{x}_3$ lie on H, while $\mathbf{x}_2, \mathbf{x}_5 \in H^+$ and $\mathbf{x}_4 \in H^-$. Figure 2.16 shows this to be true.

Let $sign(f_H(\mathcal{X}))$ be the row vector given by

$$(sign(f_H(\mathbf{x}_1)), sign(f_H(\mathbf{x}_2)), \ldots, sign(f_H(\mathbf{x}_m))).$$

We call $\mathbf{c}_i^*$ =sign$(f_{H_i}(\mathcal{X}))$ a *cocircuit* of $\mathcal{X}$ if $H \in \mathcal{H}_\mathcal{X}$. We then define $-\mathbf{c}_i^*$ to be $sign(-f_{H_i}(\mathcal{X}))$. Thus $\mathbf{c}^* = (0, +, 0, -, +)$ is the cocircuit corresponding to H in example 2.5.2, and $-\mathbf{c}^* = (0, -, 0, +, -)$. The set of cocircuits, written $\mathcal{C}^*(\mathcal{X})$, of a point configuration $\mathcal{X}$ is the set $\{sign(f_H(\mathcal{X})) : H \in \mathcal{H}_\mathcal{X}\}$. It is easy to define the boundary of the convex hull of $\mathcal{X}$ from its set of cocircuits. A point $\mathbf{x}_i \in X$ is on the boundary of the convex hull of $\mathcal{X}$ if and only if there exists a cocircuit $\mathbf{c} \in \mathcal{C}^*(\mathcal{X})$ such that $c_i = 0$ and either $c_j \in \{0, +\}$ for all $j \neq i$ or $c_j \in \{0, -\}$ for all $j \neq i$.

The description of a set of points by its circuits and cocircuits is actually equivalent. In other words, the set of cocircuits for a point configuration is completely determined by its set of circuits and vice versa. Two point sets which have the same set of circuits and cocircuits for some ordering of their members are said to be *oriented matroid equivalent*. Any two point sets which are oriented matroid equivalent have the same set of possible triangulations up to reordering the vertices. It is interesting, however, that while the existence of non-regular triangulations is determined by the oriented matroid, the number and identities of non-regular triangulations may not be the same across oriented matroid equivalent point configurations. As an example, recall the point configuration shown in figure 2.9. Figure 2.17 shows this configuration as well as two more configurations with equivalent oriented matroids under the given point labeling. The triangulations shown are the only non-regular triangulations for each configuration, which means that the first and third configurations have different non-regular triangulations and that both triangulations are non-regular for the second configuration. In the next section, we will explore a construction which will distinguish such configurations. It is a dual configuration which will make the relationship between circuits and cocircuits more apparent, and it will serve as an invaluable tool for enumerating regular triangulations.

2.6 Gale Diagrams

In this section, we will assume $\mathcal{V}$ to be an acyclic vector configuration in $\mathbb{R}^n$. Recall from section 2.2 that $\mathcal{V}$ must satisfy the following:

- $\mathcal{V}$ has no nonnegative dependence: there is no vector $\mathbf{y} \in \mathbb{R}^m$ with $y_i \geq 0$ for all i and $y_i > 0$ for some i, such that $\mathcal{V}\mathbf{y} = \mathbf{0}$.
- There exists some central hyperplane H for which $l_H(\mathbf{v_i}) > 0$ for all i.

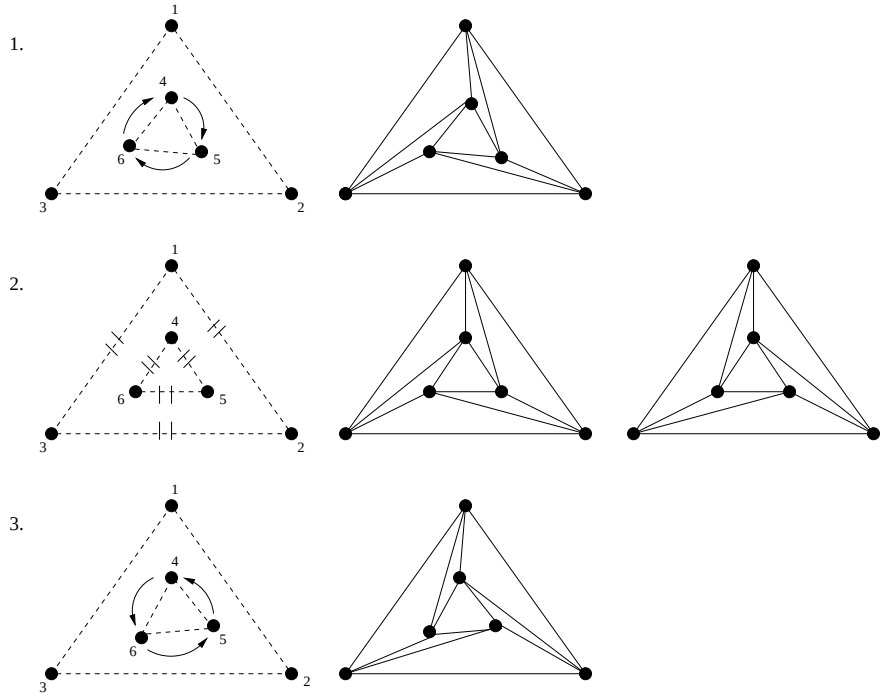

Figure 2.17: Three different point configurations with equivalent oriented matroids. The numbers and identities of the non-regular triangulations are different for each.

Furthermore, let $\mathcal{X}_\mathcal{V}$ be the point configuration obtained from some affine slice of $\mathcal{V}$. For instance, $\mathcal{V}$ might be the phase vectors in composition space for some chemical system with chemography given by $\mathcal{X}_\mathcal{V}$.

Suppose $|\mathcal{V}| = m$. Recall that the vector $\mathbf{t} \in \mathbb{R}^m$ is a linear dependence of $\mathcal{V}$ if $\mathcal{V}\mathbf{t} = \mathbf{0}$. The restriction $\mathcal{V}\mathbf{t} = \mathbf{0}$ sets up a system of n linear equations with m unknowns. Linear algebra tells us that such a system will have $m - n$ linearly independent solution vectors. It follows that the set of all linear dependences of $\mathcal{V}$ forms a linear subspace (which we will call $U_\mathcal{V}$) of $\mathbb{R}^m$ of dimension $m - n$. We note that $U_\mathcal{V} = A_{\mathcal{X}_\mathcal{V}}$. It is true, then, that $U_\mathcal{V}$ is spanned by a set of $m - n$ vectors in $\mathbb{R}^m$. We let $\mathcal{U}_\mathcal{V}$ be such a spanning set for $U_\mathcal{V}$. Then $\mathcal{U}_\mathcal{V}$ has the matrix representation:

$$\mathcal{U}_\mathcal{V} = \begin{pmatrix} u_{11} & u_{21} & \cdots & u_{(m-n)1} \\ u_{12} & u_{22} & \cdots & u_{(m-n)2} \\ \vdots & \vdots & \ddots & \vdots \\ u_{1m} & u_{2m} & \cdots & u_{(m-n)m} \end{pmatrix}$$

for which the transpose is:

$$\mathcal{U}_\mathcal{V}^T = \begin{pmatrix} u_{11} & u_{12} & \cdots & u_{1m} \\ u_{21} & u_{22} & \cdots & u_{2m} \\ \vdots & \vdots & \ddots & \vdots \\ u_{(m-n)1} & u_{(m-n)2} & \cdots & u_{(m-n)m} \end{pmatrix}$$

Let $\mathcal{G}_\mathcal{V}$ be the set of vectors whose expanded matrix form is $\mathcal{U}_\mathcal{V}^T$. Then $\mathcal{G}_\mathcal{V}$ is a set of m vectors in $\mathbb{R}^{m-n}$. The set $\mathcal{G}_\mathcal{V}$ is called the *Gale diagram* of $\mathcal{V}$ and is a dual vector configuration of $\mathcal{V}$. It is important to note that the vectors in the Gale diagram (which we call Gale vectors) always form a totally cyclic configuration. That is, every vector lies in some affine dependence with all positive coefficients. We can still, however, slice the vectors in $\mathcal{G}_\mathcal{V}$ by an affine hyperplane H, provided we negate some of the vectors. Each resulting point is then labeled positive or negative depending on whether the corresponding vector was oriented positively or negatively to intersect the hyperplane. This operation arranges the vectors of $\mathcal{G}_\mathcal{V}$ as points in a subspace of $\mathbb{R}^{m-n}$ of dimension $m - n - 1$. The arrangement, phrased as signed points in $\mathbb{R}^{m-n-1}$, is called the *affine Gale diagram* and we label it $\mathcal{G}_{\mathcal{X}_\mathcal{V}}$. We can compute the set of circuits and cocircuits for $\mathcal{G}_{\mathcal{X}_\mathcal{V}}$ as before, with the slight modification that we invert the signs corresponding to negatively signed points in $\mathcal{G}_{\mathcal{X}_\mathcal{V}}$. We then find that the circuits of $\mathcal{G}_{\mathcal{X}_\mathcal{V}}$ are the cocircuits of $\mathcal{X}_\mathcal{V}$ and the cocircuits of $\mathcal{G}_{\mathcal{X}_\mathcal{V}}$ are the circuits of $\mathcal{X}_\mathcal{V}$. In this way, the two point configurations $\mathcal{X}_\mathcal{V}$ and $\mathcal{G}_{\mathcal{X}_\mathcal{V}}$ are combinatorially linked and considered dual to one another. Notice that this implies the oriented matroid of the affine Gale diagram is completely independent of our choice of a slicing affine hyperplane. We now demonstrate this characteristic of point configurations with an example.

Example 2.6.1 Recall the point configuration from example 2.5.1:

$$\mathcal{X}_\mathcal{V} = \begin{pmatrix} 0 & 4 & 3 & 0 & 2 \\ 2 & 3 & 0 & -1 & 2 \end{pmatrix}$$

We used a computer to generate:

$$\mathcal{C}(\mathcal{X}_\mathcal{V}) = \begin{pmatrix} 0 & + & + & + & + \\ + & 0 & + & - & + \\ - & + & + & + & 0 \\ + & - & 0 & - & + \\ - & - & - & 0 & - \end{pmatrix}$$

and

$$\mathcal{C}^*(\mathcal{X}_\mathcal{V}) = \begin{pmatrix} 0 & + & 0 & - & + \\ + & 0 & - & - & 0 \\ 0 & 0 & + & + & + \\ + & + & 0 & 0 & + \\ + & 0 & - & 0 & + \\ + & 0 & 0 & + & + \\ 0 & + & - & - & 0 \\ + & - & - & 0 & 0 \\ 0 & + & + & 0 & + \\ + & - & 0 & + & 0 \end{pmatrix}$$

We can reverse-construct a set of vectors $\mathcal{V}$ which has an affine slice given by $\mathcal{X}_\mathcal{V}$ by appending a '1' to every column:

$$\mathcal{V} = \begin{pmatrix} 0 & 4 & 3 & 0 & 2 \\ 2 & 3 & 0 & -1 & 2 \\ 1 & 1 & 1 & 1 & 1 \end{pmatrix}.$$

We computed a spanning set for $U_\mathcal{V}$ to get

$$\mathcal{U}_\mathcal{V} = \begin{pmatrix} -\frac{7}{4} & \frac{5}{4} \\ 0 & 1 \\ -\frac{3}{2} & \frac{1}{2} \\ 1 & 0 \\ \frac{9}{4} & -\frac{11}{4} \end{pmatrix}.$$

Taking the transpose gives us the Gale diagram:

$$\mathcal{G}_\mathcal{V} = \begin{pmatrix} -\frac{7}{4} & 0 & -\frac{3}{2} & 1 & \frac{9}{4} \\ \frac{5}{4} & 1 & \frac{1}{2} & 0 & -\frac{11}{4} \end{pmatrix}.$$

The vector configuration $\mathcal{G}_\mathcal{V}$ is shown in figure 2.18, along with a slicing hyperplane H and the resulting affine Gale diagram. In the affine Gale diagram shown, solid dots represent positively signed points, and open dots represent negatively signed points. We can now easily check that every circuit of $\mathcal{X}_\mathcal{V}$ is a cocircuit of $\mathcal{G}_{\mathcal{X}_\mathcal{V}}$ and every cocircuit of $\mathcal{X}_\mathcal{V}$ is a circuit of $\mathcal{G}_{\mathcal{X}_\mathcal{V}}$. For example, the first column of $\mathcal{C}(\mathcal{X}_\mathcal{V})$ translates to the cocircuit $(0, +, -, -, +)$ when we apply the sign assignments of $\mathcal{G}_{\mathcal{X}_\mathcal{V}}$. This means that the hyperplane passing through

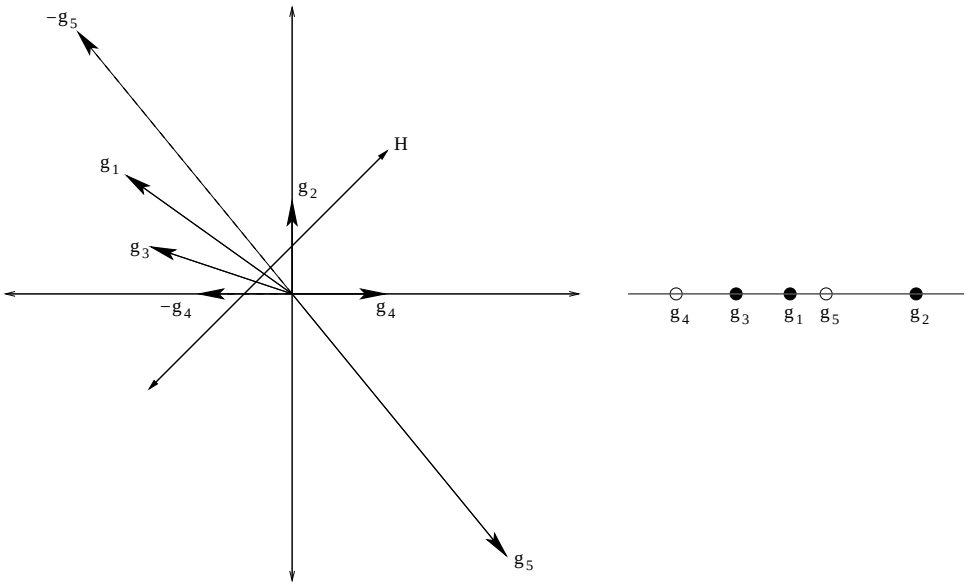

Figure 2.18: (left) The two-dimensional Gale diagram for the vector configuration in example 2.6.1 and a slicing hyperplane H (right). The resulting one-dimensional affine Gale diagram with filled dots representing positively signed points and open dots representing negatively signed points.

$\mathbf{g}_1$ must have $\{\mathbf{g}_2, \mathbf{g}_5\}$ on one side and $\{\mathbf{g}_3, \mathbf{g}_4\}$ on the other side. Figure 2.18 shows this to be true. Similarly, the first row of $\mathcal{C}^*(\mathcal{X}_\mathcal{V})$ translates to the circuit

$$\begin{pmatrix} 0 \\ + \\ 0 \\ + \\ - \end{pmatrix}$$

when we apply the sign assignments of $\mathcal{G}_{\mathcal{X}_\mathcal{V}}$. This means that there must be an affine dependence among $\{\mathbf{g}_2, \mathbf{g}_4, \mathbf{g}_5\}$, for which $(\mathcal{G}_{\mathcal{X}_\mathcal{V}})_\mathcal{P} = \{\mathbf{g}_2, \mathbf{g}_4\}$ and $(\mathcal{G}_{\mathcal{X}_\mathcal{V}})_\mathcal{N} = \{\mathbf{g}_5\}$. The geometric implication is that the segment from $\mathbf{g}_2$ to $\mathbf{g}_4$ intersects $\mathbf{g}_5$. Looking at the affine Gale diagram in figure 2.18, we see that this is true.

It is important to point out that only the combinatorial structure of the Gale diagram corresponding to a point or vector configuration is uniquely determined. Because we only require that $\mathcal{U}_\mathcal{V}$ span $U_\mathcal{V}$, there is an infinite number of coordinatizations of the Gale vectors. In particular, if $\mathbf{u}_i \in \mathcal{U}_\mathcal{V}$, then we can construct $\mathcal{U}_\mathcal{V}^{-i}$ by replacing $\mathbf{u}_i$ by $-\mathbf{u}_i$. Indeed, $\mathcal{U}_\mathcal{V}^{-i}$ spans $U_\mathcal{V}$ as required and yields the alternatively coordinatized Gale diagram $\mathcal{G}_\mathcal{V}^{-i}$. It is easy

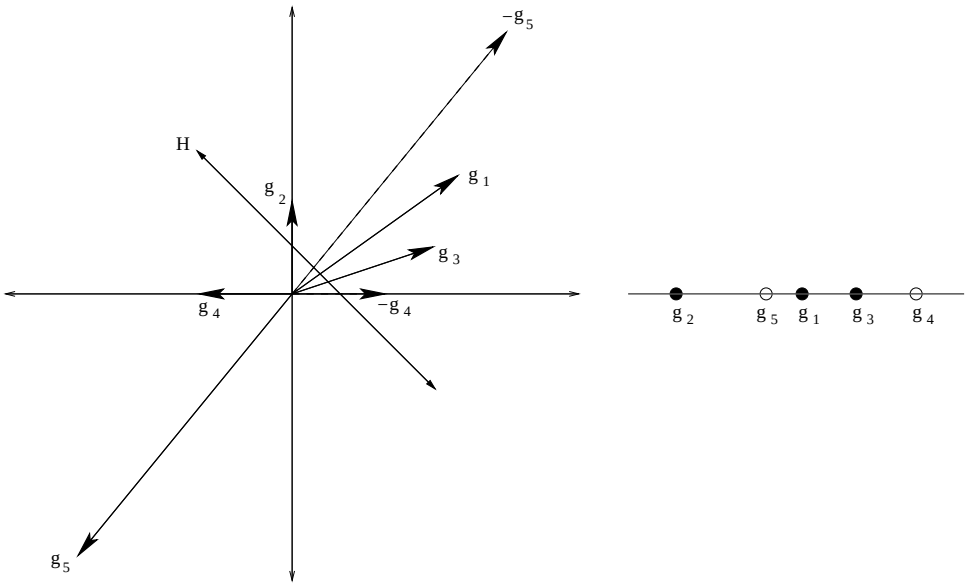

Figure 2.19: (left) An alternative Gale diagram with reversed parities from the one shown in 2.18. (right) The corresponding one-dimensional affine Gale diagram.

to see that every Gale vector $\mathbf{g}_j = (g_{j1}, \ldots, g_{ji}, \ldots, g_{j(m-n)}) \in \mathcal{G}_\mathcal{V}$ maps to $\mathbf{g}_j^{-i} = (g_{j1}, \ldots, -g_{ji}, \ldots, g_{j(m-n)}) \in \mathcal{G}_\mathcal{V}^{-i}$. Thus $\mathcal{G}_\mathcal{V}^{-i}$ is just $\mathcal{G}_\mathcal{V}$ reflected across the hyperplane spanned by $\{\{\mathbf{e}_1, \mathbf{e}_2, \ldots, \mathbf{e}_{m-n}\} \setminus \mathbf{e}_i\}$. The result is a vector configuration whose parities are reversed from the original. In terms of circuits, if $\mathbf{c} \in \mathcal{C}(\mathcal{G}_{\mathcal{X}_\mathcal{V}})$, then $-\mathbf{c} \in \mathcal{C}(\mathcal{G}_{\mathcal{X}_\mathcal{V}}^{-i})$. Similarly, if $\mathbf{c}^* \in \mathcal{C}^*(\mathcal{G}_{\mathcal{X}_\mathcal{V}})$, then $-\mathbf{c}^* \in \mathcal{C}^*(\mathcal{G}_{\mathcal{X}_\mathcal{V}}^{-i})$. Figure 2.19 shows $\mathcal{G}_\mathcal{V}^{-1}$ for $\mathcal{G}_\mathcal{V}$ from example 2.6.1. Also shown is the picture of $\mathcal{G}_{\mathcal{X}_\mathcal{V}}^{-1}$ corresponding to the one for $\mathcal{G}_{\mathcal{X}_\mathcal{V}}$ shown in figure 2.18.

We end this section by explaining the link between the Gale diagram of a vector configuration $\mathcal{V}$ and the regular triangulations of $\mathcal{X}_\mathcal{V}$. To do this, we must introduce a little more terminology. A *polyhedral cone* $\mathcal{W}$ in $\mathbb{R}^n$ is an intersection of halfspaces H_i^+ defined by finitely many linear hyperplanes H_i. A *fan* $\mathcal{F} \subseteq \mathbb{R}^n$ is a set of nonempty polyhedral cones $\mathcal{W}_\mathcal{F}$ which pairwise intersect only along a face of each. We call $\mathcal{F}$ a *complete fan* in $\mathbb{R}^n$ if and only if

$$\bigcup_{\mathcal{W}_i \in \mathcal{F}} \mathcal{W}_i = \mathbb{R}^n.$$

From the vectors in $\mathcal{G}_\mathcal{V}$, we construct what is called the *secondary fan* of $\mathcal{V}$. This is the fan $\mathcal{F}_\mathcal{V}$ consisting of all polyhedral cones which arise as intersections of simplicial cones spanned by vectors in $\mathcal{G}_\mathcal{V}$. We refer to the full-dimensional polyhedral cones of $\mathcal{F}_\mathcal{V}$ as *chambers*. Recall that the vectors in $\mathcal{G}_\mathcal{V}$ are totally cyclic and therefore $\mathcal{F}_\mathcal{V}$ is always a complete fan in $\mathbb{R}^{m-n}$.

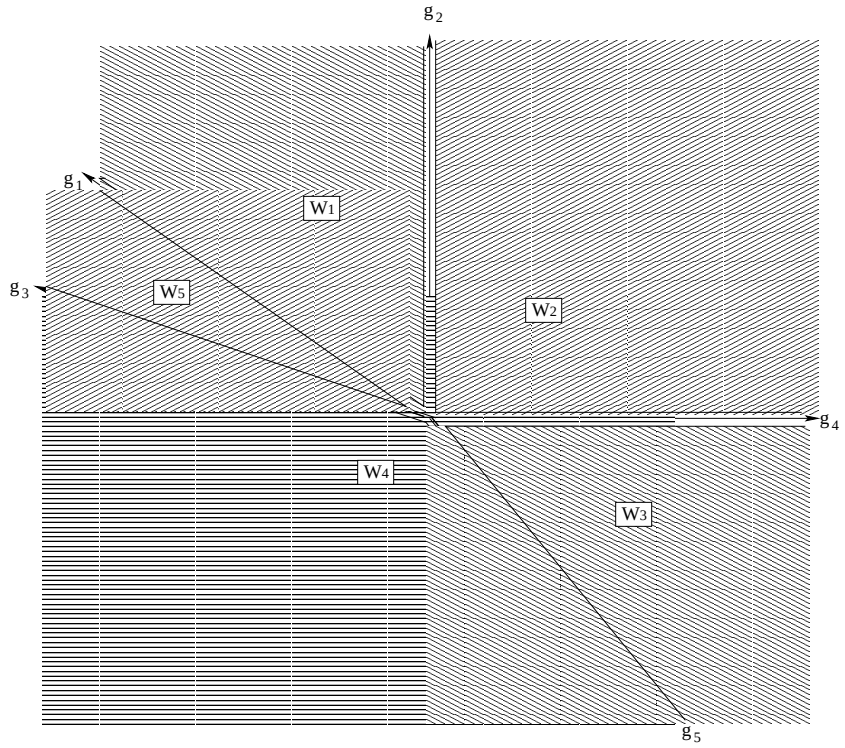

Figure 2.20: The secondary fan $\mathcal{F}_{\mathcal{V}}$ computed from the Gale diagram $\mathcal{G}_{\mathcal{V}}$ in example 2.6.1

We can somewhat easily picture the secondary fan when the number of vectors in $\mathcal{V}$ is only a few more than the number of dimensions. If $m = n$, then the Gale diagram lives and secondary fan live in $\mathbb{R}^0$ as just a single point. For $m = n + 1$, the Gale diagram is always realized by two vectors pointing in opposite directions on the real number line. The secondary fan, in this case, consists of two chambers given by the half-open intervals: $(-\infty, 0]$ and $[0, +\infty)$. When the Gale diagram is two-dimensional (as in example 2.6.1, the chambers of $\mathcal{F}_{\mathcal{V}}$ are just the regions between the Gale vectors. Figure 2.20 shows the five chambers of the secondary fan computed from the Gale diagram from example 2.6.1. The chambers are labeled $\mathcal{W}_1$ through $\mathcal{W}_5$.

When $\mathcal{G}_{\mathcal{V}} \subset \mathbb{R}^3$ (i.e. when $m = n + 3$), the secondary of $\mathcal{V}$ can be visualized by intersecting it with the unit sphere. In this representation, the Gale vectors appear as points on the sphere and the chambers of $\mathcal{F}_{\mathcal{V}}$ appear as polygonal regions. Figure 2.21 shows such a representation of the secondary fan $\mathcal{F}_{\mathcal{V}}$ for $\mathcal{V}$ a set of six vectors in three dimensions, and therefore $\mathcal{X}_{\mathcal{V}}$ a set of six points in two dimensions. The figure consists of two pictures representing top down views of two opposing hemispheres of the unit sphere intersected with $\mathcal{F}_{\mathcal{V}}$.

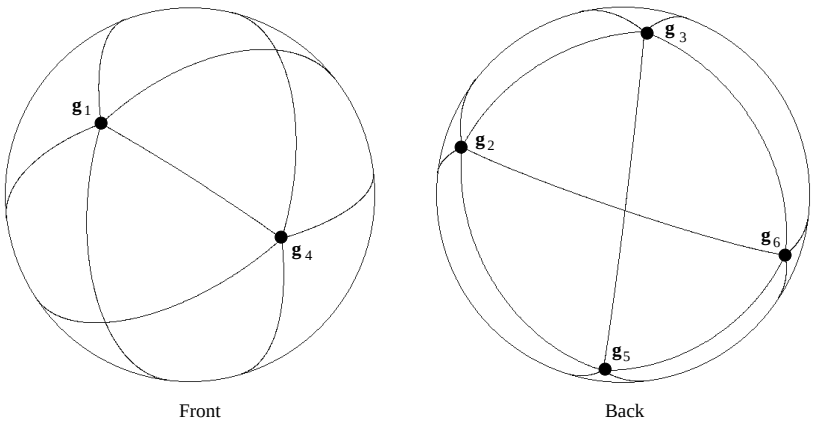

Figure 2.21: A representation of a three dimensional secondary fan for a set of six vectors in $\mathbb{R}^3$. The secondary fan has been intersected with the unit sphere and the two hemispheres are shown. The black dots show where the Gale vectors poke through the sphere.

The secondary fan was introduced by Gelfand, Kapranov, and Zelevinsky [7]. They proved that the chambers of $\mathcal{F}_\mathcal{V}$ are in one-to-one correspondence with the regular triangulations of $\mathcal{X}_\mathcal{V}$. We will not prove this fact, as it is beyond the scope of this paper, but we do give the correspondence. Take $\mathcal{W}$ to be some chamber in $\mathcal{F}_\mathcal{V}$. Then $\mathcal{V}$ has a regular triangulation $\mathcal{T}_\mathcal{W}$ uniquely defined by:

$$\mathcal{T}_\mathcal{W} = \{\{\mathbf{x}_{\sigma_1}, \ldots, \mathbf{x}_{\sigma_{n+1}}\} \subset \mathcal{X}_\mathcal{V} : \mathcal{W} \subset cone(\mathcal{G}_\mathcal{V} \setminus \{\mathbf{g}_{\sigma_1}, \ldots, \mathbf{g}_{\sigma_{n+1}}\})\}$$

In other words, $\sigma = \{\mathbf{x}_{\sigma_1}, \ldots, \mathbf{x}_{\sigma_{n+1}}\}$ is a simplex in $\mathcal{T}_\mathcal{W}$ if and only if $\mathcal{W}$ is contained in the cone spanned by the complement of the Gale vectors $\{\mathbf{g}_{\sigma_1}, \ldots, \mathbf{g}_{\sigma_{n+1}}\}$. Also, since the correspondence is one-to-one, the converse is also true. So if $\mathcal{T}$ is a regular triangulation of $\mathcal{X}_\mathcal{V}$, then there is a chamber $\mathcal{W}_\mathcal{T} \in \mathcal{F}_\mathcal{V}$ such that $\mathcal{W} \subset cone(\mathcal{G}_\mathcal{V} \setminus \{\mathbf{g}_{\sigma_1}, \ldots, \mathbf{g}_{\sigma_{n+1}}\})$ for every simplex $\sigma = \{\mathbf{g}_{\sigma_1}, \ldots, \mathbf{g}_{\sigma_{n+1}}\} \in \mathcal{T}$.

Adjacent chambers of the secondary fan are always divided by a hyperplane which is spanned by vectors in $\mathcal{G}_\mathcal{V}$, and thus correspond geometrically to cocircuits of $\mathcal{G}_{\mathcal{X}_\mathcal{V}}$. By the duality with the point configuration, these boundaries between chambers can be labeled by the circuits of $\mathcal{X}_\mathcal{V}$. The triangulations associated with any two adjacent chambers in $\mathcal{F}_\mathcal{V}$ differ only with respect to the circuit along their boundary. In one triangulation, all pairs of positive elements of the circuit are involved in a simplex, and in neighboring triangulation it is the negative elements. The act of transforming a triangulation into another triangulation by "flipping out" the positive elements of the circuit and "flipping in" the negative elements or vice versa is called a *bistellar operation.* Returning to our example, we illustrate the relationship of the Gale diagram of $\mathcal{V}$ to the triangulations of $\mathcal{X}_\mathcal{V}$.

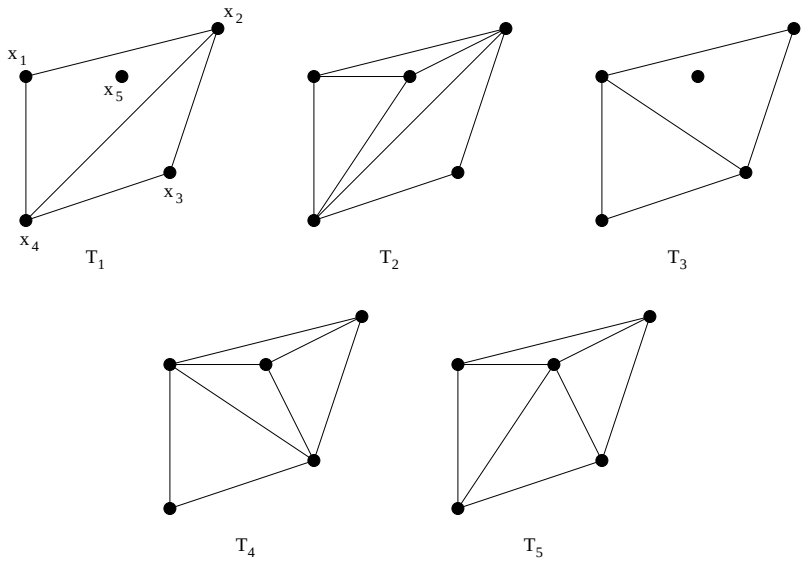

Figure 2.22: All possible triangulations of the point configuration $\mathcal{X}_{\mathcal{V}}$ from example 2.5.1

Example 2.6.2 Recall the point configuration $\mathcal{X}_{\mathcal{V}}$ from example 2.5.1. There are only five possible triangulations for this point set and we show them in figure 2.22. In example 2.6.1 we computed the Gale diagram of $\mathcal{V}$ and showed $\mathcal{F}_{\mathcal{V}}$ in figure 2.20. Beginning with chamber $\mathcal{W}_1$, the sets $\{\mathbf{g}_1, \mathbf{g}_2\}$, $\{\mathbf{g}_1, \mathbf{g}_4\}$, $\{\mathbf{g}_2, \mathbf{g}_3\}$, and $\{\mathbf{g}_3, \mathbf{g}_4\}$ all contain $\mathcal{W}_1$ in their positive cone. We construct $\mathcal{T}_{\mathcal{W}_1}$ by taking the complement of $\mathcal{G}_{\mathcal{V}}$ with each of these sets and then referencing back to $\mathcal{X}_{\mathcal{V}}$ to get

$$\mathcal{T}_{\mathcal{W}_1} = \{\{\mathbf{x}_3, \mathbf{x}_4, \mathbf{x}_5\}, \{\mathbf{x}_2, \mathbf{x}_3, \mathbf{x}_5\}, \{\mathbf{x}_1, \mathbf{x}_4, \mathbf{x}_5\}, \{\mathbf{x}_1, \mathbf{x}_2, \mathbf{x}_5\}\}$$

We can see that $\mathcal{T}_{\mathcal{W}_1}$ is $\mathcal{T}_5$ from figure 2.22. The sets which contain $\mathcal{W}_2$ in their positive cones are: $\{\mathbf{g}_1, \mathbf{g}_4\}$, $\{\mathbf{g}_2, \mathbf{g}_4\}$, $\{\mathbf{g}_2, \mathbf{g}_5\}$, and $\{\mathbf{g}_3, \mathbf{g}_4\}$. Thus,

$$\mathcal{T}_{\mathcal{W}_2} = \{\{\mathbf{x}_2, \mathbf{x}_3, \mathbf{x}_5\}, \{\mathbf{x}_1, \mathbf{x}_3, \mathbf{x}_5\}, \{\mathbf{x}_1, \mathbf{x}_3, \mathbf{x}_4\}, \{\mathbf{x}_1, \mathbf{x}_2, \mathbf{x}_5\}\} = \mathcal{T}_4.$$

The reader may check that $\mathcal{T}_{\mathcal{W}_3} = \mathcal{T}_3$, $\mathcal{T}_{\mathcal{W}_4} = \mathcal{T}_1$, and $\mathcal{T}_{\mathcal{W}_5} = \mathcal{T}_2$.

We further note that chambers $\mathcal{W}_1$ and $\mathcal{W}_2$ border along the Gale vector $\mathbf{g}_2$. Vector $\mathbf{g}_2$ spans a hyperplane which divides the remaining Gale vectors into $\{\mathbf{g}_1, \mathbf{g}_3\}$ (on the side of chamber $\mathcal{W}_1$) and $\{\mathbf{g}_4, \mathbf{g}_5\}$ (on the side of chamber $\mathcal{W}_2$). The implication is that the triangulation associated with $\mathcal{W}_1$ can be transformed into the triangulation associated with $\mathcal{W}_2$ by the bistellar operation which flips *in* the edge from $\mathbf{x}_3$ to $\mathbf{x}_1$ and flips *out* the edge from $\mathbf{x}_4$ to $\mathbf{x}_5$. Looking at the corresponding triangulations $\mathcal{T}_5$ and $\mathcal{T}_4$, respectively, in figure 2.22, we see that this is indeed the case. The curious reader could establish the bistellar operations which link the remaining adjacent chambers.

The Gale diagram constitutes the final link between the geometry of the chemography and the behavior of the system. We describe the relationship in the next section and provide some practical examples of how the theory is applied.

2.7 Determining Phase Diagram Topology

As we have said, the oriented matroid and the Gale diagram give us a full combinatorial description of a set of points in $\mathbb{R}^{n-1}$. Thus, by our chemical model, the oriented matroid yields a full description of the relative positions of phases in the chemography. Included in this is the set of all possible regular triangulations which is in one to one correspondence with the set of all possible stable equilibria for the system. However, just knowing the possible stable equilibria says nothing about the pressure and temperature configurations which yield them. For this information, we need to turn back to the phase diagram and look for its place among the mathematics we have presented.

If $\mathcal{X}_\mathcal{V}$ represents the chemography of a particular reaction system whose phase vectors in composition space are given by $\mathcal{V}$, then the regular triangulations of $\mathcal{X}_\mathcal{V}$ define stable phase equilibria for the system and the circuits of $\mathcal{X}_\mathcal{V}$ are associated with the mass balance equations. We have seen that the circuits of $\mathcal{X}_\mathcal{V}$ correspond to the boundaries between adjacent chambers of $\mathcal{F}_\mathcal{V}$, which themselves represent regular triangulations of $\mathcal{X}_\mathcal{V}$. Substituting the chemistry into this relationship says that mass balance relations exist between two stable equilibria for the reaction system. Indeed, this is consistent with the topology of the phase diagram described in Chapter 1, whereby stable regions border along univariant curves corresponding to some reaction in the system. All that is missing is how the topology of the secondary fan for the chemography, which has the same dimensionality as the Gale diagram, is represented on a two-dimensional phase diagram.

The first non-trivial case is a reaction system with n components and $n+1$ phases. For this system, the phase vectors $\mathcal{V}$ have a Gale diagram $\mathcal{G}_\mathcal{V}$ which is a set of $n+1$ vectors in $\mathbb{R}^1$. There is only one circuit for the point configuration, and the secondary fan consists of just two vectors pointed in opposite directions on the real line. In total, then, there are only two possible triangulations of $\mathcal{X}_\mathcal{V}$. The phase diagram has just a single univariant curve (the one mass balance equation) which divides it into two divariant regions of stable equilibria. This system can only have three different stable equilibria. In one case, the phases on the left hand side of the reaction have a higher Gibbs energy than those on the right and the reaction runs from left to right. In the second case, the right side has higher Gibbs energy than the left, causing the reaction to run right to left. For the third case, the Gibbs energies of both sides are equal and there is no tendency for the reaction to run in either direction. The topology of the phase diagram, in this case, is given uniquely by the secondary fan of $\mathcal{V}$.

When a system has $n+2$ phases, the situation is only a little more complicated. Here, the Gale diagram $\mathcal{G}_\mathcal{V}$ for the chemography is a set of $n+2$ vectors in

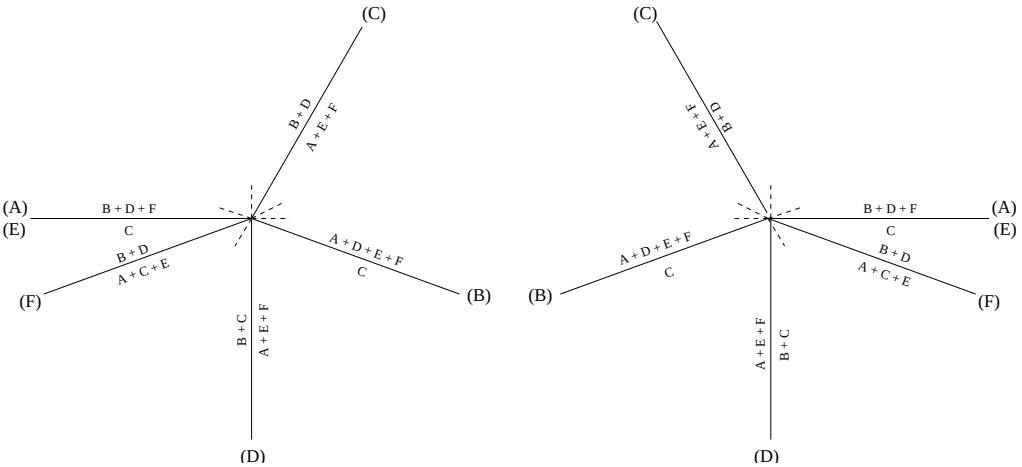

Figure 2.23: The two potential solutions for a particular $n+2$ system.

$\mathbb{R}^2$. In two dimensions, the Gale diagram and the secondary fan look identical. Therefore, in the generic case, the number of chambers in the secondary fan (and therefore the number of regular triangulations), as well as the number of circuits, is $n+2$. On the phase diagram, there is a single invariant point surrounded by $n+2$ univariant reaction curves which separate the $n+2$ stable divariant fields. If the phases are degenerate, the number of regions is potentially less, as some of the Gale vectors may overlap. In $n+2$ systems, the phase diagram topology is represented by an *invariant point map* (see [10]) which looks identical to the Gale diagram itself. However, without thermodynamic data, the handedness of the univariant reaction curves around the invariant point is unknown. Thus there are two possible invariant point maps given by $\mathcal{G}_{\mathcal{V}}$ and $\mathcal{G}_{\mathcal{V}}^{-1}$.

Geologists represent the phase diagram topology much like the Gale diagram and secondary fan for $n+2$ systems. Stable reaction lines (with short, dashed negative extensions), labeled with the phase(s) missing from the reaction in parentheses, intersect at the invariant point. This representation dates back to the work of F. A. H. Schreinemakers almost a century ago which was summarized by Zen in [18]. Figure 2.23 shows the two possible configurations for a system with four components and six phases. This system has a degeneracy exhibited by the reaction $B+D+F \rightleftharpoons C$, from which two phases (A and E) are missing.

The simple ice, water, steam system provides a simple example of an $n+2$ system.

Example 2.7.1 Consider the $n+2$ system with the single component H_2O, and the three phases ice, water, and steam. The phases in composition space are just given by the one dimensional vectors (1), (1), and (1), so our matrix is

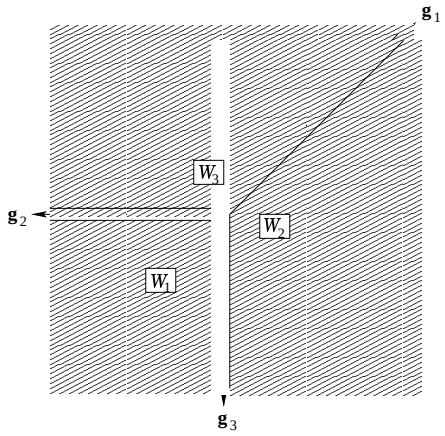

Figure 2.24: The secondary fan for the chemography of the ice-water-steam system.

just $\mathcal{V} = (1, 1, 1)$. A spanning set for the linear dependences of $\mathcal{V}$ is

$$\mathcal{U}_{\mathcal{V}} = \begin{pmatrix} 1 & 1 \\ -1 & 0 \\ 0 & -1 \end{pmatrix}$$

Taking the transpose gives the Gale vectors:

$$\mathcal{G}_{\mathcal{V}} = \begin{pmatrix} 1 & -1 & 0 \\ 1 & 0 & -1 \end{pmatrix}$$

The circuits are given by:

$$\mathcal{C}(\mathcal{X}) = \begin{pmatrix} + & + & 0 \\ - & 0 & + \\ 0 & - & - \end{pmatrix}$$

We can easily see that the circuits correspond to the three mass balance equations (from Chapter 1): $H_2O_{(s)} \rightleftharpoons H_2O_{(l)}$, $H_2O_{(s)} \rightleftharpoons H_2O_{(g)}$, and $H_2O_{(l)} \rightleftharpoons H_2O_{(g)}$. We show the secondary fan in figure 2.24 and the two possible phase diagrams in figure 2.25. We know that the actual phase diagram for this system (given in Chapter 1) has the stable divariant fields of ice, water, and steam in counter-clockwise order. Given this fact, we immediately see that potential solution 2 is the correct solution.

The case of n components and $n + 3$ phases is much more complicated than the preceding two. For systems of this type, the phase chemography is a set of $n + 3$ points in $\mathbb{R}^{n-1}$ and thus the Gale diagram is a set of $n + 3$ vectors in $\mathbb{R}^{n+3-n} = \mathbb{R}^3$. A unit sphere intersects each of these vectors at a stable invariant

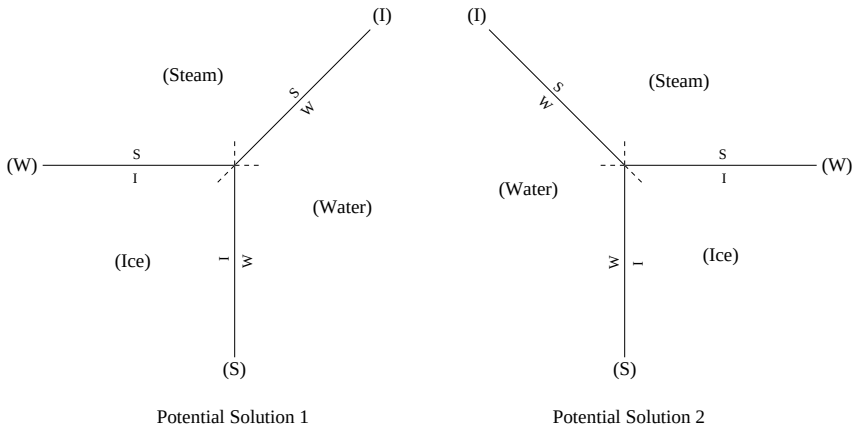

Figure 2.25: The two potential phase diagram solutions for the ice-water-steam system.

point and their negatives at a metastable invariant point. These points and their connecting lines on the unit sphere constitute the closed net from Zen [21].

Of course, the three dimensional secondary fan does not fit inside the two dimensional phase diagram. Empirically, the topology of the true phase diagram corresponds to some *affine* slice of the secondary fan by a two dimensional hyperplane. The Gale vectors intersect the slicing hyperplane as points, the planar boundaries between the chambers of the secondary fan (corresponding to circuits of the phase chemography) intersect the slicing plane as a series of lines, and the chambers themselves (corresponding to triangulations of the phase chemography) map to polygonal regions on the slicing plane. These three intersection types correspond to invariant points, univariant curves, and divariant fields on the phase diagram, respectively. The arrangement that is formed on the slicing plane is a possible description of the topology of the phase diagram. Unfortunately, there are many different slices which yield distinct topologies, and each is equivalent to a potential solution of Mohr and Stout [10]. What we *can* do is enumerate all of the possible arrangements which can be generated in this manner. The diagrams produced by the slicing planes differ by which chambers of the secondary fan are intersected. Ignoring planes which are degenerate with the secondary fan, geologists characterize each slice by the Gale vectors which intersect it. Therefore, we can enumerate all of the topologically different (non-degenerate) slices by counting the number of combinations of Gale vectors which lie on the same side of some affine hyperplane. Note that each of these slices is just a different construction of the affine Gale diagram from section 2.6. Again, the parity of the solution is unknown, and we must therefore consider slices of both $\mathcal{G}_{\mathcal{V}}$ and $\mathcal{G}_{\mathcal{V}}^{-1}$.

There is a convenient combinatorial trick for determining the set of topologically distinct slices. In order to explain it, we must introduce some notation.

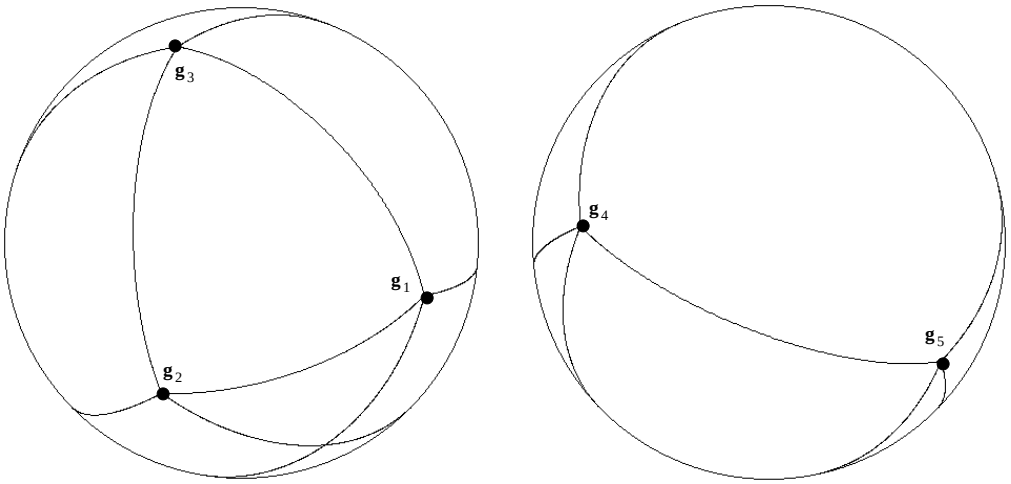

Figure 2.26: Two hemispheres of the unit sphere intersected with the secondary fan for a particular set of five Gale vectors in $\mathbb{R}^3$.

Given any non-zero vector $\mathbf{v}$ we define $H_{\perp\mathbf{v}}$ to be the unique central hyperplane to which $\mathbf{v}$ is normal. In other words, $H_{\perp\mathbf{v}}$ is the hyperplane for which $l_{H_{\perp\mathbf{v}}}(\mathbf{v}) = 0$. Secondly, if H is a central hyperplane and $\mathbf{v}$ is a vector ($\mathbf{v} \notin H$), then $(H + \mathbf{v})$ is the affine hyperplane resulting from the translation of H by one unit in the direction of $\mathbf{v}$. Now, let the Gale vectors for a particular $n+3$ system be given by $\{\mathbf{g}_1, \mathbf{g}_2, \ldots, \mathbf{g}_{n+3}\} \subset \mathbb{R}^3$. The set $\{H_{\perp\mathbf{g}_1}, H_{\perp\mathbf{g}_2}, \ldots, H_{\perp\mathbf{g}_{n+1}}\}$ defines a complete fan $\mathcal{F}_{\perp\mathcal{G}_\mathcal{V}}$ in $\mathbb{R}^3$. We emphasize that this is different from the secondary fan, $\mathcal{F}_\mathcal{V}$! Let $\{\mathcal{W}_1, \mathcal{W}_2, \ldots, \mathcal{W}_k\}$ be the chambers of $\mathcal{F}_{\perp\mathcal{G}_\mathcal{V}}$. Then the following two assertions are true:

(1) If $\mathbf{a}_{i_1}$ and $\mathbf{a}_{i_2}$ are two vectors properly contained in $\mathcal{W}_i$, then the phase diagrams given by affine slices of the secondary fan by the planes $(H_{\perp\mathbf{a}_{i_1}} + \mathbf{a}_{i_1})$ and $(H_{\perp\mathbf{a}_{i_2}} + \mathbf{a}_{i_2})$ are topologically equivalent.

(2) If $\mathbf{a}_i$ and $\mathbf{a}_j$ are two vectors properly contained in $\mathcal{W}_i$ and $\mathcal{W}_j$, respectively $(i \neq j)$, then the affine slices of the secondary fan by the planes $(H_{\perp\mathbf{a}_i} + \mathbf{a}_i)$ and $(H_{\perp\mathbf{a}_j} + \mathbf{a}_j)$ are topologically distinct.

This implies that all of the topological possibilities of the phase diagram are in one to one correspondence with the chambers of $\mathcal{F}_{\perp\mathcal{G}_\mathcal{V}}$. We can easily visualize $\mathcal{F}_{\perp\mathcal{G}_\mathcal{V}}$ by intersecting it with the unit sphere, as was done with the secondary fan. This manner of representation is used by geologists and referred to as the *Euler Sphere* in Kletetschka and Stout [9]. Figure 2.26 shows two opposing hemispheres of a unit sphere intersected with a secondary fan of five vectors in $\mathbb{R}^2$. The Euler Sphere for this configuration has been computed and two opposing hemispheres are shown in figure 2.27. Each hyperplane $H_{\perp\mathbf{g}_i}$ intersects

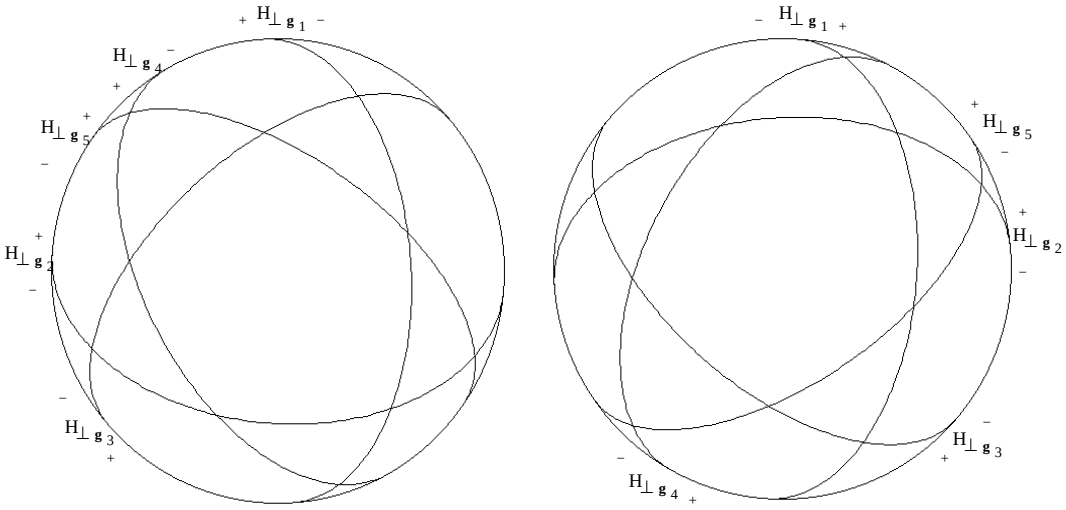

Figure 2.27: Two hemispheres of an Euler Sphere for a particular set of five Gale vectors in $\mathbb{R}^3$.

the sphere along a great circle and each chamber of $\mathcal{F}_{\perp \mathcal{G}_\mathcal{V}}$ maps to a polygon on the sphere. Notice that since each great circle splits the sphere exactly in half, any pair of opposing hemispheres are mirror images of one another.

Each polygonal region on the Euler Sphere corresponds to a chamber of $\mathcal{F}_{\perp \mathcal{G}_\mathcal{V}}$ and thus defines a family of affine hyperplanes whose slicings of the three dimensional Gale vectors (or possibly some of their negative extensions) all yield a topologically equivalent point arrangements. For example, figure 2.28 shows a highlighted region on the Euler Sphere and the resulting slice of the secondary fan from figure 2.26. From each of these regions arises an arrangement of stable and metastable invariant points and stable, metastable, and doubly metastable univariant reaction curves. The invariant points are stable where the Gale vectors poke through with their positive ends, and metastable where the Gale vectors poke through with their negative ends. A univariant reaction curve is stable when it represents a true chamber boundary in the secondary fan which intersects the slicing hyperplane. If the curve represents a true chamber boundary which does not intersect the slicing plane, it is doubly metastable. Curves which run between the positive end of one Gale vector and the negative end of another are metastable. Geologists represent the phase diagram topology for a potential solution in the $n+3$ case with a *straight line net*. In this representations, stable invariant points are drawn as solid black circles and metastable invariant points are drawn as open circles. The invariant points are labeled by the phase missing from all of the incident reactions, surrounded by square brackets. Stable, metastable, and doubly metastable reactions are denoted by solid lines, dashed lines, and dotted lines, respectively. Figure 2.29 shows the

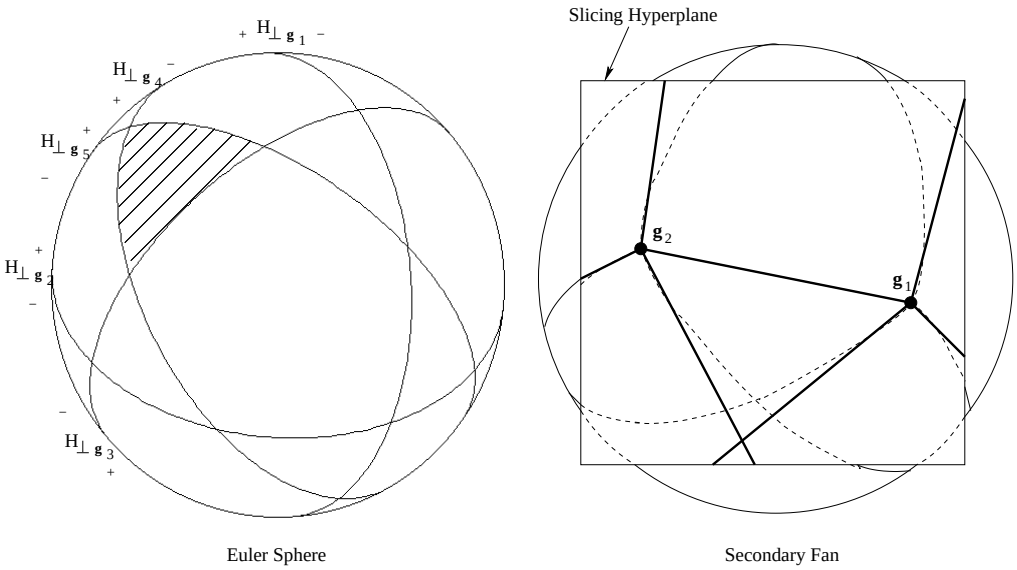

Figure 2.28: The slice of the secondary fan yielded by the highlighted region on the Euler Sphere.

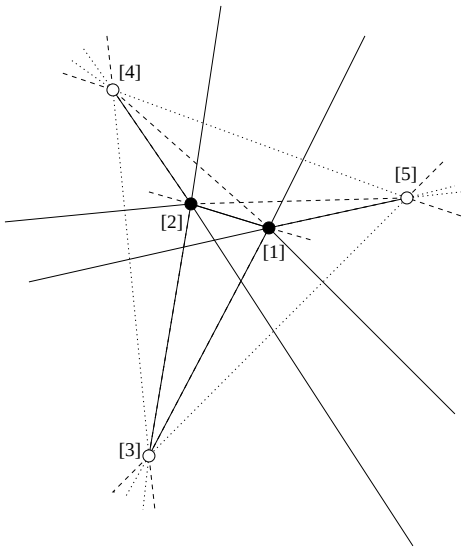

Figure 2.29: The straight line net produced by the highlighted region on the Euler Sphere from figure 2.28.

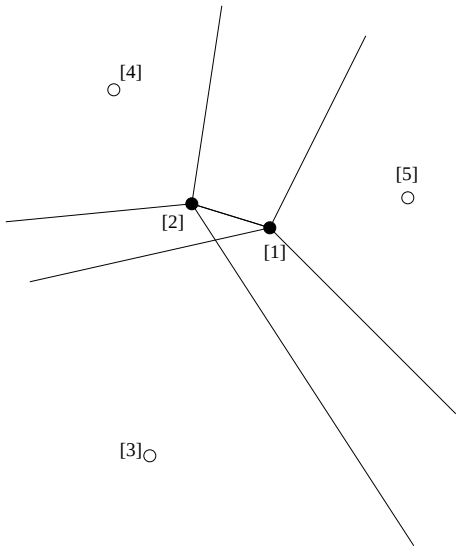

Figure 2.30: The straight line net from figure 2.29 shown with the stable reactions only.

straight line net for the potential solution defined by the Euler Sphere region from figure 2.28. The stable divariant fields correspond to polygonal regions defined by the stable univariant reaction curves. This is consistent with the secondary fan analogy, since each polygonal region is merely the intersection of a chamber with the slicing hyperplane.

If we draw the straight line net without the metastable or doubly metastable reactions, the regions are much more apparent (see figure 2.30). Because of the reflective symmetry between opposing hemispheres on the Euler Sphere, any polygonal region has an identical region on the other side of the sphere. In terms of the slicing hyperplanes given by two diametrically opposite regions, the Gale vectors which are sliced at their positive ends for one are exactly the Gale vectors whose negative ends are sliced for the other, and vice-versa. The result is that the straight line nets generated have inverse stabilities: stable invariant points go to metastable invariant points, stable reaction curves go to doubly metastable reaction curves, and metastable reaction curves remain metastable. Two potential solutions which arise from diametrically opposite regions on the Euler Sphere are called *trivial conjugates* of each other [10]. Figure 2.31 shows the Euler Sphere region opposite the one shown in figure 2.28 and the corresponding slice of the secondary fan. We show the resulting straight line net in figure 2.32.

Similarly, taking corresponding slices of $\mathcal{G}_{\mathcal{V}}$ and $\mathcal{G}_{\mathcal{V}}^{-1}$ yields potential solutions for which the stability of invariant points is the same, but the parity of the arrangement of univariant curves is reversed. Figure 2.33 shows the reversed-

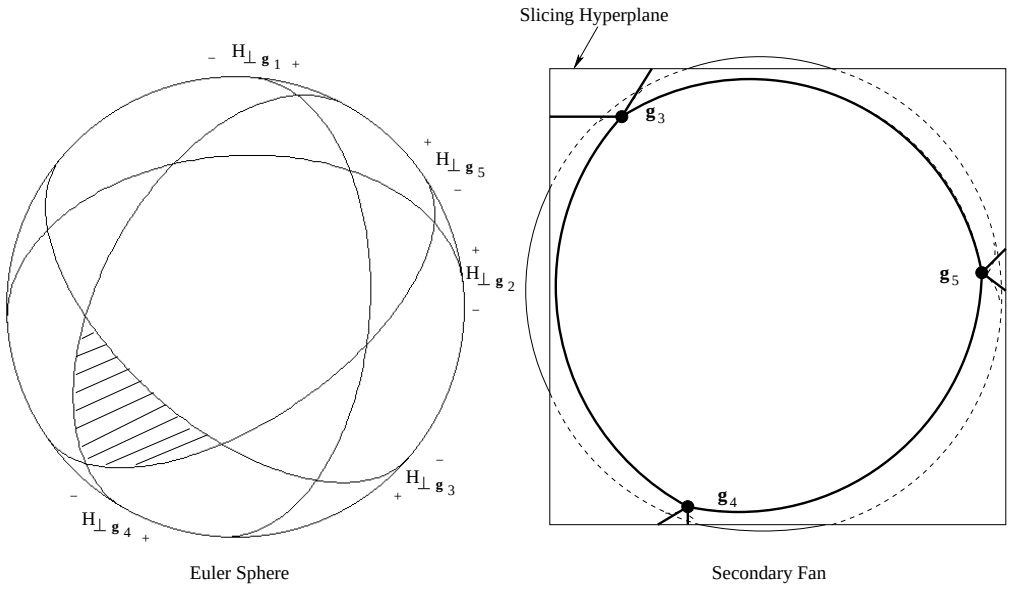

Figure 2.31: The opposite Euler Sphere region from figure 2.28 and the induced slice of the secondary fan.

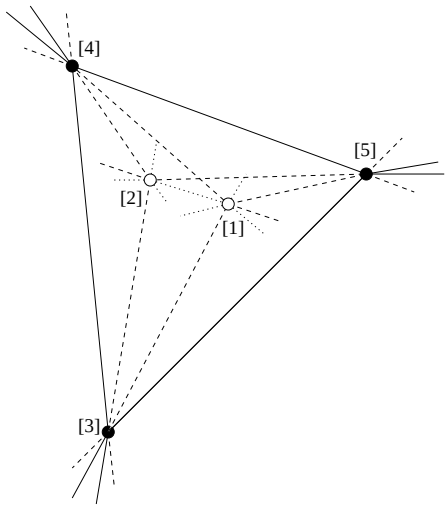

Figure 2.32: The straight line net for the trivial conjugate of the potential solution from 2.29.

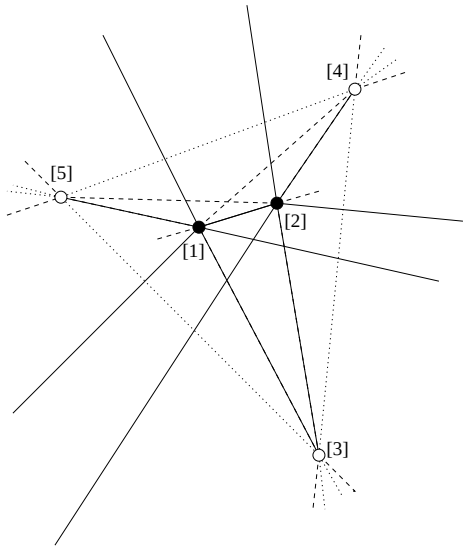

Figure 2.33: The straight line net with reversed parity from the one given in figure 2.29.

parity straight line net of figure 2.29.

We now give an example of the geometrical analysis described above for a well-studied geological system from [9] and given in Chapter 1. Note that we only give potential solutions for one of the two parity choices.

Example 2.7.2 Consider the chemical system with the following six phases: andalusite (Al_2SiO_5), diaspore ($AlO(OH)$), kaolinite ($Al_2Si_2O_5(OH)_4$), pyrophyllite ($Al_2Si_4O_{10}(OH)_2$), quartz (SiO_2), and water (H_2O). This system has three components, given by Al_2O_3, SiO_2, and H_2O. The vectors in the composition space form the following matrix:

$$\mathcal{V} = \begin{pmatrix} 1 & \frac{1}{2} & 1 & 1 & 0 & 0 \\ 1 & 0 & 2 & 4 & 1 & 0 \\ 0 & \frac{1}{2} & 2 & 1 & 0 & 1 \end{pmatrix}$$

The chemography for the system is the set of points in $\mathbb{R}^2$, shown in figure 2.34. Notice the degeneracy among the phases quartz (Q), pyrophyllite (P), and diaspore (D). The circuits for the chemography are:

$$\mathcal{C}(\mathcal{X}_\mathcal{V}) = \begin{pmatrix} 0 & 0 & 0 & 0 & + & + & + & + & - & - & - & + & - \\ + & + & + & 0 & 0 & 0 & 0 & 0 & + & + & + & - & + \\ - & 0 & - & + & - & + & + & 0 & 0 & 0 & - & 0 & - \\ 0 & - & + & - & 0 & - & - & - & 0 & + & 0 & - & + \\ + & + & 0 & + & + & + & 0 & + & + & 0 & + & 0 & 0 \\ + & 0 & + & - & + & 0 & + & + & - & - & 0 & + & 0 \end{pmatrix},$$

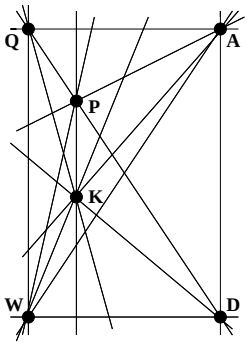

Figure 2.34: Two dimensional chemography for the system in example 2.7.2 with phases andalusite (A), diaspore (D), kaolinite (K), pyrophyllite (P), quartz (Q), and water (W). The arrangement is degenerate, as the three phases (Q), (P), and (D) are collinear.

which correspond, column-wise, to the mass balance equations:

(1) $2HAlO_2 + 2SiO_2 + H_2O \rightleftharpoons Al_2Si_2O_5(OH)_4$

(2) $2HAlO_2 + 4SiO_2 \rightleftharpoons Al_2Si_4O_{10}(OH)_2$

(3) $2HAlO_2 + Al_2Si_4O_{10}(OH)_2 + 2H_2O \rightleftharpoons 2Al_2Si_2O_5(OH)_4$

(4) $Al_2Si_2O_5(OH)_4 + 2SiO_2 \rightleftharpoons Al_2Si_4O_{10}(OH)_2 + H_2O$

(5) $Al_2SiO_5 + SiO_2 + 2H_2O \rightleftharpoons Al_2Si_2O_5(OH)_4$

(6) $Al_2SiO_5 + Al_2Si_2O_5(OH)_4 + 5SiO_2 \rightleftharpoons 2Al_2Si_4O_{10}(OH)_2$

(7) $2Al_2SiO_5 + Al_2Si_4O_{10}(OH)_2 + 5H_2O \rightleftharpoons 3Al_2Si_2O_5(OH)_4$

(8) $Al_2SiO_5 + 3SiO_2 + H_2O \rightleftharpoons Al_2Si_4O_{10}(OH)_2$

(9) $2HAlO_2 + SiO_2 \rightleftharpoons Al_2SiO_5 + H_2O$

(10) $6HAlO_2 + Al_2Si_4O_{10}(OH)_2 \rightleftharpoons 4Al_2SiO_5 + 4H_2O$

(11) $4HAlO_2 + 3SiO_2 \rightleftharpoons Al_2SiO_5 + Al_2Si_2O_5(OH)_4$

(12) $2Al_2SiO_5 + 3H_2O \rightleftharpoons 2HAlO_2 + Al_2Si_2O_5(OH)_4$

(13) $10HAlO_2 + 3Al_2Si_4O_{10}(OH)_2 \rightleftharpoons 4Al_2SiO_5 + 4Al_2Si_2O_5(OH)_4$

The Gale diagram is given by the vectors:

$$\mathcal{G}_{\mathcal{V}} = \begin{pmatrix} 1 & -2 & 0 & 0 & -1 & 1 \\ 1 & -4 & 1 & 0 & -3 & 0 \\ 0 & -2 & 0 & 1 & -4 & 0 \end{pmatrix}$$

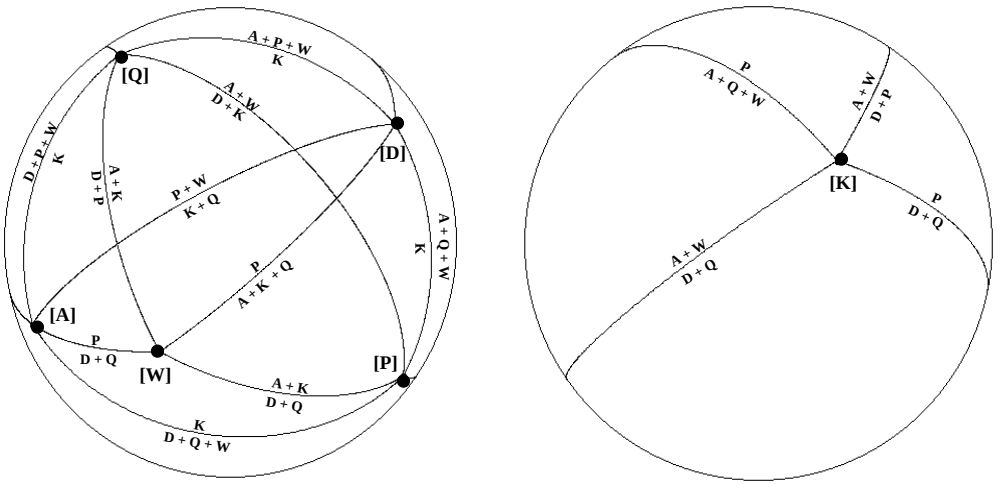

Figure 2.35: Two hemispheres of the unit sphere intersected with the secondary fan for the system in example 2.7.2. Gale vectors are labeled as invariant points with the missing phase in square brackets. The region borders are labeled according to the phases in its associated mass balance equation.

In figure 2.35, we show two opposite hemispheres of the unit sphere intersected with the secondary fan for the chemography. The Gale vectors represent invariant points labeled by the missing phase and each region border is labeled by the phases of the mass balance equation of the associated circuit. Mohr and Stout showed in [9] that the Euler Sphere for this system consists of 30 polygonal regions and so there are 30 potential solutions for the system. The reader should be aware that in the case where the phases are in general position, the Euler Sphere has 32 polygonal regions. One hemisphere of the Euler Sphere for this degenerate system is shown in figure 2.36 with the associated configuration of stable and metastable invariant points drawn for each region. Note that in terms of the invariant points, the degeneracy of the system is exhibited by the reaction which is missing the three phases A, K, and W.

So far, we have only discussed how to generate possible phase diagrams for systems with $n+3$ or fewer phases. In fact, systems with $n+4$ or more phases are not yet completely understood. There is not a way in which to enumerate the possible topologies for phase diagrams in such systems. This is a very big open problem in thermochemistry and may stretch the limits of current enumeration techniques.

In the next chapter, we give user instructions for a Java applet called `CHEMOGALE`, which computes and displays the possible phase diagram topologies in the manner described above for systems of $n+2$ and $n+3$ phases. We recognize that systems of $n+4$ or more phases are not exempt from chemical consideration, so

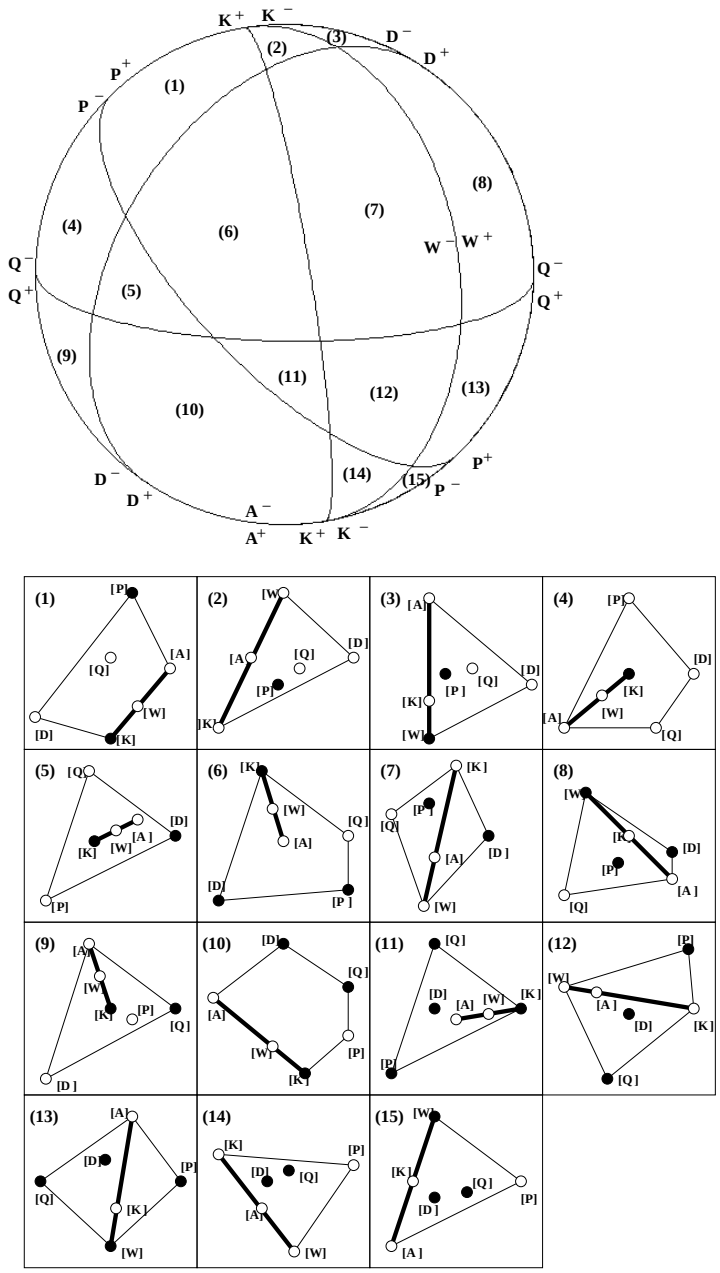

Figure 2.36: One hemisphere of the Euler Sphere for the system in example 2.7.2. The regions are labeled 1 through 15 and the invariant point configuration corresponding to each visible region is given in the boxes. The collinearity among the invariant points with missing phases A, K, and W is denoted by a thick line between the points.

in these cases we offer the list of all possible triangulations (divariant equilibria) and the set of mass balance equations without a graphical interface.

Chapter 3

In this chapter, we give complete user instructions for a computer program called CHEMOGALE. Similar information may be found on the introductory web-pages for CHEMOGALE at http://www.math.umn.edu/~reiner/CHEMOGALE.html. For a user-input chemical system, the program computes the chemical information described in the previous chapter based on the phase vectors in composition space. When the Gale diagram lives in viewable two and three dimensions (i.e. when the system input has n components and $n+2$ or $n+3$ phases), the output is displayed with a graphical user interface for ease of data analysis. When graphic output is not possible (i.e. when the Gale diagram has dimension greater than three), the program provides text information including the list of mass balance equations and all possible triangulations (divariant equilibria). The program is limited to systems with number of components, $2 \leq n \leq 6$, and number of phases $n+1 \leq p \leq 8$. CHEMOGALE will handle most degenerate systems unambiguously. However, we assert the following disclaimer:

> **NOTE:** As with most freely available software, there is no guarantee that the program is totally bug-free. Also, degeneracies in a system may cause some errors due to the computer's limited level of numerical precision.

We advise that the user verify the program's output whenever possible. The introductory web page contains the email address to which you may submit detailed bug reports, including specific information about the input system.

3.1 Preliminaries

CHEMOGALE was written as a Java applet for easiest remote usability. As with all applets, it is required that the user's web browser understand Java. To use this program, the user must have a browser which supports Java 1.1 or higher. Many of the images shown in this chapter are screen-grabs of CHEMOGALE run in Netscape Navigator 4.7. We recommend running the program with either Microsoft Internet Explorer (version 5.0 or later) or Netscape Navigator (version 4.7 or later). To download either of these for free, the reader is referred to either of

`http://cgi.netscape.com/cgi-bin/upgrade.cgi`

`http://www.microsoft.com/downloads`.

NOTE: If you are installing `Netscape Navigator`, be sure that the installation includes Java support. For this, you may have to select **custom installation**.

Once you have a Java enabled browser, you can launch access `CHEMOGALE` by going to `http://www.math.umn.edu/~reiner/CHEMOGALE.html`. Clicking **Enter** from the lead-in page should bring up the introduction page. From here, we provide a brief outline of the program's features as well as a guided tour of `CHEMOGALE` in addition to the program itself. If possible, we recommend running the program as you read this text. To begin the program from the introduction page, click on the link **Start CHEMOGALE** at the bottom of the page. If the program does not load properly, it is most likely that your browser is not properly configured.

Before getting on with the tutorial we make one further note to `Netscape` users. For some `Netscape` browsers, the command to resize the browser window may cause Java applets to restart. This is especially annoying if you have completed the user input portion and the applet restarts when you resize the window to view the output.

NOTE: Resizing a `Netscape` browser window may restart the applet. If you are using a `Netscape` browser, you should not attempt to resize the browser window after proceeding from the first screen.

The program's output should fit into the default size for most browser windows. We make the point, however, that too big is always better than too small.

3.2 User Input

The first three screens of the program prompt the user for input about the chemical system. Screen one is shown in figure 3.1 and contains fields in which to enter the number of components and the number of phases. As mentioned earlier, the program is limited to systems in which the number of components is at least two and at most six. Note that the components must be independent, i.e., there can be no linear dependences among them. Also the number of phases must be at least one more than the number of components and no more than eight altogether. After entering the appropriate numbers of components and phases for a system, the **Continue** button proceeds to the second screen.

Figure 3.2 shows the second screen, in which the user must enter the names of the components and phases of the system. The example shown happens to be for a system with three components and six phases. To avoid cluttering in the forthcoming screens, the phase names will be truncated to be at most two letters long. The user should only enter one or two meaningful letters for each phase. On this page (and all pages to follow) there is a **Previous** button which

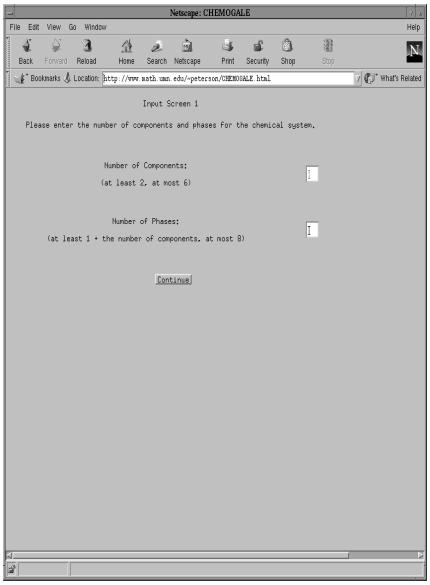

Figure 3.1: The first input screen of CHEMOGALE, with fields for the numbers of components and phases of the system.

allows the user to go back to the previous screen. If erroneous data was entered in a previous screen, clicking the **Previous** button allows the user to change prior fields.

> **NOTE:** DO NOT use the browser's **Back** button to return to a previous screen. Doing so will exit `CHEMOGALE`. Instead, always use the **Previous** or **New Input** button (described later).

After the names of all system components and phases, click **Continue** to proceed.

The third screen asks the user to input the relative amounts of each component for every phase. In other words, the user should enter the coordinates of the phase vectors in composition space. Typically, the input coordinates for a mineral are the mass balance coefficients in moles of the oxides chosen as components. Figure 3.3 shows what the third screen looks like for a system of three components and six phases. The fields are set up so that each row corresponds to the phase shown on the far left, and each column corresponds to the component shown at the top. For each phase, the user should fill in the columns according to the amounts of the corresponding components. Fields which are left empty are assumed to be zero. To insure the maximum amount of precision, all values must be input as integers or rationals. Rationals are represented by an integer numerator, followed immediately by a slash symbol "/", and then an integer denominator - with no spaces in between. So the fraction one-half is

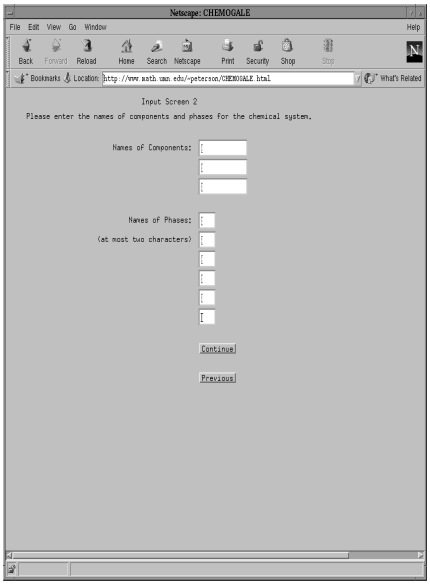

Figure 3.2: The second input screen of CHEMOGALE for a system of three components and six phases, with fields for the names of the system's components and phases.

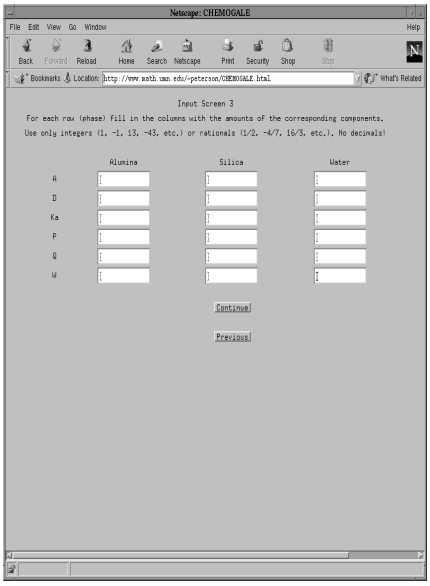

Figure 3.3: The third input screen of CHEMOGALE for a system of three components and six phases, with fields for the names of the phase vector coordinates in composition space.

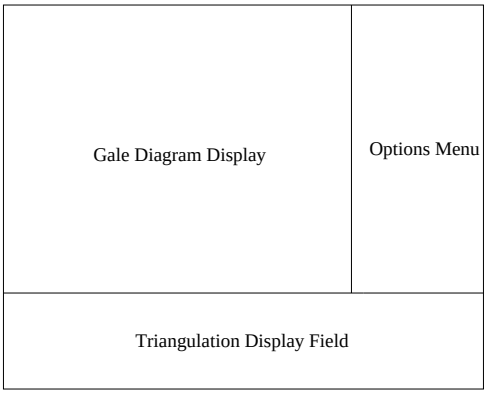

Figure 3.4: The main display screen layout for $n + 2$ or $n + 3$ systems.

represented by "1/2" and not "1 / 2." The program automatically restricts the size of any integer to a maximum of 999,999 in absolute value. If zero is ever entered as a denominator, the program will output an error message and the user will not be able to continue until it has been changed. Once all of the coordinates have been entered, the user input portion is complete. The next screen displays the computed output for the system. For a system with n components and $n + q$ phases, the program will display the output in one of three modes, depending on q. The three modes correspond to the cases $q = 2$, $q = 3$, and $q = 1$ or $q > 3$. Before discussing the specifics of each mode, we briefly outline the generalized output environment.

3.3 The Output Environment

Among the three output modes of the program, there are some global features which we now discuss. Upon clicking **Continue** from the third input screen, the program computes all relevant information for the given system. When the number of components and/or phases of the system is high, the calculations become somewhat intensive and the program may take up to a few minutes to prepare the output. Because of the restrictions we have placed on the size of the system, however, the computation time should never exceed five minutes (depending on the speed of transmission). Once the computations are completed, the main display screen will appear. When $q = 2$ or $q = 3$, the main display screen consists of a graphical representation of the Gale diagram and secondary fan, a text-based triangulation display field, and a menu of option buttons. Figure 3.4 shows the layout of the main display screen for such systems. For systems with $q = 1$ or $q > 3$, the main display screen consists solely of a set of menu of option buttons, as shown in figure 3.5. The main display screen will remain in the browser window until the user wishes to input a new system. Each

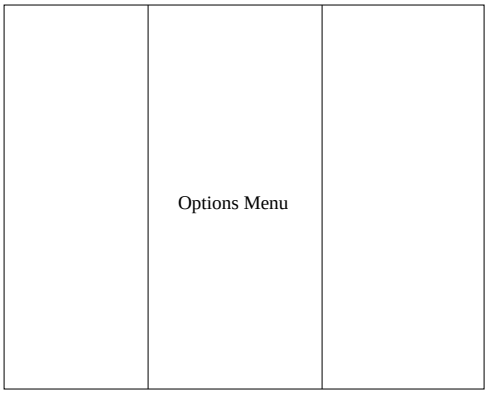

Figure 3.5: The main display screen layout for $n + q$ systems with $q = 1$ or $q > 3$.

output mode has an option button labeled **New Input**. Selecting this will exit the main display screen and recall the third user-input screen. From here, the user may correct erroneously entered phase coordinates or change options from an earlier input screen by clicking the **Previous** button.

Additional information about an input system is displayed at the user's request in *pop-up windows*. Pop-up windows are just additional display windows which are independent from the main browser window. They may be re-sized, minimized, moved, etc., without affecting other windows. Each pop-up window has its own menu bar at the top. The menu options vary depending on the content of the window. Every pop-up window, however, has a **Close** command under **File** in the menu bar.

> **NOTE:** Closing a pop-up window should only be done using the **Close** command under the **File** menu on the window's menu bar. Other system-dependent means of window disposal may be destructive to the applet and/or browser session itself.

It is possible to have any number of pop-up windows open at one time. However, all pop-up windows will be closed automatically when **New Input** is selected.

There are two pop-up windows which are accessible in all three display modes. The first one we describe contains all of the possible triangulations of the input chemography and can be opened by selecting **All Triangulations** from the options menu on the main display screen. The triangulations are numbered $T1, T2$, etc., and described by their sets of simplices. Each simplex, in turn, is described by the set of phases $\{p_{\sigma_1}, \ldots, p_{\sigma_n}\}$ which make up the corresponding divariant assemblage. Non-regular triangulations are denoted by a "*." For systems with $q = 3$, the window contains the menu item **Select Region**, which we discuss later. Figure 3.6 shows the triangulations pop-up window for a sample system.

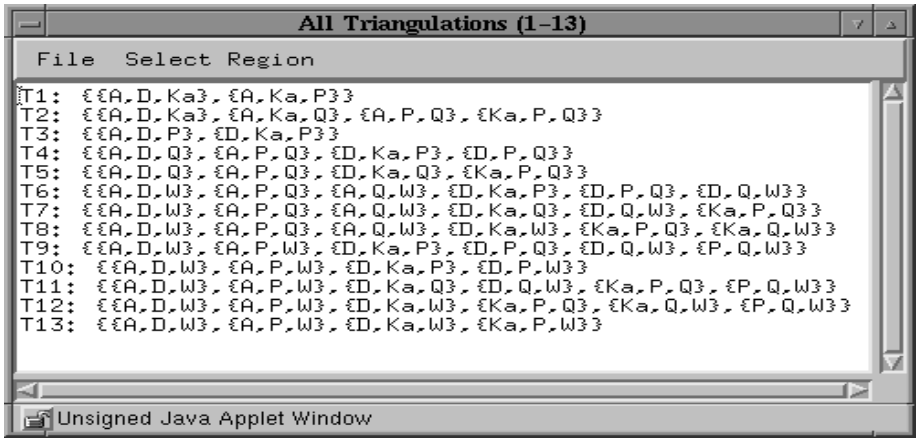

Figure 3.6: The pop-up window containing all possible triangulations for a particular system.

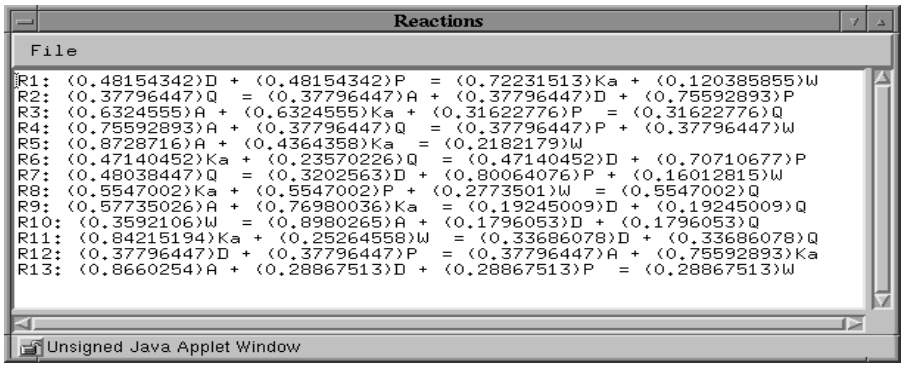

Figure 3.7: The pop-up window containing all of the mass balance equations for a particular system.

Another window common to the three modes is displayed by clicking **Display Reactions** from the options menu on the main display screen. This window gives the set of all mass balance equations and approximate coefficients for the input system. The reactions are numbered $R1, R2$, etc., and consist of a left and right hand set of phases separated by a "=" sign. The reactions window for a sample system is shown if figure 3.7.

In the two graphic modes, the user may view a list of warning messages by clicking the **Display Warnings** button. These warnings inform the user of any degeneracies or irregularities detected for the system. For instance, if two Gale vectors are coincident on a line in an $n+3$ system, the straight line nets of the potential solutions may be inaccurate. The user is always encouraged to verify any degeneracies when they come up, and so the program will notify the user with a pop-up window when warnings exist.

It is possible for the user to capture information from the main display screen or any additional information window. Any data which appears as text in a white text field can be cut and pasted into almost any word processing program, such as `Notepad`, `Microsoft Word`, `Emacs`, etc, by highlighting the text and performing the cut and paste key commands for the particular operating system. As for printing and saving graphics, many browsers have such capabilities but the results are not always predictable. For this reason, we recommend saving all graphical information using a suitable screen capture software. Most systems have a built-in screen capture utility. For example, in the `Windows` operating system, the key sequence alt-printscreen will put the image from the current window onto the clipboard where it may be then pasted into any graphics manipulation software or printed directly. For `Macintosh` users, the key sequence `Apple-Shift-4` will provide a cursor which will enclose any area of interest as simple text for printing. If you are unsure how to use the screen capture utility for your system, we recommend the following informative web sites:

`http://www.lanl.gov/orgs/cic/cic6/bits/97august/Dale_images.html`,

`http://hale.pepperdine.edu/ capratt/index.html`,

`http://hale.pepperdine.edu/ scorcora/screen_shot.htm`.

Having dealt with the general user interface, we now discuss the individual aspects of each of the three output modes.

3.4 Input Systems of $n+2$ Phases

Systems of n components and $n+2$ phases are very easy to interpret (and display) graphically. Recall from the previous chapter that such systems have Gale diagrams (and thus secondary fans) in $\mathbb{R}^2$. We now describe `CHEMOGALE`'s various features for analyzing this type of system. Throughout this section, we use an example ternary system from [18] with components Al_2O_3, SiO_2, and H_2O and the five phases andalusite (Al_2SiO_5), kaolinite ($Al_2Si_2O_5(OH)_4$),

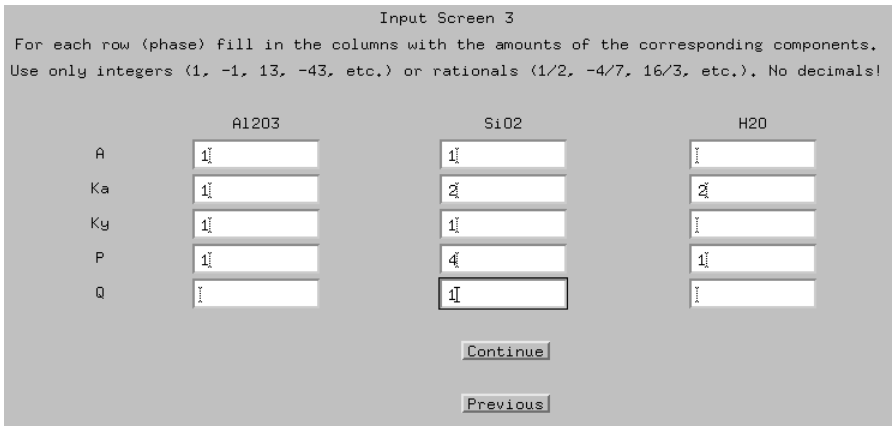

Figure 3.8: The completed third input screen for the example $n + 2$ system.

kyanite (Al_2SiO_5), pyrophyllite ($Al_2Si_4O_{10}(OH)_2$), and quartz (SiO_2). Figure 3.8 shows the completed third input screen for this system. If possible, we recommend that the reader run this example on his or her own computer while following along with this guide.

Figure 3.9 shows the main display screen for the example system. The two-dimensional Gale diagram is displayed as a set of lines emanating from a single point. The reader will recall that this is equivalent to the stable univariant reaction curves intersecting at the invariant point. The endpoint of each line is labeled by the particular phase which is/are missing from the corresponding univariant reaction. The standard notation is used with "( )" around the missing phase(s). Each line is also labeled according to the number of its associated mass balance equation. Accompanying the equation number, each side of a line is labeled with an "l" or an "r". These letters denote left-handed (l) and right-handed (r) sides of each reaction as tabulated in the **Reactions** pop-up window. An "l" denotes stability of the phases on the left hand side of the equation and an "r" denotes stability of the phases on the right hand side of the equation. To see, this, we may bring up the reactions window (shown in figure 3.10) by clicking **Display Reactions** on the main display screen. Notice that there are three reactions listed, which matches the fact that there are three lines total on the Gale diagram. We can see that reaction two involves only andalusite and kyanite, which are two distinct phases with the same chemical formula. The reaction is listed with andalusite on the left side and kyanite on the right side. Labels "l2" and "r2" on the Gale diagram relate which side of the reaction curve has the left side and right side of the equation stable, respectively. This reaction is a degeneracy in the Gale diagram, putting three of the Gale vectors coincident on the same line.

Recall from chapter 2 that reversing the parity of the phase diagram results in a second potential solution. This solution corresponds to a reflection of the

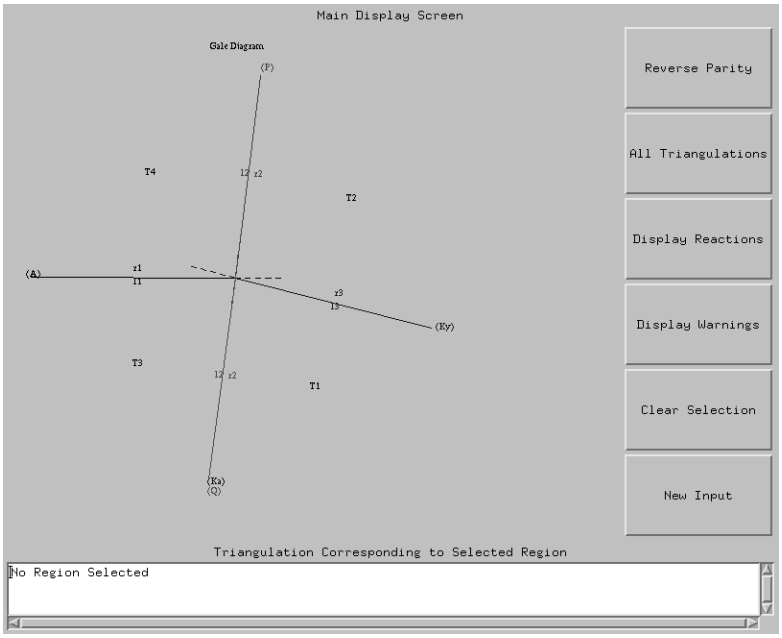

Figure 3.9: The main display screen for the example $n + 2$ system.

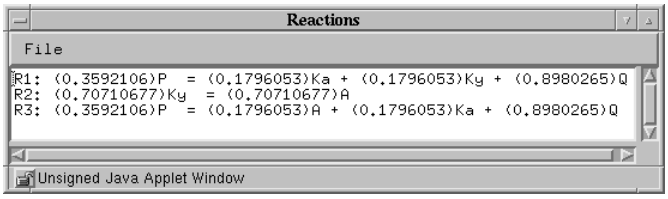

Figure 3.10: The reactions window for the example $n + 2$ system.

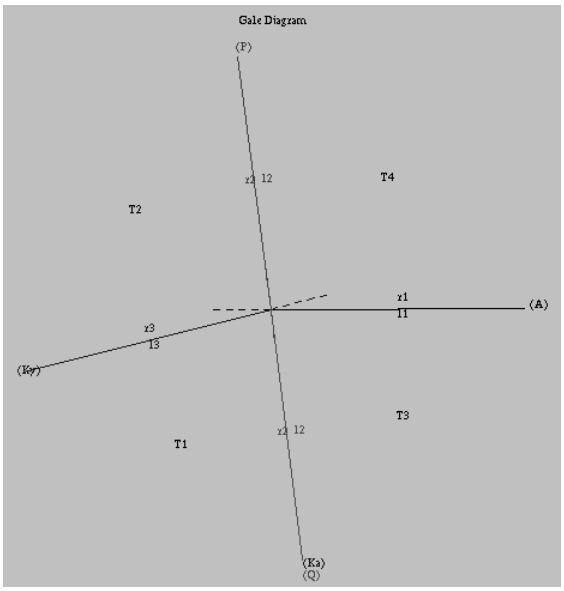

Figure 3.11: The Gale diagram with parities reversed from figure 3.9.

Gale diagram about some arbitrary axis. The user can view this solution by clicking the **Reverse Parity** button on the main display screen. In figure 3.11, we show the potential solution given by inverting the original. The user may go back to the originally displayed solution by clicking the **Reverse Parity** button again.

In both solutions, the regions in between the Gale vectors (i.e. the chambers of the secondary fan) are labeled according to their corresponding triangulation number. These are all of the potential stable divariant fields on the phase diagram. Clicking anywhere in a desired region will highlight the region and display the associated triangulation in the triangulation field at the bottom of the screen. The triangulation is displayed exactly as it appears in the pop-up window of all triangulations. In figure 3.12, we show the result of clicking on the region labeled $T1$ in the originally displayed Gale diagram. If the user wishes for no region to appear selected, he or she may click the button labeled **Clear Selection**.

3.5 Input Systems of $n+3$ Phases

Of course, things get much more complicated when we move to systems with three more phases than components. Just from a visualization standpoint, the upgrade of the Gale diagram (now constituting a closed net) to three dimensions makes things much harder to keep track of. Because of the increased

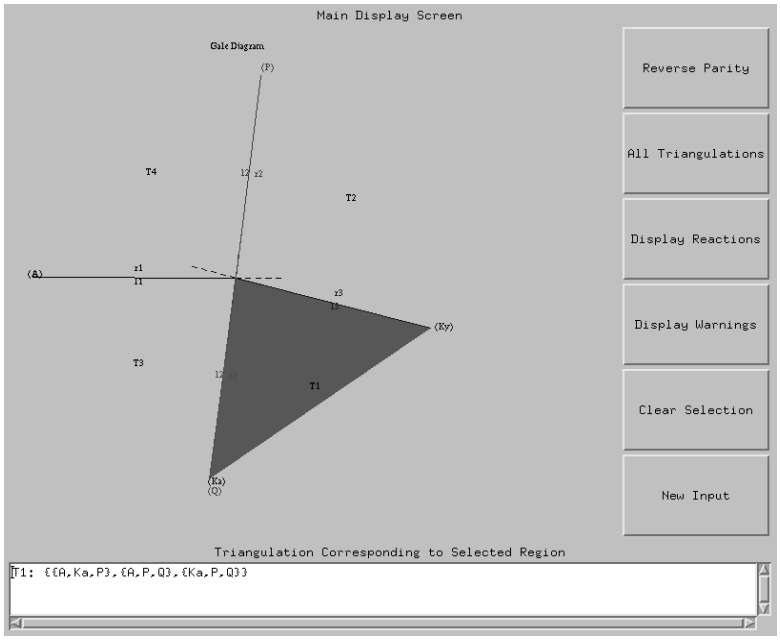

Figure 3.12: The Gale diagram with the $T1$ region selected for the example $n+2$ system.

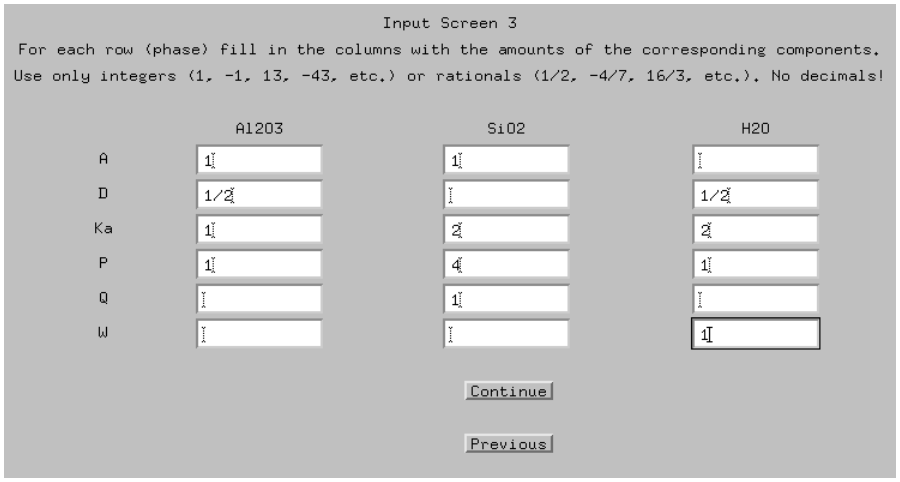

Figure 3.13: The completed third input screen for the example $n+3$ system.

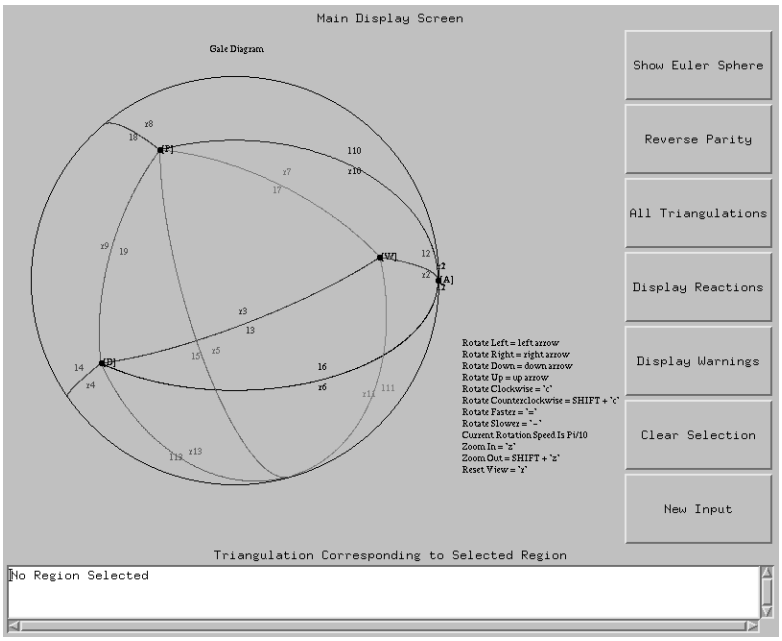

Figure 3.14: The main display screen for the example $n+3$ system.

complexity, CHEMOGALE has some additional features besides what was seen in the last section. To help illustrate all of them, we use the example system from [9] with the three components Al_2O_3, SiO_2, and H_2O and six phases: andalusite (Al_2SiO_5), diaspore ($AlO(OH)$), kaolinite ($Al_2Si_2O_5(OH)_4$), pyrophyllite ($Al_2Si_4O_{10}(OH)_2$), quartz (SiO_2), and water. The coordinates for these phases have been entered into the third input screen, shown in figure 3.13. Again, we recommend that the user run this example on his or her own machine while reading along.

The Gale diagram and secondary fan are shown in the main display screen intersected with the unit sphere (figure 3.14). Of course, we can only view one hemisphere at a time and so comes the need to rotate the sphere so that it can be viewed from any angle. Because mouse movements can be very clumsy and imprecise, we have designed the program to accept only keyboard commands for graphical manipulations. The various key commands and their effects are always displayed in a key to the right of the Gale diagram. In order to activate them, click once inside the display region (but outside the sphere itself). Now the sphere may be rotated about the horizontal axis (using up and down arrows), the vertical axis (using right and left arrows), or clockwise and counter clockwise (using c for clockwise and SHIFT-c for counter-clockwise). The speed of rotation can be decreased with the - key and increased with the = key. The current speed of rotation is given in the key as the angle (in radians) swept by each rotational

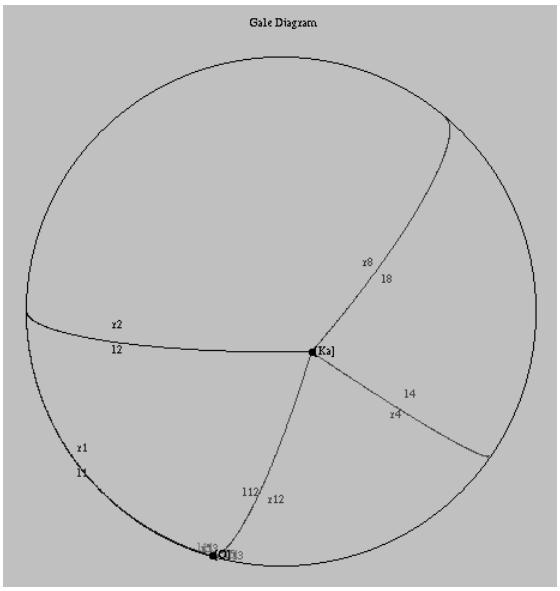

Figure 3.15: Rotation of the Gale diagram by π in the example $n+3$ system.

key stroke. We can view the opposite hemisphere by pressing = until the rotation speed is $\frac{\pi}{1}$ and pressing any arrow key. The result of doing this with the right arrow key yields the picture in figure 3.15. It is also possible to zoom in on the center of the displayed portion of the sphere by using `z`. Zooming back out is accomplished by pressing `SHIFT-z`. The amount of zoom is maintained by the zoom level. Initially, the zoom level is 1 and increases when zooming in. The current zoom level is always displayed in the key. The zoom level and rotation speed may be reset to the default by typing with `r`.

On the unit sphere, Gale vectors (stable invariant points) are represented as labeled black dots at the points where they poke through the sphere's surface. Univariant reaction curves are shown as colored arcs between invariant points. Just as in the two dimensional case, the arcs are labeled with an l_i on one side and an r_i on the other. The letters represent the stability of the left hand side (l_i) and right hand side (r_i) of the corresponding ith mass balance equation in the reaction pop-up window. Recall that the univariant reaction curves define the boundaries of the chambers in the secondary fan. Given these curves and their various intersections at the indifferent crossings, it is easy to see the chambers of the secondary fan as polygonal regions on the unit sphere. As we explained in the last chapter, these regions are in one-to-one correspondence with the regular triangulations of the phases in the chemography. As in the two-dimensional case, the user can click inside any region to display the corresponding triangulation. The triangulation will appear as a list of simplices (divariant assemblages) in the triangulation display field at the bottom of the screen and the selected region

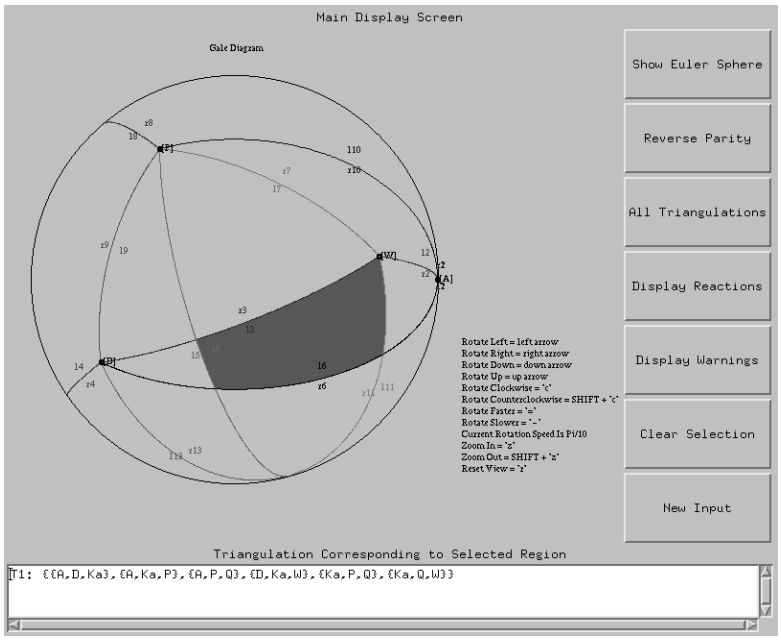

Figure 3.16: The Gale diagram with a secondary fan chamber selected in the example $n + 3$ system.

will be highlighted in red. In figure 3.16 we show a particular selected region for the input example system. The selected region on the unit sphere will remain highlighted in red until another region is selected or the **Clear Selection** button is clicked. Instead of selecting a triangulation from a particular region, the user may also select a region from a triangulation. Bringing up the pop-up window with all of the possible triangulations (the button labeled **All Triangulations**), the user will notice a **Select Region** heading on the menu bar. Clicking this will bring up a list of numbers corresponding to all of the regular triangulations. Selection of any number from this list will highlight the corresponding region in the Gale diagram and display the triangulation in the triangulation bottom window.

To see all of the potential phase diagram solutions for the system, one could attempt to find all possible orientations of the Gale diagram which yield a different topological configuration of regions. Recall from the previous chapter that systems with $n + 3$ phases have a set of potential solutions given by the regions on the Euler Sphere. Clicking the button **Show Euler Sphere** will open a display window (shown in figure 3.17) containing the Euler Sphere for the system. The sphere may be rotated and zoomed with the same key commands as the Gale diagram on the main display screen. Recall that the Gale vectors are represented as great circles on the Euler sphere. We label each great circle

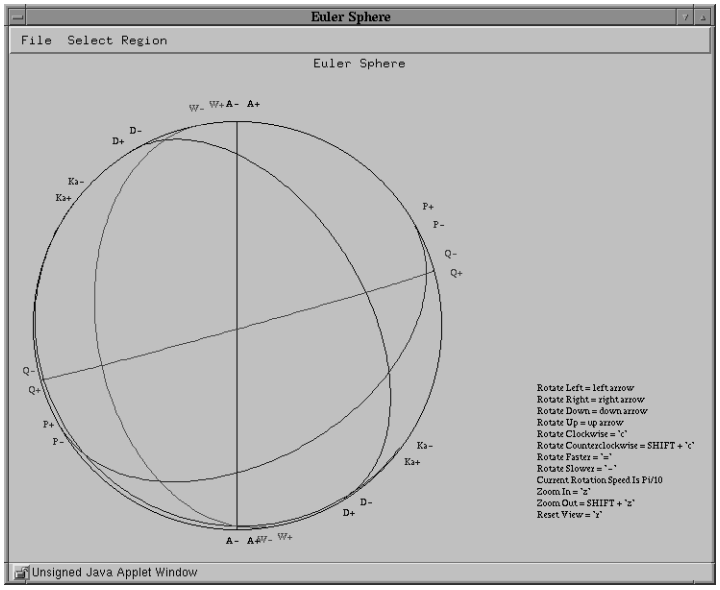

Figure 3.17: One hemisphere of the Euler Sphere in the example $n+3$ system.

by its corresponding Gale vector and assign + to the side of the great circle from which the Gale vector emanates and − to the opposing side. The regions defined by the arrangement of great circles can be selected with the mouse or from the list of region numbers under the **Select Region** heading on the menu bar. Selecting a region by either method will highlight the region and open a display window with the straight line net for the associated potential solution.

Figure 3.18 shows an example of a straight line net describing the potential solution for region number 26 on the Euler Sphere. The solution is displayed in the conventional format of straight line nets with solid dots at stable invariant points and open circles at metastable invariant points. Solid lines represent stable univariant curves, with dashed and dotted lines for metastable and doubly metastable reactions, respectively. The l and r on either side of the lines have the same meaning as in the Gale diagram, with labels corresponding to the numbered list of mass balance equations in the reactions window. The user may move the straight line net around in the window using the arrow keys for translation, `z` to zoom in, `SHIFT-z` to zoom out, and `r` to reset. To clearly see that each potential solution is really just a particular hemispheric view of the secondary fan, the user may refer back to the main display screen and notice that it has been automatically oriented so that the visible hemisphere is in line with the selected region of the Euler Sphere. Thus the configuration of stable univariant curves and stable invariant points on the straight line net is matched by the visible chamber boundaries and Gale vectors on the Gale diagram (after some clockwise or counterclockwise rotation). The metastable invariant points

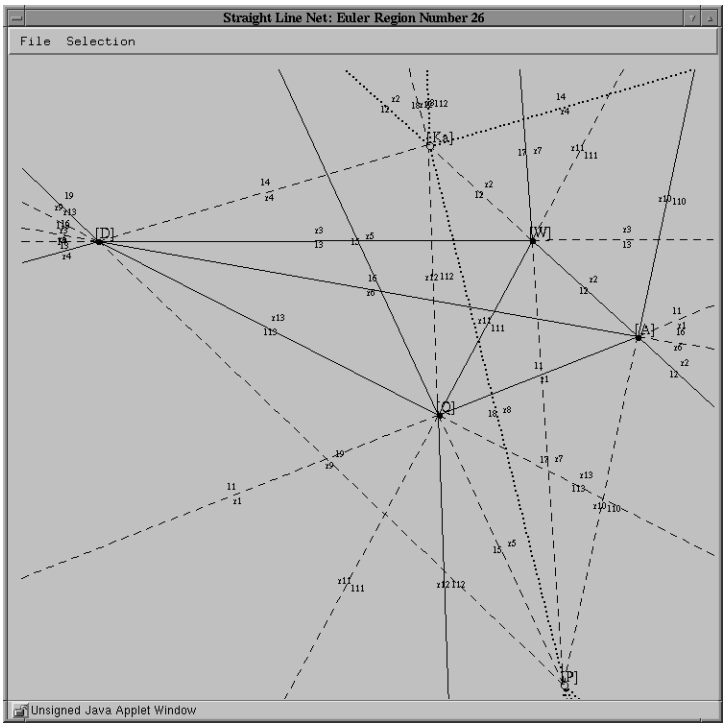

Figure 3.18: Potential solution 26 selected from the Euler Sphere in the example $n + 3$ system.

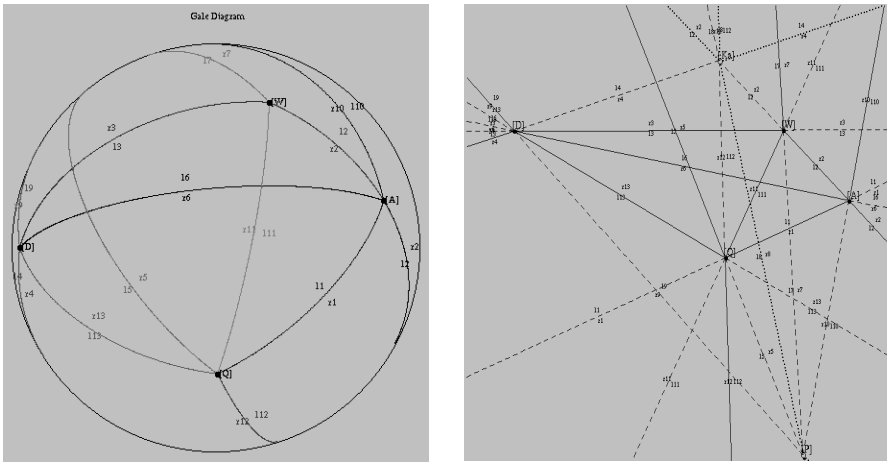

Figure 3.19: Potential solution 26 with the aligned orientation of the Gale diagram in the example $n+3$ system.

and the metastable and doubly metastable univariant reactions are the image of what is currently on the other side of the currently displayed hemisphere. Stable equilibria for the potential solution are existent in regions bounded by stable univariant reactions.

We performed the prescribed clockwise rotation of the Gale diagram to orient it consistent with the selected potential solution. Both are shown in figure 3.19. Clicking inside any stable region places a label in the clicked location with the triangulation number associated with that region. The clicked region is also highlighted in on the main display screen, and the triangulation is shown in the triangulations window at the bottom. To make the stable regions more apparent, the user may select the option **Display Stable Reactions Only** from the **Selection** menu (the option **Display All Reactions** redisplays the metastable and doubly metastable lines). Now the alignment should be very obvious and in figures 3.20 and 3.21 we show the effect on the main display screen of selecting the stable region (labeled $T5$) in the straight line net. For a particular potential solution, we can label every region with its corresponding triangulation number by clicking inside all of them. In figure 3.22 we show a completely labeled potential solution.

Recall that reversing the parities (handedness of invariant points) of each potential solution results in another valid potential solution for the system. As in the case of the two dimensional Gale Diagram, this corresponds to reflecting the Gale vectors across an arbitrary axis. By clicking the **Reverse Parity** button, the user may view the mirror image of the Gale diagram whose Euler Sphere contains all of the potential solutions resulting from reversing parities of the original solutions. Figure 3.23 shows two opposing hemispheres of the parity-reversed Gale diagram. In figures 3.24 and 3.25, we show the straight

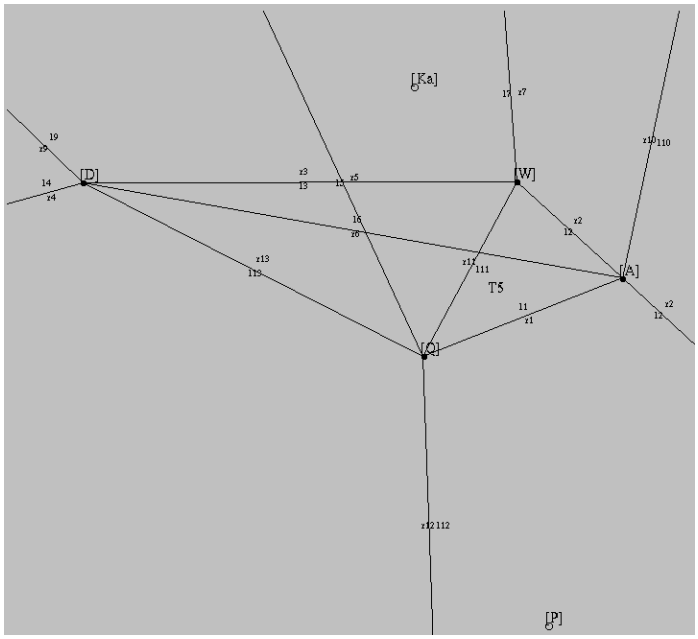

Figure 3.20: The stable region associated with triangulation 5 was selected in the straight line net for potential solution 26.

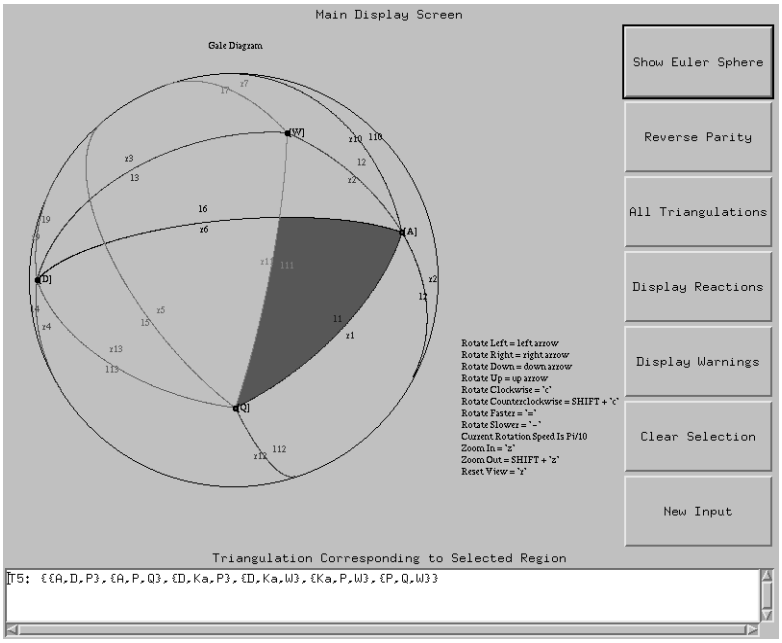

Figure 3.21: The corresponding Gale diagram region is highlighted as a result of selecting a stable region in the straight line net.

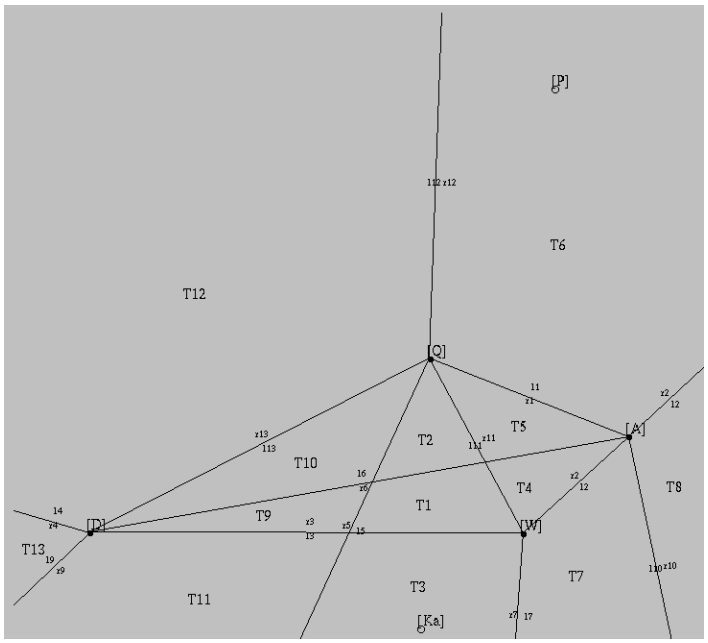

Figure 3.22: Potential solution 26 showing stable reactions only and all stable regions labeled in the example $n + 3$ system.

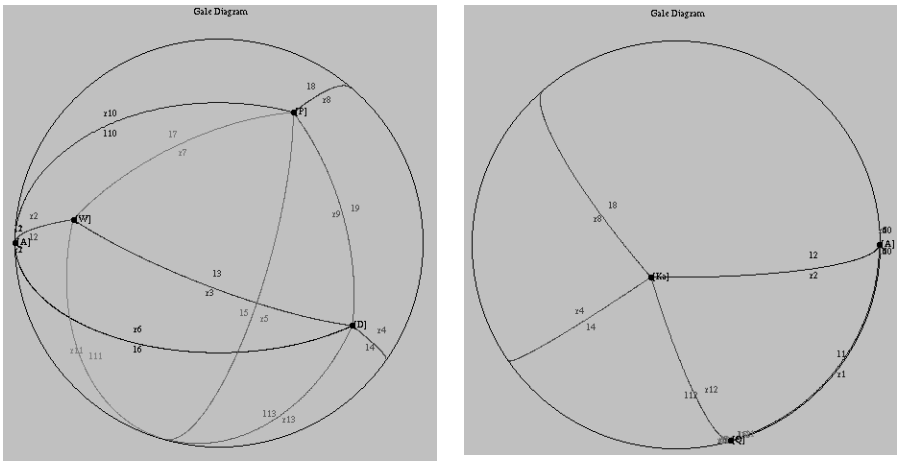

Figure 3.23: Two opposing hemispheres of the inverted Gale diagram for the example $n + 3$ system.

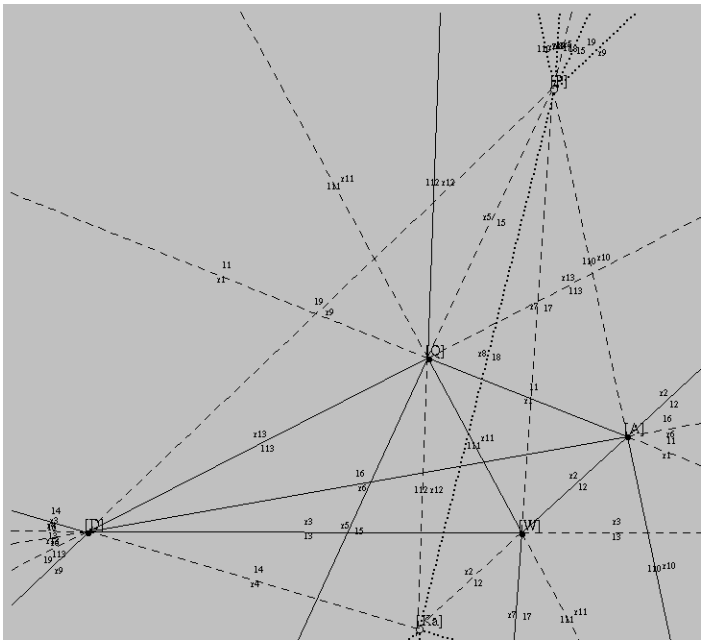

Figure 3.24: Potential solution 26 for the inverted Gale diagram.

line net for potential solution number 26 of the new Euler Sphere. It is easy to see that this solution is just like potential solution number 26 of the original Euler Sphere with the parities of every invariant point reversed.

3.6 Input Systems of $n+q$ Phases, $q = 1$ or $q > 3$

In the case of a chemical system with n components and $n + q$ phases, where $q > 3$, the dimension of the Gale diagram makes it very hard to visualize, let alone display on a computer. On the other hand, when $q = 1$, the phase diagram has trivially simple topology. Because of this, we only provide relevant triangulation and mass-balance information in such cases. We give a brief summary of the program's output for a sample system with the three components Al_2O_3-SiO_2-H_2O and seven phases: andalusite (Al_2SiO_5), diaspore ($AlO(OH)$), kaolinite ($Al_2Si_2O_5(OH)_4$), kyanite (Al_2SiO_5), pyrophyllite ($Al_2Si_4O_{10}(OH)_2$), quartz (SiO_2), and water. Figure 3.26 shows a completed third input screen for this system.

The main display screen (shown in figure 3.27) consists of just the three menu buttons: **New Input**, **All Triangulations**, and **Display Reactions**. All of these buttons have the same functionality as described above. Figures 3.28 and 3.29 show the triangulations and reactions windows, respectively. Until a convenient way is found in which to visualize systems with $n+4$ or more phases,

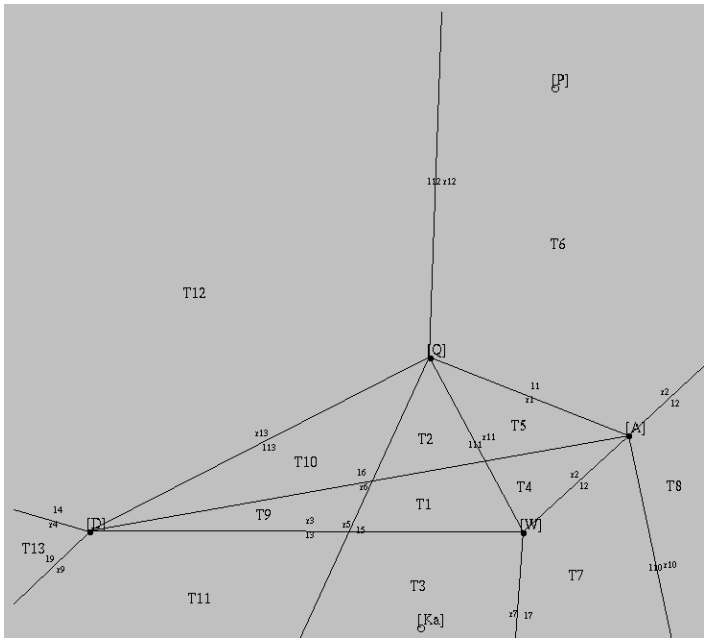

Figure 3.25: Potential solution 26 for the reverse parity Gale diagram shown with stable reactions only and all stable regions labeled.

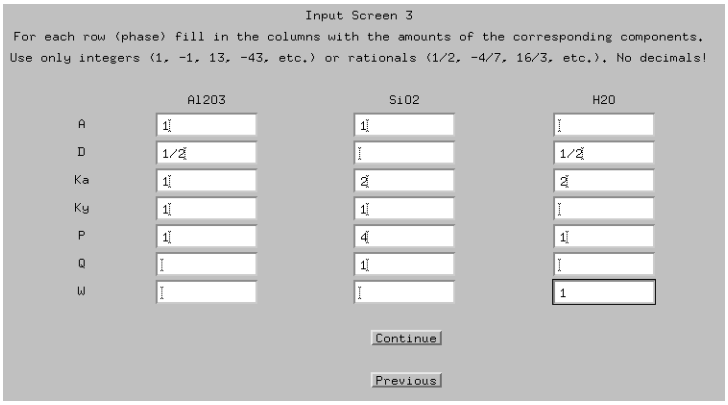

Figure 3.26: The third input screen completed for the example $n + 4$ system.

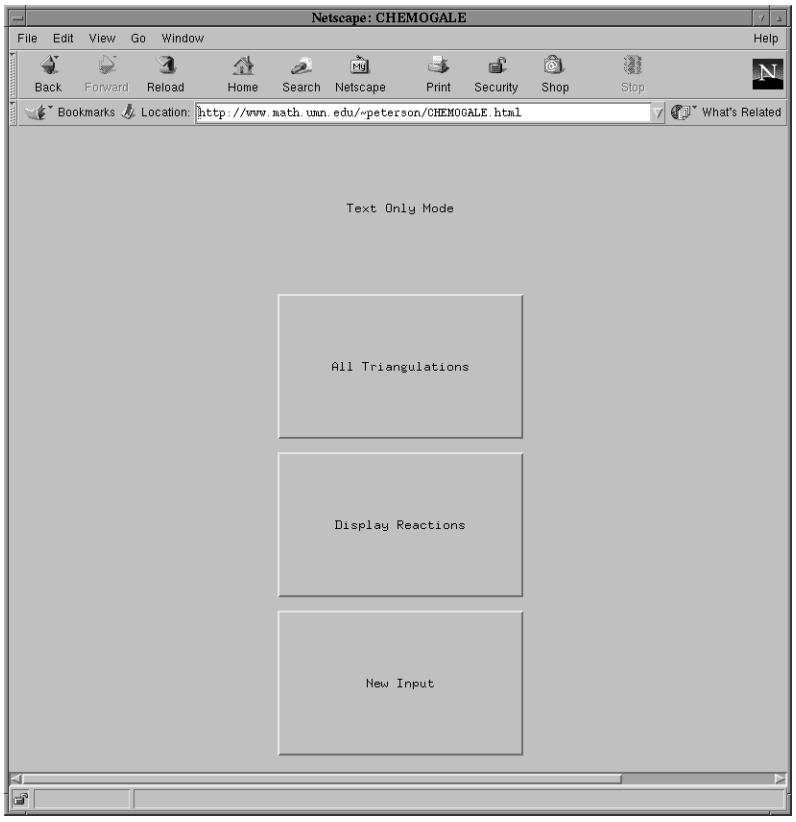

Figure 3.27: The main display screen for the example $n + 4$ system.

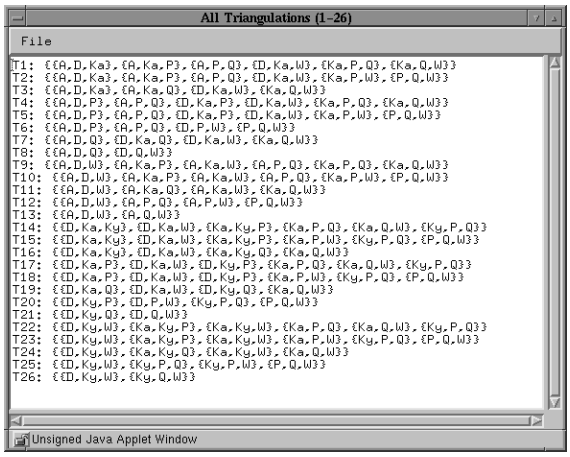

Figure 3.28: The window of all triangulations for the example $n + 4$ system.

the program is limited to only this output.

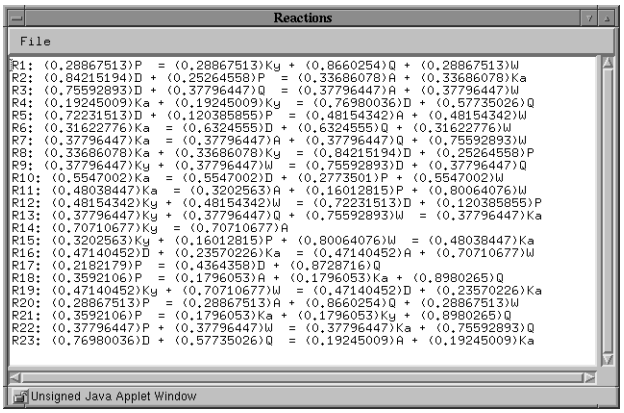

Figure 3.29: The set of all mass balance equations for the example $n+4$ system.

Appendix A

We have seen that the oriented matroid is a very powerful tool for studying point and vector configurations. Aside from encoding useful information about spatial relationships, we will see that oriented matroids provide us with a way of classifying and distinguishing sets of points or vectors based on combinatorial differences. In this appendix, we discuss how oriented matroids enable us to enumerate the entire set of combinatorially different point arrangements for a fixed small number of generically positioned points in low dimensions. The discussion becomes easier if we deal with acyclic vector configurations (i.e. the phase vectors in composition space) rather than affine point arrangements. Therefore, we will discuss oriented matroids as applied to some acyclic vector configuration, $\mathcal{V}$ in $\mathbb{R}^n$. We wrote a C++ program which exploits the theory, and we give results for acylic orientations of seven vectors in $\mathbb{R}^4$ (i.e. point configurations in $\mathbb{R}^3$) at the end of this appendix.

Recall from chapter two that the oriented matroid is completely defined by the list of signed circuits or, equivalently, by the list of signed cocircuits. Let us assume that we are dealing with a generic set $\mathcal{V}$ of m vectors in $\mathbb{R}^n$, whose oriented matroid is given by $\mathcal{M}_{\mathcal{V}}$. We know that every cocircuit in $\mathcal{M}_{\mathcal{V}}$ is given by some hyperplane spanned by a set of $n-1$ vectors in $\mathcal{V}$. This means that $\mathcal{M}_{\mathcal{V}}$ will contain a total of $\binom{m}{n-1}$ cocircuits. For each choice of $n-1$ spanning vectors, the columns of these $n-1$ vectors will be zero in the cocircuit and the remaining $m-(n-1) = m-n+1$ columns will be either a "+" or a "−." Naively counting all of the possibilities gives a total of $(2^{m-n+1})^{\binom{m}{n-1}}$ different oriented matroids. This bound is impractically large, yielding $1,073,741,824$ possibilities for as few as five vectors in $\mathbb{R}^3$. Fortunately, oriented matroid theory provides that there is a set of circuit axioms which the circuits and cocircuits of every oriented matroid must satisfy, thus limiting the possibilities. The axioms have been taken from [2], in which a circuit, $X \in \mathcal{C}$ is composed of (X^+, X^-) and $-X = (X^-, X^+)$. Here, X^+ is the set of indices which are "+" in the circuit and X^- is the set of indices which are "−" in the circuit. The axioms are as follows:

(C0) $\emptyset$ is not a circuit.

(C1) If X is a circuit, then so is $-X$.

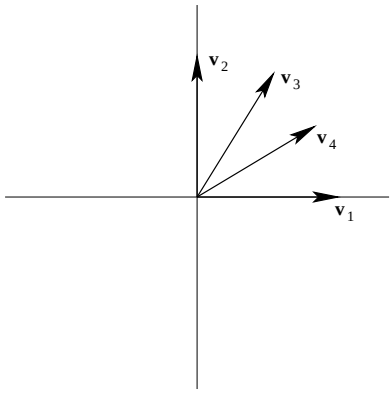

Figure A.1: An acyclic configuration of four vectors in $\mathbb{R}^2$.

(C2) No proper subset of a circuit is a circuit.

(C3) If X_0 and X_1 are circuits with $X_1 \neq -X_0$ and $e \in X_0^+ \cap X_1^-$, then there is a third circuit $X \in \mathcal{C}$ with $X^+ \subseteq (X_0^+ \cup X_1^+) \backslash \{e\}$ and $X^- \subseteq (X_0^- \cup X_1^-) \backslash \{e\}$.

It is guaranteed that the circuits and cocircuits of the oriented matroid for any acyclic vector configuration satisfy the above axioms. The converse, however, is not true. There are oriented matroids (i.e. sets of signed circuits which satisfy the circuit axioms) which do not correspond to any acyclic configuration of vectors. Such oriented matroids are said to be *non-realizable*. It is proven in [2] that all oriented matroids are realizable by a set of m vectors $\mathcal{V}$ in $\mathbb{R}^n$ for at least the following cases:

(1) $n \leq 2$

(2) $n = 3$ and $m \leq 8$

(3) $n = 4$ and $m \leq 7$

(4) $n = 5$ and $m \leq 8$

(5) $n \geq 6$ and $m \leq n + 2$

As we should expect, swapping any of these with its oriented matroid dual (replacing (n, m) with $(m - n, m)$) gives back a case which is also listed. For any pair (n, m) which satisfies one of the five cases, we can theoretically generate acyclic vector configurations from every oriented matroid of the corresponding size.

The main advantage to working with acyclic vector configurations rather than affine point configurations is that the acyclic vector arrangements can be counted in a very natural way. Consider the two-dimensional, acyclic vector configuration shown in figure A.1. If we replace $\mathbf{v}_1$ with $-\mathbf{v}_1$, we get the new

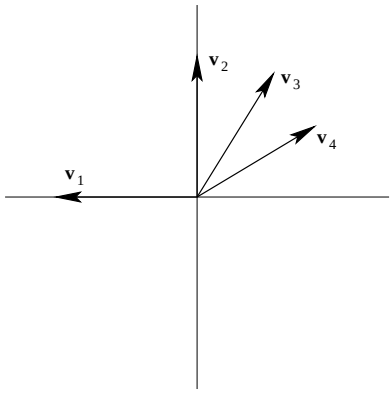

Figure A.2: An acyclic reorientation of the vector configuration in figure A.1.

acyclic arrangement shown in figure A.2. The new arrangement is an *acyclic reorientation* of the original vectors. We can iterate this process many times and in different combinations to yield six more configurations. Of course, there are other acyclic arrangements which are not reorientations of the vectors from figure A.1. One such arrangement is shown in figure A.3. This concept applies to sets of vectors in any dimension and provides a way to group acyclic vector orientations into large reorientation families.

At first glance, the oriented matroids might look different from one acyclic reorientation to the next. However, much of the appearance of the circuits and cocircuits depends on how we label the vectors. For example, the acyclic arrangement shown in figure A.1 can be made to look just like its reorientation in figure A.2 by imposing the label permutation $\{\mathbf{v}_2 \to \mathbf{v}_1, \mathbf{v}_3 \to \mathbf{v}_2, \mathbf{v}_4 \to \mathbf{v}_3, \mathbf{v}_1 \to \mathbf{v}_4\}$. Certainly, we do not want two arrangements to be considered different if the only distinguishing characteristic is the labeling scheme. Therefore, we are only interested in acyclic vector arrangements up to re-labeling their vertices. Even vector configurations which are not reorientations of one another can be equivalent after a relabeling. The reader should convince him or herself that any two generic arrangement of m vectors in $\mathbb{R}^2$ can be labeled such that they are equivalent. For this reason, we require that any two reorientation families be distinct for any possible relabeling. Now, relabeling equivalence can only exist between acyclic orientations of the same reorientation family.

In terms of oriented matroids, all of the reorientations from a particular family belong to the same *reorientation class* of oriented matroids. The enumeration of the oriented matroid classes is beyond the scope of this paper, but extensive work has been done by Ulli Kortenkamp, Bokowski, Jürgen Richter-Gebert and others to construct them for small sets in few dimensions [13], [2]. The particular problem of counting the generic, acyclic orientations of 7 vectors in $\mathbb{R}^4$ falls into case (3) from above, so we know that all of the oriented matroids are realizable. Oriented matroid duality helps to simplify things a lot. For it is

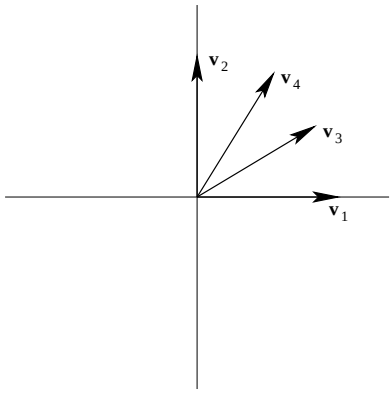

Figure A.3: An acyclic arrangement of four vectors in $\mathbb{R}^2$ which is not a reorientation of the vectors in A.1.

known that the number of different oriented matroid classes is invariant under duality. A configuration of seven vectors in $\mathbb{R}^4$ has the dual configuration of seven vectors in $\mathbb{R}^{7-4} = \mathbb{R}^3$. Replacing the seven vectors in $\mathbb{R}^3$ by the hyperplanes to which they are normal and then taking an affine slice by a non-central affine hyperplane yields a configuration of seven lines in $\mathbb{R}^2$. This configuration is topologically invariant across different slices. In [8], Grünbaum proves that there are eleven topologically distinct ways to arrange seven lines in the plane. This implies that there are eleven oriented matroid classes for a set of seven acyclic vectors in $\mathbb{R}^3$ and thus also in $\mathbb{R}^4$.

Several steps were involved for us to count the number of point configurations up to relabeling. Jürgen Richter-Gebert kindly provided us with *chirotopes* (see [2]) for the line arrangements from [8] to construct the 11 oriented matroid classes. We then manually realized each of these oriented matroid classes as a set of seven vectors in $\mathbb{R}^4$. All that was needed from here was to count the number of acyclic reorientations of these vectors and eliminate duplications from relabeling. Enumerating the acyclic orientations employs the interchangeability of vector configurations and hyperplane arrangements shown in [2]. Recalling our notation from chapter two, we can use the acyclic vector arrangement $\mathcal{V} = \{\mathbf{v}_1, \mathbf{v}_2, \ldots \mathbf{v}_7\}$ to construct the hyperplane arrangement $\mathcal{H}_\mathcal{V} = \{H_{\perp\mathbf{v}_1}, H_{\perp\mathbf{v}_2}, \ldots, H_{\perp\mathbf{v}_7}\}$. We have seen that $\mathcal{H}_\mathcal{V}$ defines a complete fan, $\mathcal{F}_\mathcal{V}$, in $\mathbb{R}^4$. Now every chamber $C_i \in \mathcal{F}_\mathcal{V}$ is in one to one correspondence with an acyclic reorientation of $\mathcal{V}$. Specifically, the reorientation is defined by replacing each $\mathbf{v}_j \in \mathcal{V}$ by $SIGN_{H_{\perp\mathbf{v}_j}}(C_i)\mathbf{v}_j$, where $SIGN_{H_{\perp\mathbf{v}_j}}(C_i) = 1$ if $C_j \subset H^+_{\perp\mathbf{v}_j}$ and $SIGN_{H_{\perp\mathbf{v}_j}}(C_i) = -1$ if $C_j \subset H^-_{\perp\mathbf{v}_j}$.

We used C++ to implement an algorithm based on the Farkas lemma (found in [14]), for enumerating all of the chambers of $\mathcal{F}_\mathcal{V}$, given $\mathcal{V}$. After collecting all of the acyclic reorientations of $\mathcal{V}$, the program weeded out any repeats from relabeling. After running the program for each of the eleven reorientation families,

we found 246 combinatorially different sets of seven points in general position in $\mathbb{R}^3$. We used another C++ program called TOPCOM, written by Jörg Rambau [12], to produce the list of all triangulations for each unique point configuration. Finally, we used a maple program called PUNTOS, written by Jesus de Loera [5], to identify non-regular triangulations.

We can classify each point configuration by the structure of its convex hull. If $\mathcal{X}$ is a set of m points in $\mathbb{R}^n$ and $\mathbf{x} \in \mathcal{X}$ is a point on the convex hull, then the *degree* of $\mathbf{x}$ is the total number of external edges incident on $\mathbf{x}$. The degree of vertex $\mathbf{x}$ must be at least n and at most $m-1$. For any point configuration, we can specify its *degree sequence*, written $(d_n, d_{n+1}, \ldots, d_{m-1})$, which relates the number of occurrences of each feasible degree value. For instance, if $m = 7$ and $n = 3$, the degree sequence $(2, 3, 0, 2)$ implies that there are two vertices with degree three, three vertices with degree four, and two vertices with degree six. Figures A.4 and A.5 show the possible degree sequence types for generic sets of at most six points in $\mathbb{R}^2$ and at most seven points in $\mathbb{R}^3$, respectively. We used a program called `PORTA`, written by T. Christof [4], to compute vertex degree information for all 246 configurations of seven points in $\mathbb{R}^3$. Table A.1 lists the number of combinatorially different configurations for each degree sequence type of six points in general position in $\mathbb{R}^2$, sorted by the four oriented matroid classes. Similar information for six points in general position in $\mathbb{R}^3$ (for which there is only one oriented matroid class) is shown in table A.2. Finally, we present our program's results for the case of seven points in general position in $\mathbb{R}^3$ in table A.3. The number of point configurations in each category for which there exist non-regular triangulations is given in parentheses.

OM Class	Triangle	Quadrilateral	Pentagon	Hexagon	total
1	1	2	0	1	4
2	1	0	1	0	2
3	2	2	1	0	5
4	2 (1)	2	1	0	5
total	6 (1)	6	3	1	16 (1)

Table A.1: Number of distinct point configurations (grouped by number of external vertices) generated by the 4 oriented matroid classes for six generically positioned points in $\mathbb{R}^2$. Numbers in parentheses denote the number of configurations for which non-regular triangulations exist.

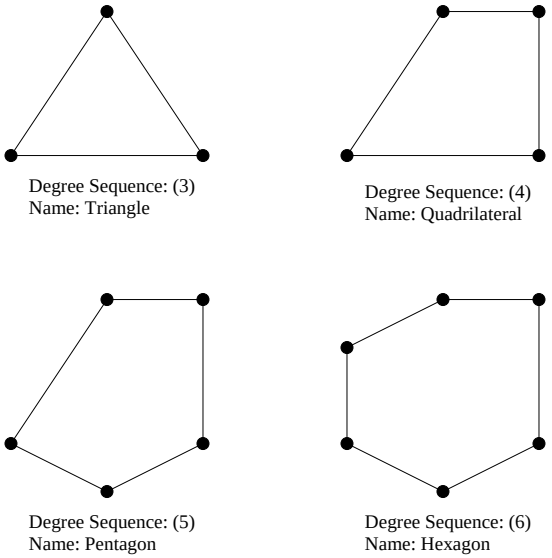

Figure A.4: The four possible degree sequence types for at most six points in $\mathbb{R}^2$.

OM Class	T	B	O_s	O_a	total
1	1	1	1	1	4

Table A.2: Number of distinct point configurations (grouped by degree sequence types from figure A.5 of the external vertices) generated by the 1 oriented matroid class for six generically positioned points in $\mathbb{R}^3$.

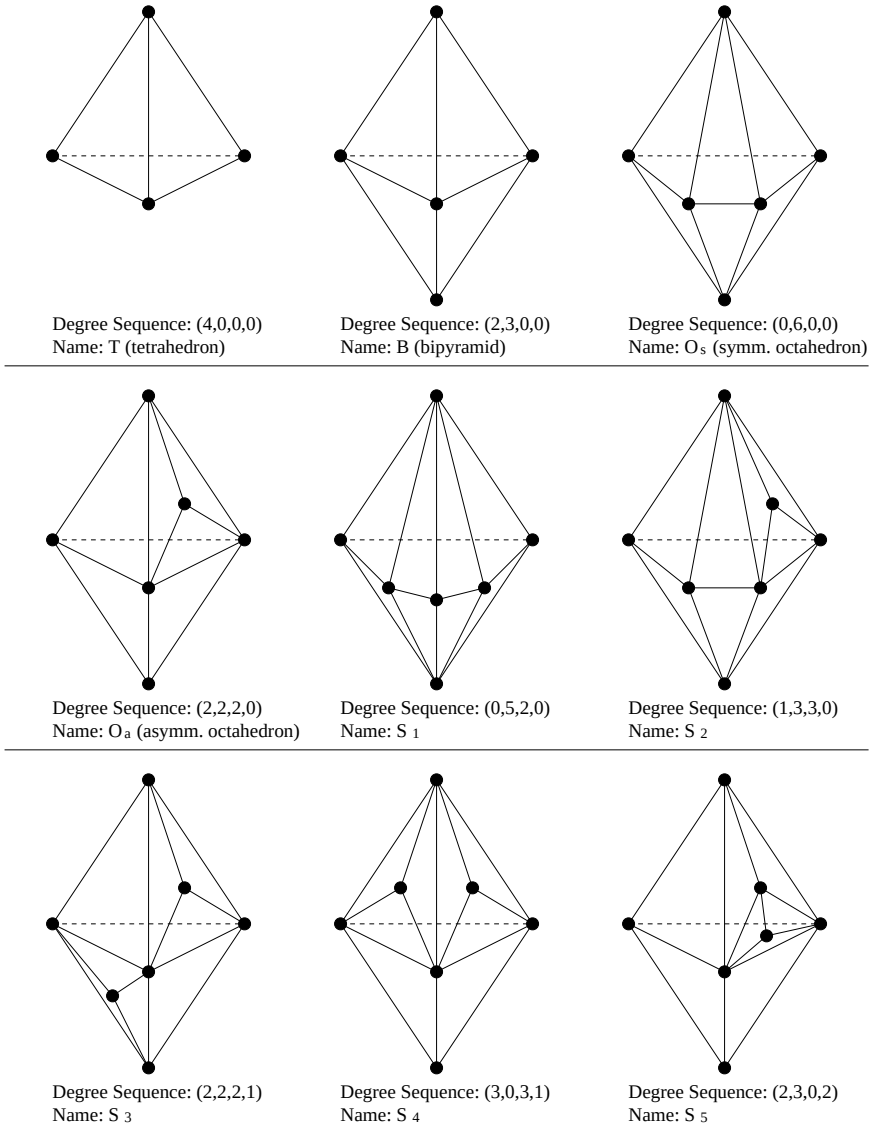

Figure A.5: The nine possible degree sequence types for at most seven points in $\mathbb{R}^3$.

OM Class	T	B	O_s	O_a	S_1	S_2	S_3	S_4	S_5	total
1	1	2 (1)	1	0	0	0	0	0	1	5 (1)
2	4 (2)	10 (3)	3	3	1	0	1	0	1	23 (5)
3	8 (3)	17 (8)	4	8 (2)	1	1	1 (1)	1	1	42 (14)
4	4 (2)	9 (4)	3	5	0	1	1	0	0	23 (6)
5	4 (3)	9 (1)	3 (1)	4	1	0	2	0	0	23 (5)
6	5 (3)	7 (4)	2	6 (1)	0	1	2	0	0	23 (8)
7	6 (3)	6 (3)	0	8 (5)	1	1	0	1	0	23 (11)
8	3 (1)	6 (2)	2	3	0	2 (1)	0	0	0	16 (4)
9	8 (4)	16 (3)	2 (2)	12 (4)	2	2	0	0	0	42 (13)
10	4 (1)	4 (3)	1 (1)	5 (1)	0	2	0	0	0	16 (6)
11	2 (1)	3	1 (1)	2 (2)	1	0	0	1	0	10 (4)
total	49 (23)	89 (32)	22 (5)	56 (15)	7	10 (1)	7 (1)	3	3	246 (77)

Table A.3: Number of distinct point configurations (grouped by degree sequence type from figure A.5 of the external vertices) generated by the 11 oriented matroid classes for seven generically positioned points in $\mathbb{R}^3$. Numbers in parentheses denote the number of configurations for which non-regular triangulations exist.

Bibliography

[1] **T. Banchoff and J. Werner**, *Linear Algebra Through Geometry*, Springer-Verlag, New York, (1983).

[2] **A. Björner, M. Las Vergnas, B. Sturmfels, N. White, and G. Ziegler**, *Oriented Matroids*, Cambridge University Press, Cambridge, 1993.

[3] **R. G. Bland and M. Las Vergnas**, *Orientability of matroids*, J. Combinatorial Theory, Ser. B 24, (1978), 94-123.

[4] **T. Christof**, *PORTA - A Polyhedron Representation Transformation Algorithm*, version 1.3.1, available at `http://www.iwr.uni-heidelberg.de/iwr/comopt/soft/PORTA/readme.html` and at `ftp://elib.zib.de/pub/mathprog/polyth/index.html`

[5] **J. de Loera**, *Triangulations of Polytopes and Computational Algebra*, PhD Thesis, Cornell University, (1995).

[6] **J. Folkman and J. Lawrence**, *Oriented matroids*, J. Combinatorial Theory, Ser. B 25, (1978), 199-236.

[7] **I. M. Gelfand, M. Kapranov, and A. Zelvisky** *Multidimensional Determinants, Discriminants and Resultants*, Birkhäuser, Boston (1994).

[8] **B. Grünbaum**, *Convex Polytopes*, Wiley Interscience, New York, (1967), 456 p.

[9] **G. Kletetschka and J. H. Stout**, *Stability analysis of invariant points using Euler spheres, with an application to FMAS granulites*, J. metamorphic Geol., 17 (1999), pp. 1-14.

[10] **R. E. Mohr and J. H. Stout**, *Multisystem nets for systems of $n + 3$ phases*, American Journal of Science, 280 (1980), pp. 143-172.

[11] **W. H. Press, B. P. Flannery, S. A. Teukolsky, W. T. Vetterling** *Numerical Recipes in C*, Cambridge University Press, Cambridge, 1989.

[12] **J. Rambau**, *TOPCOM - Triangulations of Point Configurations and Oriented Matroids*, version 0.2.0, (1999). Available at `http://www.zib.de/rambau/TOPCOM.html`

[13] **J. Richter-Gebert**, *On the realizability problem for combinatorial geometries*, Dissertation, TH Darmstadt, (1991).

[14] **A. Schrijver, Alexander**, *Theory of Linear and Integer Programming*, Wiley-Interscience, (1998).

[15] **J. H. Stout**, *A general chemographic approach to the construction of ternary phase diagrams. With application to the system Al_2O_3-SiO_2-H_2O*, American Journal of Science, 285 (1985), pp. 385-408.

[16] **J. H. Stout**, *Phase chemographies in quaternary systems of seven phases, I: The five convex polytopes*, American Journal of Science, 290 (1990), pp. 719-738.

[17] **J. H. Stout and Q. Guo**, *Phase diagram topology and the intrinsic stability rule*, American Journal of Science, 294 (1994), pp. 337-360.

[18] **E-an Zen**, *Construction of pressure-temperature diagrams for multicomponent systems after the method of Schreinemakers - a geometric approach*, U.S. Geol. Survey Bull., 1225 (1966), pp. 1-56.

[19] **E-an Zen**, *Some topological relationships in multisystems of $n + 3$ phases I. General theory; unary and binary systems*, American Journal of Science, 264 (1966), pp. 401-427.

[20] **E-an Zen**, *Some topological relationships in multisystems of $n + 3$ phases II. Unary and binary metastable sequences*, American Journal of Science, 265 (1967), pp. 871-897.

[21] **E-an Zen and E. H. Rosenboom, Jr.**, *Some topological relationships in multisystems of $n + 3$ phases III. Ternary systems*, American Journal of Science, 272 (1972), pp. 677-710.

[22] **G. M. Ziegler** *Lectures on Polytopes*, Springer-Verlag, New York, 1995.